STUDY OF ANCHORING BEHAVIOR OF NEMATIC FLUIDS AT THE INTERFACE OF POLYMER-DISPERSED LIQUID CRYSTALS

A Dissertation

Presented to

The Academic Faculty

By

Jian Zhou

In Partial Fulfillment

Of the Requirements for the Degree

Doctor of Philosophy in School of Polymer, Textile and Fiber Engineering

Georgia Institute of Technology

November, 2003

Study of Anchoring Behavior of Nematic Fluids at The Interface of Polymer-Dispersed Liquid Crystals

Approved by:

Dr. Mohan Srinivasarao, advisor

Dr. David M. Collard, advisor

Dr. Mostafa El-Sayed

Dr. Anselm C. Griffin

Dr. Andrew Lyon

Dr. Jung O. Park

Date Approved 11/21/2003

ACKNOWLEDGEMENTS

I am very grateful to many people who helped me in this thesis work. First, I would like to sincerely thank both of my thesis advisors, Prof. Mohan Srinivasarao and Prof. David Collard, for guiding me through the process of this graduate research and development of this thesis. I appreciated the freedom and space which they gave me in exploring this research project. In particular, I would like to thank Prof. Srinivasarao for his teaching and support, his mentoring on how to work professionally in scientific areas, his time in answering me so many questions and critically reading the draft of this thesis, his encouragements and giving me many chances to attend academic conferences during my graduate years. I thank Prof. Collard for his support in providing me the lab space and facilities to work on synthesis since the starting of this research, his time, patience and many insightful suggestions on our meetings. I am also very grateful to Dr. Jung O. Park for many fruitful discussions, her encouragements and helpful suggestions as a senior member of our group. I also thank the three of them for making detailed comments in revising the manuscripts for publication.

I would like to thank the other members of my committee, Prof. Haskell Beckham, Prof. Mostafa El-Sayed, Prof. Anselm Griffin, Prof. Satish Kumar, Prof. Andrew Lyon, and Prof. Laren Tolbert for their valuable criticisms, suggestions, and reading the proposal of this thesis and the final thesis.

Many thanks to my former and current labmates from both Srinivasarao group and Collard group, whom I learned a great deal from and enjoyed collaborative relations with. In particular, on the experimental work, I thank David Jenkins, Raymond René and Lulu Song for their help with using the instruments of the group. I thank Marian Vargas

for helping me to start on synthesis, and Susanna Coons, Michael Hong, Ling Li, Fouad Salhi, and Shannon Watt for the helpful discussions. I thank Vivek Sharma for the proof reading of Chapter 3. In addition, my thanks extend to Joel Pollino, James Russum, Swati Singla and Walter P. Watson for their help with GPC and DSC measurements, to Dr. Tao Liu for the helpful discussions.

I am grateful to Prof. Satyendra Kumar and Dr. Tony Wang (Kent State University) for the collaborations on the work of Chapter 4 and help in measurement of the refractive indexes of a liquid crystal sample (Appendix C).

I also wish to express my gratitude to Dr. Karl Amundson (E Ink Corp.) for the helpful discussions on anchoring transitions, to Dr. Mark Kimmel and Xun Gu for allowing me to use their lab space and assistance for measurement of electro-optical properties of diffraction gratings.

The financial support from NSF (CAREER Award for Prof. Srinivasarao, Grant No. 0096240) on this research project is greatly acknowledged.

I also would like to thank the staffs of School of Polymer, Textile and Fiber Engineering and Georgia Tech library for their assistance to my graduate study.

Finally, I want to thank my wife, Wei, and my parents who have always given me love and support through this research work. I must also thank my friends who give me support by prayers during my graduate study.

Glory and praise to our God for HE made all things possible.

TABLE OF CONTENTS

LIST OF FIGURES

LIST OF TABLES

LIST OF SYMBOLS

n and n (r)	nematic director and nematic director field
f	azimuthal angle of nematic director
q	tilt angle of nematic director
α	out-of-plane angle of nematic director, $\alpha=90°-q$
T_{NI}	nematic-isotropic transition temperature
T_t	anchoring transition temperature
S	Orientation order parameter or strength of defect in liquid- crystals (depending on the context)
n_e,	extraordinary refractive index of a nematic fluid
n_o	ordinary refractive index of a nematic fluid
n_{eff}	effective refractive index for a extraordinary ray
(n_e-n_o) or Δn	birefringence
R	optical retardation
K_{11}, K_{22} and K_{33}	elastic constants for splay, twist and bend deformation of a nematic liquid crystalline phase respectively.
γ_1	rotational viscosity coefficient
H	magnetic field
E	electric field
$\Delta\chi$	anisotropy of magnetic susceptibility
$\Delta\varepsilon$	dielectric anisotropy
ξ_m	magnetic coherence length of nematics

LIST OF SYMBOLS (cont'd)

τ_{rise}	response time of nematics when swichting on an electric or magnetic field
τ_{decay}	response time of nematics when swichting off an electric or magnetic field
E_c and V_c	threshold electric field and threshold voltage respectively
V_{90}	voltage required for the LC cell to reach 90% of the maximum transmittance
I_{det}	intensity collected by the detector
I_{em}	fluorescent emission intensity
λ	the wavelength of light
h	sample thickness
d	width of wall defect
b	extrapolation length
b_m	Diffraction angle of the m^{th} order diffraction beam
W_s	anchoring energy
$W_p(q)$	polar anchoring energy
W_p	polar anchoring strength or coefficient of polar anchoring energy
$W_a(f)$	azimuthal anchoring energy
W_a	azimuthal anchoring strength or coefficient of azimuthal anchoring energy

LIST OF ABBREVIATIONS

LC	liquid crystal
NLC	nematic liquid crystal
PDLC	polymer-dispersed liquid crystal
TN	twisted nematic devices
2-EHxA	2-ethylhexyl acrylate
C6A	*n*-hexyl acrylate
C7A	*n*-heptyl acrylate
C8A	*n*-octyl acrylate
C10A	*n*-decyl acrylate
MHA	methylheptyl acrylates
DMH_xA	dimethylhexyl acryaltes
H-to-P	homeotropic-to-planar
C-to-H	conical-to-homeotropic
DE	diffraction efficiency
FCPM	fluorescence confocal polarizing microscopy
OM	optical microscopy
PLM	polarized light microscopy
LSCM	laser scanning confocal microscopy
SEM	scanning electronic microscopy

SUMMARY

A liquid crystal (LC) at its boundary surface adopts a preferential alignment, which is referred to as anchoring. The direction of this alignment (i.e., anchoring direction) may be perpendicular, parallel or tilted with respect to the surface. Transitions from one anchoring condition to another may occur when the parameters (e.g., temperature) charactering the surface change, as referred to as anchoring transitions. In the LC-polymer composite systems under our study, the anchoring and temperature-driven anchoring transitions of nematic fluids is very sensitive to the structure of the side chain of poly (alkyl acrylate) matrixes that encapsulate the LC. We have shown that the anchoring transition temperature of these systems can be tuned far below the nematic-to-isotropic transition temperature, by varying either the length, branching structure of the side chains of homopolymers, or the composition of copolymer of two dissimilar monomers. Both sharp and broad anchoring transitions with respect to the temperature range over which a transition occurs were observed. It is postulated that microscopic interactions between the polymer side chains and LC molecules play an important role in determining the anchoring. In particular, the conformation of the polymer side chain is proposed to have important control over the anchoring. Anchoring strength and tilt angle as a function of temperature during the anchoring transitions were experimentally investigated, which contribute to understanding of the microscopic mechanism for such transitions.

Based on the LC-polymer composites with controlled anchoring, a LC display with reverse switching mode and a novel electrically switchable diffraction grating have

been demonstrated. The advantages of these devices are ease of manufacturing, low operation voltage, and mechanical stability offered by polymer matrix.

Moreover, a detailed study of the director configuration of wall defects found in these composite films was carried out using fluorescence confocal polarized microscopy.

CHAPTER 1

INTRODUCTION

A liquid crystalline phase is a phase of matter between a isotropic liquid and a solid crystal: it is a fluid phase and also has some degree of order (rotational order, and in some cases as well) of its components. The fluidity and partial order in the liquid crystalline phase gives rise to many interesting properties.[1] The existence of liquid crystals (LC) has been known for more than a hundred years.[2] Yet it is only in the last 30 or 40 years that research in LC has been very active. It was mainly driven by interests in technological applications of the LC (e.g., display devices, sensors, light valves) and fundamental study of new phenomena related to LC phases.[3] The anisotropy of a LC phase dictates that its physical properties depend on its bulk alignment. This alignment can be affected by both external forces, like electrical, magnetic, and mechanical forces and the boundary conditions of the LC. In absence of external forces, a LC phase in contact with any surface adopts a preferential alignment that minimizes the surface energy, which is commonly referred to as anchoring. The preferred alignment direction (i.e., anchoring direction) may be perpendicular (homeotropic), parallel (planar) or tilted with respect to the surface. Transitions fom one anchoring condition to another (for example, from homeotropic to planar) may occur when the parameters charactering the surface change, and are referred to as anchoring transitions. Anchoring plays an essential role in the preparation and operation of liquid crystal devices. Numerous surface treatment techniques have been widely investigated to control the anchoring of LC at solid substrates.[4,5,6] An important example of this control is using rubbed polymer layers as the substrates to achieve the uniform slight tilted anchoring of a nematic LC (the

simplest form of LC phases) in many LC displays (e.g., those used for laptop computer screens).[7,8] Polymeric materials are the most commonly used solid substrates in LC devices to provide a desirable anchoring. This arises from their ease of processing (e.g., readily forming smooth and uniform layers), ease of tuning surface structure and bulk physical properties, and chemical, thermal and mechanical stability relative to small molecules. In display devices constructed from polymer-dispersed liquid crystal (PDLC), a polymer is used as the encapsulating matrix that provides not only control of surface anchoring but also the mechanical stability of the device.[9,10]

The major focus of this thesis is to understand the relationships between the anchoring behavior of nematic fluids and the chemical structure of matrix polymers, and to exploit this knowledge to fabricate novel electro-optical LC devices based on LC-polymer composites. In particular, we focus our attention on temperature-driven anchoring transitions, the effect of the side chain structure of the matrix polymers on such transitions, and the microscopic mechanisms of the anchoring transitions.

In this chapter, we briefly introduce the types of LC phases, the physical properties of the nematic LC phase (NLC), the responses of the NLC to an external magnetic or electric field, and its typical microscopic textures.

1.1. Type of liquid crystals

Based on the component materials, LCs are classified as either thermotropic, or lyotropic LCs.[3] Thermotropic LC phases are obtained by controlling temperature while the lyotropic LC phases are obtained by controlling both concentration and temperature.

Thermotropic LCs are made of organic molecules (single component or multi-component) that are either rod-like, e.g., 8CB (4-n-octyl-4'-cynobiphenyl)

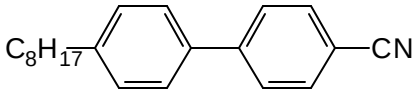

or disc-like (discotic), e.g., hexapentoxytriphenylene:

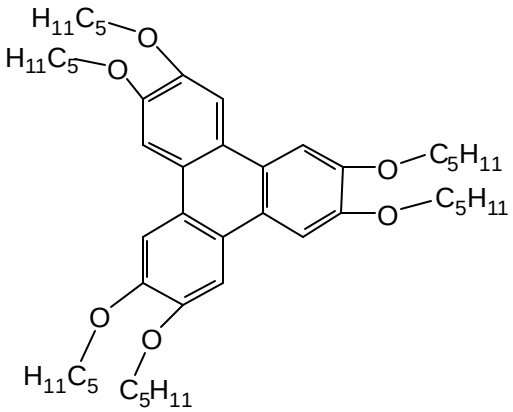

Lyotropic LCs are made of components (small molecules or a component in the nanometer or mesoscopic scale) of anisotropic shape, associated with a dispersing medium such as water, oil, alcohol, etc. Examples include the amphiphilic molecules in water, the tobacco mosaic virus in aqueous solution,[11] and rod-like nanocrystals in water.[12]

Based on ordering or packing of the components, liquid crystals are classified as (i) nematic, (ii) smectic, or (iii) columnar phases. In the nematic phase, the building blocks (thermotropic molecules or anisotropic aggregates of amphiphilic molecules) do not have long range positional order with respect to their center of mass, but display a

long range orientational order (Figure 1.1.a). The average orientation direction of the long molecular axis is represented as director **n**, a unit vector. Smectic phases are layered structures with both orientation order and positional order. There are a number of such phases, but two important cases are smectic A and smectic C phases, in which the molecules have no positional order within the plane of the layers. In the smectic A phase, the director of the layer is parallel to the layer normal (Figure 1.1.b), and the smectic C phase has a angle between the director and the layer normal (Figure 1.1.c).

If the molecules constituting these phases are chiral, they form chiral nematic phases (also called cholesteric phase) and chiral smectic phases. In a chiral nematic phase, the director rotates along a direction perpendicular to the director as shown in Figure 1.2. The distance over which the director rotates one revolution is called the pitch, although due to the symmetry between **n** and –**n** the actual spatial period is half the pitch.[13]

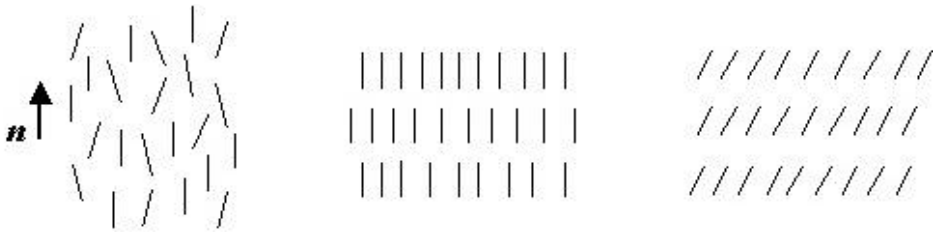

(a) **(b)** **(c)**

Figure 1.1. Schematic of LC phases (a) nematic, (b) smectic A and (c) smectic C.

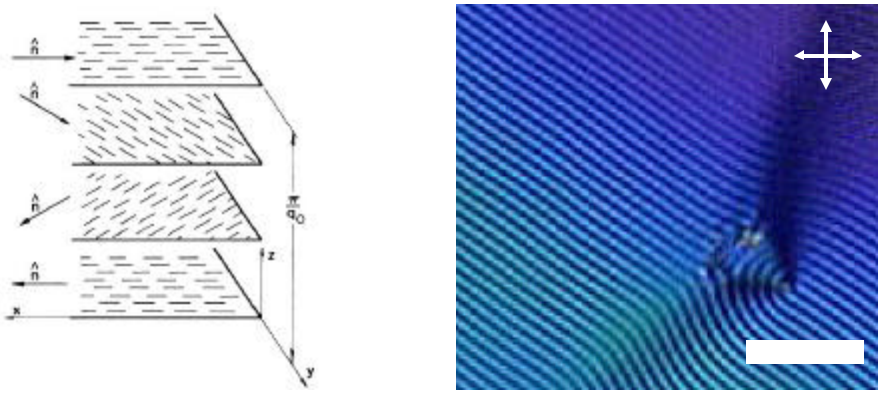

(a) **(b)**

Figure 1.2. Helical structure of chiral nematic phase (a) and finger-print texture (b). The scale bar is 10 μm. (a) is after reference 1.

1.2. Physical properties of nematic fluids

Since we focus on the nematic phases in this thesis, it is helpful to first briefly introduce the physical properties of nematic phases. Appendix A provides important physical properties of the nematic fluids used in this thesis.

1.2.1. Phase transitions

A thermotropic nematic liquid crystal usually goes through two phase transitions upon heating from a crystalline phase; the transition points are the crystalline to nematic transition temperature (T_{KN}) and the nematic to isotropic transition temperature (T_{NI}) respectively.

$$\text{Crystalline phase (K)} \xrightarrow{T_{KN}} \text{Nematic phase (N)} \xrightarrow{T_{NI}} \text{Isotropic liquid (I)}$$

1.2.2. Nematic director and director field

The nematic director **n**, a dimensionless unit vector, represents the average orientation of the long molecular axis in a small volume. In a right-handed Cartesian coordinate system (Figure 1.3), the alignment of the director at a fixed point can be described by both the tilt angle q with respect to z' axis, and azimuthal angle f (the angle between the projection of n in $x'0y'$ plane with x axis), as shown in Figure 1.3. The director can vary in space and its spatial distribution is referred to as director field **n(r)**, where **r** is the position vector from the origin.

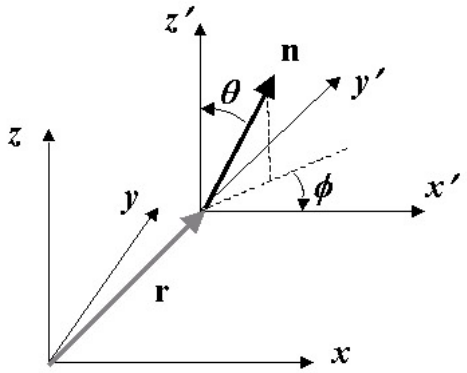

Figure 1.3. The concept of nematic director field **n (r).**

1.2.3. Orientation order parameter

The nematic molecules always fluctuate around a local average direction, the nematic director. The orientation order parameter *S* describes the average orientation over all of the molecules within the volume u_0 (a volume small compared with the size of the system but large compared with molecule size).[5] It can be given by the following equation[14]

$$S = <3\cos^2 q_{mol} - 1>/2 \qquad (1.1)$$

where q_{mol} is the angle between the long axis of a nematic molecule and the director **n**. The typical order parameter in the bulk nematic phase of small molecules is between 0.4 and 0.6. Order parameter *S* usually decreases when temperature (*T*) increases, and drops substantially when *T* is close to T_{NI}.[14] Many important physical properties of LCs are a function of *S* and are described below.

1.2.4. Anisotropy of optical, electrical and magnetic properties

The refractive indices of nematic phases are anisotropic. The optical properties of the nematics are similar to those of uniaxial crystals.[15] The largest value is called as n_e, the smallest one is called as n_o. The subscripts of n_e and n_o are used due to the fact that a

linearly polarized light passing through nematic phase usually decomposes into two rays: ordinary ray and extraordinary ray. Each ray experiences a different refractive index. The ordinary ray always experiences a constant index $n_{o,}$ while the extraordinary ray experiences a varying index, effective n_e, depending on the angle a between the vibrating direction of light (polarization plane) and the local optical axis of the nematic phase.[15] The effective n_e can be calculated using the equation:

$$n_{eff} = \frac{n_e n_o}{\sqrt{n_o \cos^2 \alpha + n_e \sin^2 \alpha}} \tag{1.2}$$

The largest difference in refractive index between e-ray and o-ray is (n_e-n_o), which is the birefringence, Δn, of the fluid phase.

When a magnetic field **H** is applied to the nematic phase, it introduces a torque $G_{m,}$ which can be given by:[16]

$$G_m = \Delta\chi(\mathbf{n} \cdot \mathbf{H})\mathbf{n} \times \mathbf{H} \tag{1.3}$$

where $\Delta\chi=\chi_{||}-\chi_{\perp,}$ the difference between two magnetic susceptibility parallel and perpendicular to the nematic director, also called the anisotropy of magnetic susceptibility, which is positive for most rod-like nematic materials.[13] When $\Delta\chi>0$, **n** aligns in the direction of the applied magnetic field. The contribution due to the applied magnetic field to the free energy density of the nematic phase is given by:[17]

$$F_m = -\frac{H^2}{2}\Delta c \cos^2 q_m \tag{1.4}$$

where H is the magnitude of the magnetic field **H**, q_m is the angle between the field direction and the nematic director.

The dielectric constants parallel and perpendicular to the average long molecular axis of bulk nematics (i.e., director) are referred to as $\varepsilon_{\parallel}$ and $\varepsilon_{\perp}$, respectively. $\varepsilon_{\parallel}$-$\varepsilon_{\perp}$ is known as dielectric anisotropy $\Delta\varepsilon$, which can be positive or negative for nematics. A nematic molecule carries a permanent dipole moment, which aligns at an angle β ($0°<\beta<90°$) to the long axis of the molecule: $\Delta\varepsilon>0$ if β is close to 0°, while $\Delta\varepsilon<0$ if β is closer to 90°. A static electric field **E** imposed on a nematic fluid has many physical effects, some of which are quite complex (e.g., convective instability under electric field).[13,18] Here we only describe the simplest one, alignment due to the dielectric anisotropy. The nematics with positive $\Delta\varepsilon$ aligns its long axis parallel to the applied electrical field direction (**E**). The nematics with negative $\Delta\varepsilon$ aligns perpendicular to **E**. Both cases exist for nematic liquid crystals, although the former case is more commonly used for LC displays. Similar to the case of the magnetic field, the contribution due to the electric field to the free energy density of the nematic phase is given by:[17]

$$F_{\mathrm{e}} = -\frac{E^2}{8\pi}\Delta\varepsilon\cos^2\theta_e \tag{1.5}$$

where E is the magnitude of the magnetic field **E**, q_{e} is the angle between the field direction and the director.

1.2.5. Elastic deformation and elastic constants of nematics

Due to the long-range orientational order of nematic phases, the molecules prefer to align parallel to each other. The continuous director field deformation gives rise to the elastic energy. There are three different basic deformations in the nematic phase: splay, twist and bend as shown in Figure 1.4.[13]

Splay **Twist** **Bend**

Figure 1.4. Splay, twist and bend deformations of nematic phases.

According to Frank,[16,19] the free energy density for the distortion of nematic phase F_d may be written in the compact form:

$$F_d = \frac{1}{2}K_{11}(\nabla \cdot n)^2 + \frac{1}{2}K_{22}(n \cdot \nabla \times n)^2 + \frac{1}{2}K_{33}(n \times \nabla \times n)^2 \quad (1.6)$$

where K_{11}, K_{22} and K_{33} are the elastic constants for splay, twist and bend respectively.

1.2.6. Defects in nematic phases

The defects in liquid crystal phases can be classified as singular defects (disclination) and non-singular defects. A disclination is a discontinuity in the alignment of the director. The discontinuity may be located at one point or a line in the nematic phase, which are referred to as a point or line disclination.[20] Dark and flexible filaments are usually observed for a thick nematic sample under a polarized light microscope. These filaments are line disclinations, which are also accountable for the origin of the name of "nematic" (thread) phase. The director fields of typical point defects are shown in Figure 1.6. The strength of disclination, S (a scalar), is defined as follows:[13] let there be a closed circuit surrounding a dislcination, give this circuit an arbitrary direction and starting from a point of origin on this circuit, trace the direction of the nematic director that the circuit meets. If the rotating direction of the director along the circuit is the same

as that of the circuit, *S* is a positive number $\Omega/2\pi$, where Ω is the angle the nematic director turned. If the rotating direction of the director is contrary to that of the circuit, S is a negative number. The strength of +1/2, -1/2, +1 and –1 are often observed for nematic phase. The defects with strength higher than 1 are rarely observed due to the high free energy they caused. It should be noted here that *S*, as the symbol of the strength of defect, is used in most literatures and happens to be the same as the symbol representing the orientation order parameter of LC phases, which is also commonly used in the literature. In this thesis, we stick to the common language. So please read the context to see what *S* represents.

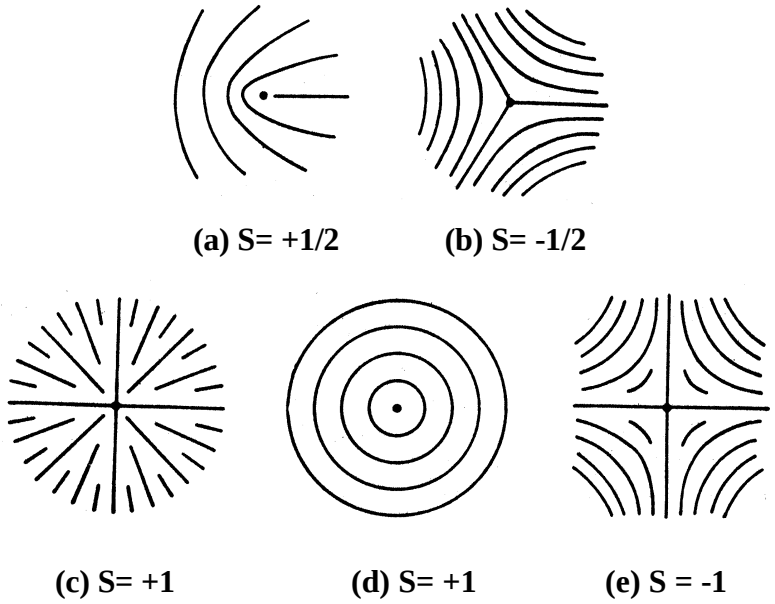

Figure 1.5. Director configurations of typical point defects with different strengths S. (after Chandrasekhar[13]).

The wall is a two-dimensional defect (point and line are 0 and 1-dimension respectively). It is usually a continuous distorted region of finite thickness within LC phase. The details of the wall defects will be described in Chapter 6.

1.2.7. Anchoring and anchoring energy

A nematic liquid crystal is aligned along a preferred direction at its boundary surface so as to minimize the surface free energy, which is referred to as anchoring.[4] The preferred alignment direction (i.e., anchoring direction) can be perpendicular (homeotropic anchoring), parallel (planar anchoring) or tilted (tilted anchoring) with respect to the surface. The anchoring direction(s) may not be a unique direction in space since the surface free energy of the nematic LC may have a certain number of minima obtained for a set of directions, $\{\boldsymbol{a}_i\}$. According to Jerome,[4] the anchoring can be classified into monostable, multistable and degenerate anchoring based on whether the number of the elements in the set $\{\boldsymbol{a}_i\}$ is one, a finite number greater than one, or infinite.

The energy needed to move the director away from the anchoring direction is referred to the anchoring energy, W_s. In the case of homeotropic anchoring (the anchoring direction is z axis), the anchoring energy is a function of tilt angle q only, referred to as polar anchoring energy, $W_p(q)$. In case of a monostable planar anchoring (e.g., the anchoring direction is along x axis in Figure 1.6), W_s is a function of both q and f; which can be decomposed into two independent parts: the energy needed to tilt LC molecules out of the plane of the surface, $W_p(q)$, and that required for in-plane twist of LC molecules, $W_a(f)$, which are referred to as polar anchoring energy and azimuthal anchoring energy respectively.

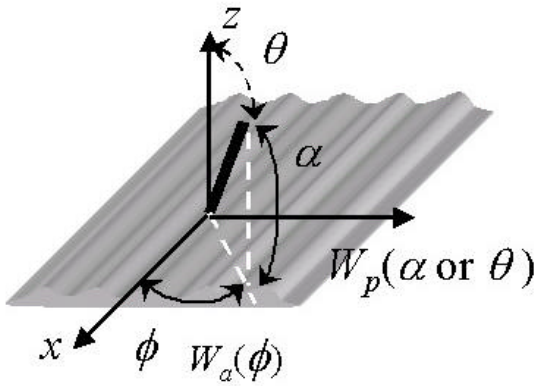

Figure 1.6. Illustration of polar anchoring energy W_p and azimuthal anchoring energy W_a of a nematics on a surface with the anchoring direction along x axis. f, q and α are azimuthal angle, tilt angle, out-of plane angle of the director (black bar at the origin), respectively (redrawn after a LC online tutorial at the website of Brown University).

The anchoring phenomenon was first discovered in 1913 by Mauguin,[21] who found that a nematic LC is aligned with its axis parallel to the surface, making an angle of 60° with the optical axis of the mica slide (using today's vocabulary, this case is called monostable planar anchoring). Following the work of Mauguin, especially since the time when liquid crystals started to be used in display devices about 30 years ago,[3,22] numerous techniques have been proposed and widely investigated to obtain alignment of liquid crystal phases on solid substrates. A detailed discussion of anchoring and surface alignment techniques will be described in Chapter 3.

1.3. Freedericksz transition and magnetic coherence length

Consider a nematic film confined between two parallel plates with homeotropic anchoring as shown in Figure 1.7a. It was first found by Freedericksz[23] that such a cell would undergo an abrupt change in the optical properties when the strength of an external magnetic field, applied normal to the director, exceeds a well-defined threshold. Freedericksz also noted that the strength of the threshold magnetic field is inversely

proportional to the cell thickness. The Freedericksz transition has important implications in LC devices and has been studied extensively.

As mentioned above, in absence of external forces, a bulk nematic fluid in contact with the surface adopts a preferential alignment determined by LC-surface interactions. Upon application of a magnetic or electrical field, the nematic switches its director to parallel to the field direction (if $\Delta\varepsilon>0$). The total free energy density of the nematic subject to a magnetic field or electrical field can be given as follows:

$$F=F_d + F_m \text{ (or } F_e) + W_s \qquad (1.7)$$

where F_d is given by equation 1.6, F_m or F_e is the free energy contributed by magnetic or electrical field (equation 1.4 or 1.5), and W_s is the anchoring energy.

In the case of the strong anchoring where the surface anchoring does not change with the external field (i.e., W_s is a constant), only ($F_d + F_m$) need to be considered to find the equilibrium state of the director field $\mathbf{n}(\mathbf{r})$ in presence of a magnetic field. The equilibrium state is given by the director configuration that minimizes the total free energy of the system with specified boundary conditions. The LC distortion in the case of Figure 1.7a can be simply described by $(\frac{d\theta'}{dz})$ (a bend deformation), where q is the angle between the director and the easy axis of the surface (i.e., z axis in Figure 1.7), equal to $\pi/2-q_m$ (i.e., q_m in equation 1.4). The free energy expression can be rewritten using the so-called one-constant approximation (i.e., $K=K_{11}=K_{22}=K_{33}$) as below.[17]

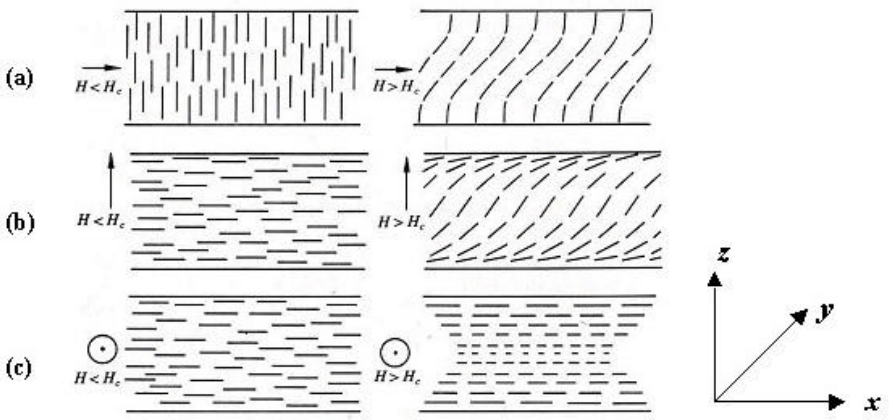

Figure 1.7. Nematic director field in a LC cell undergoing Freedericksz transition (after Chandrasekhar[13])

$$F=F_{\mathrm{d}}+F_{\mathrm{m}}=\frac{1}{2}\left\{K(\frac{d\theta'}{dz})^2-\Delta\chi\cdot H^2\sin^2\theta'\right\} \tag{1.8}$$

The optimum function $q\phi$ (z) to give the minimum of the total free energy of the system, $\int_V Fdv$, can be found by applying Euler-Lagrange equation to F:

$$\frac{\partial F}{\partial\theta'}-\frac{d}{dz}\left(\frac{\partial F}{\partial(\frac{d\theta'}{dz})}\right)=0 \tag{1.9}$$

Then we have

$$\xi_m{}^2(\frac{d^2\theta'}{dz^2})+\sin\theta'\cos\theta'=0 \tag{1.10}$$

where $\xi_m=\sqrt{\frac{K}{\Delta\chi}}\frac{1}{H}$ is referred to as the magnetic coherence length of nematics.[16] By solving differential equation (1.10) under the boundary condition, one can find that when $\xi_m > h/\pi$, the unperturbed state (i.e., state in absence of magnetic field) is stable and $q\phi=0$; only when $\xi_m < h/\pi$, a perturbed state with $q\phi(x)\neq 0$ is obtained.[17] The smallest field to produce a perturbed state H_c is given by:

$$H_c = \sqrt{\frac{K}{\Delta c}}\frac{p}{h} \tag{1.11}$$

Equation (1.11) agrees with Freedericksz's observation that the threshold field strength varies inversely with the thickness of the sample *h*. It also provides a method to determine the elastic constant of nematics. According to de Gennes,[16] the exact elastic constant measured using the geometry of Figure 1.7a is actually the bend elastic constant K_{33}. The geometries for measurement of the two other elastic constants, K_{11} and K_{22}, are shown by Figure 1.7b and Figure 1.7c. The equation (1.11) is still valid for these two cases simply by substituting K with K_{11} or K_{22} respectively.

A Freedericksz transition induced by an electric field is similar to that induced by a magnetic field. The threshold electric field, E_c, and voltage, V_c, are respectively given by:

$$E_c = \frac{p}{h}\sqrt{\frac{4Kp}{\Delta e}} \tag{1.12}$$

$$V_c = E_c \cdot h = p\sqrt{\frac{4Kp}{\Delta e}} \tag{1.13}$$

1.4. Polarized light microscopy and textures of nematic phases

The most convenient and informative technique to determine the director field of LC phases is polarized light microscopy. Using a polarized microscope, one can identify not only the azimuthal angle f of a local optical axis (i.e., f in Figure 1.3), but also the average tilt angle q through the thickness.[15,24]

The transmitted intensity of a monochromatic light through a LC sample under crossed polarizers can be described by:[24]

$$I = \sin^2(2\phi)\sin^2(\pi R/\lambda) \tag{1.14}$$

where f is the angle between the optical axis and the polarizer; λ is the wavelength and R is the optical retardation defined as effective birefringence of the sample times the thickness, having the same unit of the wavelength (e.g., nanometer). From this equation, we can see that the light is extinguished when the optical axis of LC is parallel or perpendicular (i.e., f = integral time of $\pi/2$) to the polarizer, regardless of the values of R and λ. This is the origin of the dark brushes observed in LC textures.[25] Under fixed R and λ, the transmission intensity shows a maximum when f is $\pi/4$. By rotating the sample on the microscope stage, f for a local nematic domain can be measured.

We also see from this equation that the transmission is different at different wavelengths when R is fixed. With a white light (a mixture of light with wavelength from 400 to 700nm) illumination, the intensity distribution of the transmitted light will be modified depending on the value of R, therefore showing a specific color, so-called birefringence color. The relation between birefringence color and the optical retardation is given by the Michel-Levy chart.[15] The two parameters affecting the observed color are the sample thickness h and the effective birefringence (n_{eff}-n_o). Since n_{eff} depends on n_e, n_o and tilt angle q as shown in equation 1.2, observation of birefringence color provides a way of estimating the average tilt angle q through the thickness if h, n_e and n_o are known.[26]

The defects in the textures of LC phases can also be identified by PLM. The point defect structures often look like a dark point with dark brushes radiating from it under crossed polarizers. This is observed in Schlieren textures[25,27] of nematic phase as shown in Figure 1.8. When the crossed polarizer pair is rotated, the dark brushes also rotate but

the positions of the points stay intact. The number of the brushes is related to the strength of the point defect: S=(number of the brushes)/4. For example, the point with two dark brushes has the strength of +1/2 or –1/2. The sign of the defects can be identify from comparing the rotating direction of the brushes with that of the polarizer pair: if they are along the same direction, the sign is positive; if along opposite direction, the sign is negative. The point defects of opposite sign attract each other, those of equal sign repel each other.

Both surface anchoring and sample geometry affect the director field of a nematic domain, which in turn determines the microscopic texture of that domain. We can decode the director field and surface anchoring condition from microscopic observation of nematic textures. For example:

(i) Schlieren textures mentioned above are mostly subject to continuous degenerate anchoring, either planar or tilted. [20]

(ii) A nematic slab which is confined between two parallel plates with homeotropic anchoring always looks dark under polarized light microscope as long as the light is normally incident.

(iii) A spherical droplet with homeotropic anchoring shows a cross pattern under crossed polarizers (Figure 1.9a), sometimes also with concentric color bands due to interference, while a nematic droplet with planar anchoring shows a baseball pattern or a cross under crossed polarizers (Figure 1.9b), depending on the orientation of the symmetry axis of the droplet with respect to the polarizer.

(iv) Chiral nematic molecules behave like nematic molecules within each layer that is perpendicular to the helical axis. The helical axis of chiral nematic phase aligns

perpendicular to the substrate of planar anchoring condition or parallel to the substrate of hometropic anchoring condition so that the molecules within the layers are able to satisfy the anchoring condition in each case respectively. If the latter case, the characteristic finger-print texture is observed (Figure 1.2b)

1.5. Thesis outline

This thesis focuses on the study of anchoring behavior of nematic fluids at the interfaces of LC-polymer composites. Chapter 2 describes phase separation methods to prepare polymer-dispersed liquid crystals and characterization of the resulting morphology with emphasis on cellular morphology. Chapter 3 describes the effect of the chemical structure of encapsulating polymer matrices on the anchoring and temperature-driven anchoring transitions of nematic fluids, and also discusses the measurements of anchoring strength and tilt angle as function of temperature during the anchoring transitions. Chapter 4 and Chapter 5 exploit the knowledge of control over the anchoring to fabricate new electro-optical LC devices, i.e., a LCD with reverse-switching mode (Chapter 4) and electrically switchable diffraction gratings (Chapter 5), through a one-step photopolymerization. In Chapter 6, we demonstrate an improved method to measure anchoring strength based on microscopic observations of wall defects found in the LC-polymer composite films with an anchoring transition. These wall defects are typically unstable and collapse on themselves, but are found quite stable in our systems, perhaps due to surface stabilization. A detailed study of the director configuration in three-dimensions using fluorescence confocal polarizing microscopy is described.

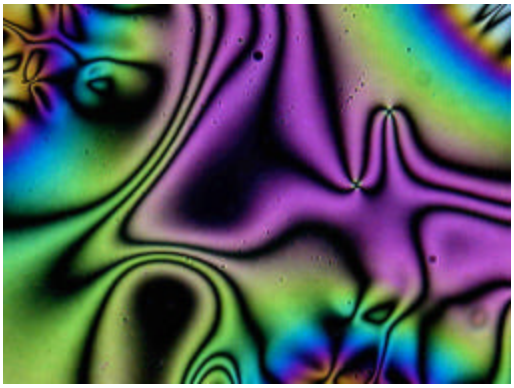

Figure 1.8. Schlieren texture of nematic phase: E7 on the surface of glycerol.

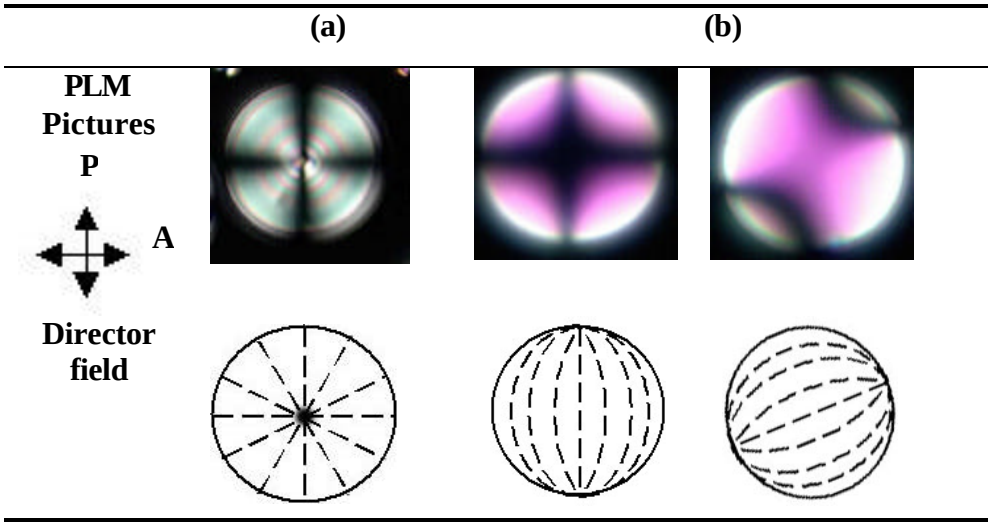

Figure 1.9. Polarized-light micrographs (under crossed polarizers) and director fields of nematic droplets: (a) radial configuration (homeotropic anchoring); and (b) bipolar configuration (planar anchoring).

REFERENCES

[1] Priestley, E.B. "Liquid crystal mesophases," in *Introduction to Liquid Crystals*; Priestley, E. B.; Wojtowicz, P. J.; Sheng, P., Eds; Plenum Press: New York, 1974.

[2] Collings, P. J. *Liquid crystals: nautres's delicate phase of matter*, 2nd ed., Princeton University Press: Princeton, 2002.

[3] Collings, P. J.; Patel, J. S. "Introduction to the science and technology of liquid crystals," in *Handbook of Liquid Crystal Research*; Collings, P. J.; Patel, J. S., Eds.; Oxford University Press: New York, 1997, ch.1.

[4] Yokoyama, H. "Interfaces and thin films," in *Handbook of Liquid Crystal Research*; Collings, P. J.; Patel, J. S., Eds.; Oxford University Press: New York, 1997, and the literatures within.

[5] Jerome, B. "Surface effects and anchoring in liquid crystals," *Rep. Prog. Phys*. **1991**, *54*, 391-451 and the literatures within.

[6] Cognard, J. "Alignment of nematic liquid crystals and their mixtures," *Mol. Cryst. Liq. Cryst*. **1982**, Suppl, 1-77 and the literatures within.

[7] Geary, J. M.; Goodby, J. M.; Kmetz, A.R.; Patel, J.S. "The mechanism of polymer alignment of liquid-crystal materials," *J. Apply. Phys.* **1987**, *62*, 4100-8.

[8] Barmentlo, M.; Vanerle, N.A.J.M.; Hollering, R.W.J.; Damen, J.P.M. **"**Surface induced liquid-crystal alignment studied by optical second-harmonic generation," *J. Apply. Phys.* **1992**, *71*, 4799-804.

[9] Drzaic, P. S. *Liquid Crystal Dispersions*; World Scientific: Singapore, 1995.

[10] *Liquid Crystals In Complex Geometry*; Crawford, G. P.; Zumer S., Eds; Taylor & Francis: London, 1996.

[11] Zasadzinski, J.A.N.; Meyer, R. B. "Molecular imaging of Tobacco Mosaic-virus lyotropic nematic phases," *Phys. Rev. Lett.* **1986**, *56*, 636-8.

[12] Lemaire, B. J.; Davidson, P.; Ferre, J.; Jamet, J. P.; Panine, P.; Dozov, I.; Jolivet, J. P. "Outstanding magnetic properties of nematic suspensions of goethite (α-FeOOH) nanorods," *Phys. Rev. Lett*. **2002**, *88*, art. No. 125507.

[13] Chandrasekhar, S. *Liquid Crystals*; Cambridge Univ. Press: Cambridge, 1977.

[14] Wojtowicz, P. J. "Introduction to the molecular theory of nematic liquid crystals," in *Introduction to Liquid Crystals*; Priestley, E. B.; Wojtowicz, P. J.; Sheng, P., Eds; Plenum Press: New York, 1974.

[15] Bloss, F. D. *Optical crystallography*; Mineralogical Society of America: Washington, D. C., 1999; ch.6. and ch. 8.

[16] de Gennes, P. G. "Static distortion in a nematic single crystal," *The Physics of Liquid Crystals*; Clarendon: Oxford, 1974, ch.3.

[17] Sheng, P. "Introduction to the elastic continuum theory of liquid crystals," in *Introduction to Liquid Crystals*; Priestley, E. B.; Wojtowicz, P. J.; Sheng, P., Eds; Plenum Press: New York, 1974.

[18] de Gennes, P. G. "Dynamic properties of nematics" *The Physics of Liquid Crystals*; Clarendon: Oxford, 1974, ch.5.

[19] Frank, F. C. "Liquid crystals: theory of liquid crystals," *Disc. Faraday Soc.* **1958**, *25*, 19-28.

[20] de Gennes, P. G. "Defects and textures in nematics," *The Physics of Liquid Crystals*; Clarendon: Oxford, 1974, ch.4.

[21] Mauguin, C. *C. R. Acad. Sci. Paris* **1913**, *156*, 1246-7.

[22] Schadt, M.; Helfrich, W.; "Voltage-dependent optical activity of a twisted nematic liquid crystal," *Appl. Phys. Lett.* **1971**, *18*, 127.

[23] Freedericksz, V.; Zolina, V. "Forces causing the orientation of an anisotropic liquid" *Tran. Faraday Soc* **1933**, *29*, 919-30.

[24] Born, M.; Wolf, E. *Principles of optics: electromagnetic theory of propagation, interference and diffraction of light*, 5th Ed., Pergamon Press: Oxford, 1975.

[25] Demus, D.; Richter, L. *Textures of Liquid Crystals*; Verlag Chemie: Weinheim, 1978. ch.4.

[26] Ryschenkow, G.; Kleman, M. "Surface defects and structural transitions in very low anchoring energy nematic thin films," *J. Chem. Phys.* **1976**, *64*, 404-12.

[27] Nehring, J.; Saupe, A. “Schlieren texture in nematic and smectic liquid crystals” *J. Chem. Soc. Faraday Trans. II* **1972**, *68*, 1-15.

CHAPTER 2

POLYMER-DISPERSED LIQUID CRYSTALS (PDLC): PREPARATION, PHASE SEPARATION AND MORPHOLOGY

2.1. Introduction

2.1.1. Liquid crystal-polymer composites, PDLC and its applications

Liquid crystal (LC)-polymer composites were first reported in 1971 as electrically controllable displays.[1] It was a cholesteric LC encapsulated in polymer matrix, which can be switched between different states. However, the extensive study in this field did not start until Fergason (1984), Doane *et al* (1986) and Drzaic (1986) reported their initial work on PDLCs.[2,3,4] Since then, LC-polymer composites have attracted many researchers' attentions and been widely studied for both fundamental science and technology. Many reviews or books have been published in this field.[5,6,7,8,9,10,11] According to Mucha,[11] most LC-polymer composites, based on their applications, can be classified into the following groups: polymer-dispersed liquid crystals; LC in colloidal templated cavities; polymer network or polymer-filled liquid crystals; LC/polymer membrane; LC/polymer/dye blends; polymer-dispersed ferroelectric liquid crystals; LC gels; LC/liquid crystalline polymer blends; phase separated composite films (PSCOF), etc. This list is by no means a complete one to cover all of LC-polymer composites reported in literature. The concentrations of polymer in various LC-polymer composites can range from only 2 wt % up to 80 wt % depending on the type of polymer and the application. Hence LC-polymer composites can also be classified into: polymer-dispersed liquid crystals where typically 50-80 wt % of low molecular LC droplets are dispersed in a *continuous* polymer matrix, and polymer-stabilized liquid crystals where only a few

percent of crosslinked polymer is distributed in a *continuous* LC phase.[9,12] Below, we shall focus on the PDLC system since it is the major system studied in this thesis.

The operating mechanism of typical PDLC electro-optical devices is illustrated in Figure 2.1. In the field-off state, the symmetry axis of liquid crystal director in the droplets are randomly oriented, which leads to the mismatch in the refractive indices of polymer matrix (n_p) and the dispersed LC phase (the average between n_e and n_o) and hence the scattering of the light. The materials therefore look milky white. In the field-on state, the liquid crystal directors are aligned along the field; for normally incident light, the liquid crystal has the ordinary refractive index n_o which is constant across the film and also matches the refractive index of the polymer. The light therefore goes through the film without scattering and the film looks transparent.

..

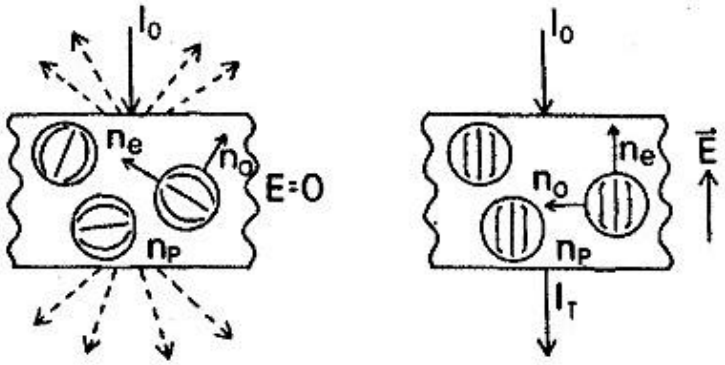

(a) Off (scattering) (b) On (transparent)

Figure 2.1. Operating mechanism of a typical PDLC electro-optical device[3]

PDLC systems are suitable for application in large area light shutters (smart windows), direct view displays, projection displays, etc. The advantages of PDLC displays over the traditional LC displays, i.e., twist nematic (TN) devices (see chapter 3), are ease of manufacturing (one-step phase separation process and no requirement for

alignment layer as used in TN devices), high brightness because no polarizer is used, and also symmetric viewing angle.[7]

The role of polymer in a PDLC system includes providing ease of film formation, mechanically supporting dispersed liquid crystal phases, providing adhesion to the substrates (i.e., polymer acting as binder), affecting the LC director configuration (hence electro-optics of devices) by confining LC phases in small cavities and also by surface anchoring.[11] Moreover, the mutual solubility between polymers and LC phase changes the properties of both phases in the final film. For example, polymer dissolved in LC phase, acting as impurity, drops the phase transition temperatures of the LC phase, on the other hand, LC dissolved in polymer matrix may change the glass transition temperature and refractive index of the polymer. In most cases, such solubility is not desired.[8]

..2.1.2. Preparation methods of PDLC films

The PDLC can be prepared by either microencapsulation process (see the early examples in references 2 and 4) or phase separation process.[7] In the former process, an emulsion of liquid crystal droplets in a polymer solution (usually aqueous) as starting materials is coated to the substrate. On removal of the solvent (e.g., water), the PDLC structure is formed. The main advantage of the emulsion method is its easy extension to large areas. Moreover, it is compatible with very different kinds of polymers including both hydrophilic (e.g., polyvinyl alcohol) and hydrophobic polymers (e.g., polyacrylates).[8] For instance, a typical hydrophobic LC doesn't dissolve in hydrophilic polymers so that it can be fully utilized in the final film. But the care needs to be taken to avoid ionic impurity with hydrophilic polymers.[8] The size of the LC droplets can be

controlled by modifying the interfacial properties, e.g., adding surfactants or adding an alcohol in water to reduce the interfacial tension.

For phase separation methods, the systems start with a one-phase mixture containing LC and polymers, prepolymers or monomers; and phase separation process is then induced by (i) cooling (referred to as thermally-induced phase separation, TIPS), (ii) by solvent evaporation (solvent-induced phase separation, SIPS), or (iii) by polymerization (polymerization-induced phase separation, PIPS) to form PDLC films.

(i) Polymers used for TIPS technique are thermoplastic polymers, like poly (methyl methacrylate), polystyrene, etc., which are miscible with LC at high temperature (the system is homogeneous and isotropic at that temperature), but not at room temperature.[4,8] During the cooling of the hot solution of polymer and LC, LC droplets are formed. This technique is easily performed and the size of the droplet can be adjusted by a careful control of cooling rate.[13]

(ii) For the solvent-induced phase separation, polymer and LC are soluble in a common solvent. For example, poly (methyl methacrylate) and E7 (a commercial low molecular weight LC mixture, EM Industries) in choloroform.[14] Phase separation occurs during evaporation of the solvent. The method is also easy to perform. But it is not easy to control the evaporation rate reproducibly, which critically determine the structure of the final composite. West reported that a SIPS process was used in conjunction with a TIPS process to make PDLC films:[15] both a thermoplastic and LC are dissolved in a common solvent. The solution is deposited on a glass substrate. The solvent is quickly removed without controlling the evaporation rate. By heating the sample until the LC dissolved back into polymer and cooled again to room temperature, the droplet size and

density can be controlled by the cooling rate. This method combines the advantages of the above two processes.

(iii) Polymerization-induced phase separation is the most studied method, especially photopolymerization-induced phase separation, since it is fast and easy to control. Polymerization can also be induced thermally, which can be either by free radical polymerization or by polycondensation mechanism. The disadvantage of thermally-induced polymerization is that the concentration of the monomers in the starting LC/monomer mixture is typically low so that induced polymerization is slow and also not easy to reach a high conversion. On the other hand, photopolymerization-induced phase separation is typically via free radical polymerization. Compared with TIPS and SIPS processes, a wide range of liquid crystal concentration can be used in this case because of the possibility of crosslinking the polymer. The rate of polymerization can be controlled by the intensity of ultraviolet (UV) light, isothermal polymerization temperature and concentration of photoinitiator.[7,16,17,18] The rule of the thumb for the size of the LC droplets formed in the final film is that the faster the polymerization is, the smaller the LC droplets are.[7]

2.1.3. Morphology of PDLCs made by photopolymerization-induced phase separation

The morphology of a PDLC film represents how the LC phase and polymer are distributed in the composite, and the size and shape of the dispersed LC droplets. The morphology is critical in determining electro-optic properties of a PDLC.[19] As mentioned above, the morphology is controlled by the kinetics of photopolymerization, which depends on UV intensity, temperature, and concentration of the photoinitiator. The amount of crosslinking (in terms of both concentration and functionality of crosslinking

agent) also controls the morphology, which determines when polymer matrix starts being solidified during a PIPS process and how much LC stays soluble in the polymer matrix of the final film.[7,18,20] A higher concentration or functionality of crosslingking agent solidifies the polymer phase at an earlier stage of the phase separation, allowing shorter time for LC droplets to grow by coalescence, and therefore smaller LC domains are obtained in the final film.

It was also found that the size of the LC droplet increase with the LC percentage in the starting mixture,[18,21,22] Amundson suggested that it is related to the temperature-composition coordinate of the starting mixture in the LC/monomer phase diagram.[22] For example, Figure 2.2 shows a series of phase diagrams for binary mixture of LC and monomer or linear polymer with increasing degree of polymerization. It is noted that the two-phase coexistence curve becomes broader with increase of the degree of polymerization, which is mainly due to the reduction in the entropy of mixing between LC and polymer.[7,23] The initial LC composition in the starting mixture is represented by solid dot in Figure 2.2. During the process of polymerization, the two-phase coexistence curve move leftward due to increasing of degree of polymerization and the phase separation starts when the coexistence curve rides over the initial temperature-composition coordinate of the system. A series of LC compositions of the starting mixture are chosen along the dotted line where the temperature is a constant (Figure 2.2): the phase separation of case B starts at a higher degree of polymerization than that of case A. It means the growth of LC droplets in case B starts later and is also slower (due to more viscous surrounding polymer matrix) than case A. As a result, the final droplet size in the case B is smaller than case A, which has a higher initial LC.

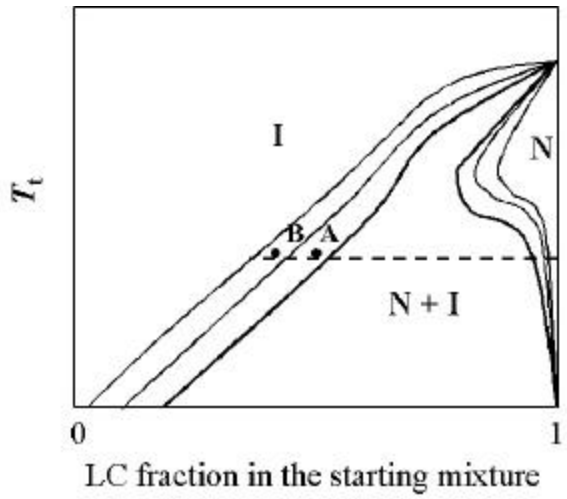

Figure 2.2. Binary phase diagram for TL205-PN393 mixtures, and speculative expansions of the two-phase region upon photopolymerization (redrawn after ref. 22).

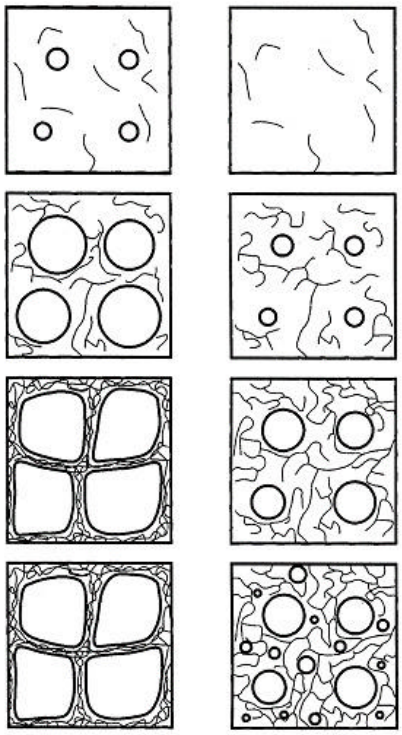

(A) (B)

Figure 2.3. Illustration of phase separation of nematic droplet from a polymerizing mixture. LC fraction in (A) is higher than in (B) (redrawn after reference 22).

Beside the "normal" droplet-like (either spherical or elliptical) morphology,[7,19] LC domains in PDLC may also have polygonal shape (i.e., cellular morphology as called in reference 24), due to a high fraction of LC and relatively slow photopolymerization process,[21,24] or irregular shape (e.g, in PDLC with reversed morphology, where LC is also a continuous phase filling up irregular space in polymer network[25]. Both the LC and polymer phases are continuous in this case).

Another interesting aspect of the morphology PDLC formed by photopolymerization-induced separation is that the minority polymer phase (even if polymer fraction is less than 20%[18,24]) often forms the continuous network of the composite. This is contrast to the common sense view of conventional liquid-liquid or liquid-solid phase separations where a minority phase forms only isolated phase.[26,27] According to Tanaka,[27] the viscoelasticity of polymer-rich phase plays an important role in two-phase pattern development during phase separation: more viscoelastic polymer-rich phase tends to form a continuous network to support stress induced by dynamic asymmetry between polymer molecules and LC molecules. This transient two-phase structure can be then "frozen" by crosslinking of polymer phase. In fact, a spongelike or cell-like morphology is universal morphology for the phase separation of any mixture in which asymmetric elasticity plays a role. For example, the physics behind the formation process of plastic foam (gas bubbles dispersed in polymer matrix) is similar to that of PIPS process making PDLC films.[27]

2.1.4. Techniques to characterize the morphology of PDLCs

Among the techniques to characterize the morphology of PDLC are optical microscopy (OM), laser scanning confocal microscopy (LSCM) and scanning electronic

microscopy (SEM).[4,22] Resolution of OM and LSCM techniques are limited by the wavelength of light, usually 0.2~0.3μm in lateral direction (i.e., perpendicular to the optic axis of the microscope) while that of SEM could be as high as several nanometers.[28] But SEM can't be applied in-situ to the sample, requires special preparation of the sample for imaging and therefore may be destructive to the original morphology. Compared with OM, which yields only the two-dimensional projection of the morphology, LSCM has ability to provide three-dimensional morphology information by optically sectioning the sample.[29] As long as the size of dispersed LC droplets in PDLC is greater than 1 μm, LSCM is well suited for obtaining the morphology in three-dimensions.

The principle of confocal microscopy is illustrated in Figure 2.4. As shown in the figure, the pinhole before the laser creates a point light source, which forms a point image (i.e., focus point of the light) in the sample so that the fluorescence is excited from a small volume around that focus point. The fluorescence light traveling backward is collected by a detector with another pinhole before it. The distance between the second pinhole and the focus point is identical to that between the first pinhole (the one before the laser) and the focus point. In other words, the two pinholes are in confocal positions. Therefore, only fluorescence light emitted from the focus point can pass the second pinhole but those from out-of focus areas is cut off. The fluorescence intensity data can be collected through the sample by scanning the beam or the sample position in three dimensions. The overall image is established by computer.[29]

For confocal imaging of the morphology of PDLCs, a small amount of fluorescent dye is added to the pre-polymerization mixture in order to generate better imaging contrast between polymer and liquid crystalline phases in the final film.[22,30] Besides

providing information on 3D morphology, LSCM techniques has also been used to image the director configuration within LC domains since LC phase may align the long axis of fluorescent molecules of anisotropic shape parallel to the director.[31,32] This topic will be addressed in more detail in Introduction of Chapter 6 of this thesis.

In results and discussion of this chapter, we will focus on characterization of the cellular morphology of PDLCs by OM and LSCM techniques. This specific morphology is mostly used for identifying anchoring of LC at polymer surfaces in this thesis.

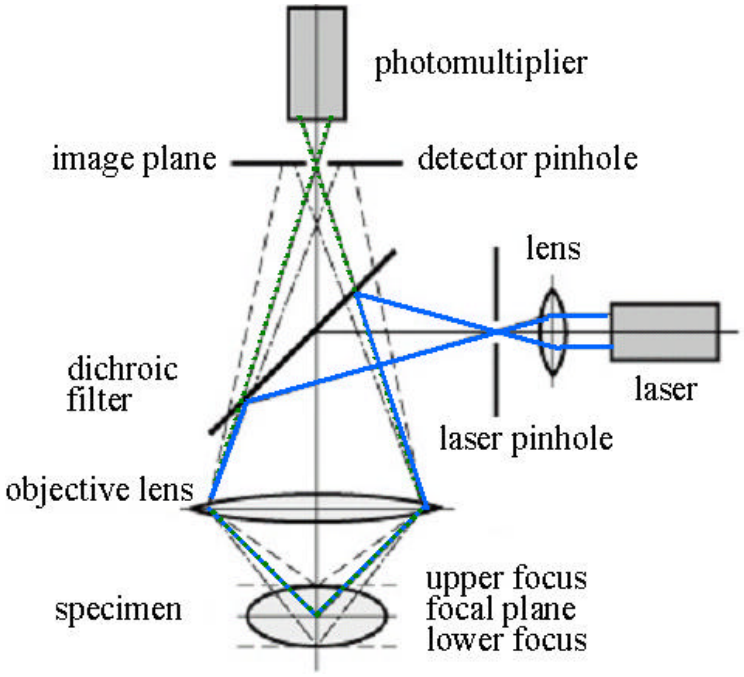

Figure 2.4. Working principle of confocal microscope.

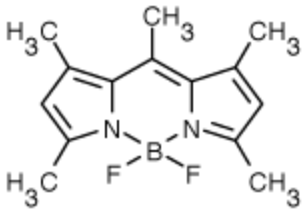

Spectral Information:

$\lambda_{max,abs}$ = 493 nm (in methanol)

$\lambda_{max,fl}$ = 519 nm (in methanol)

ε_{493} = 7.9x104 liter mol^{-1} cm^{-1}

Φ_f = 0.99 (in methanol)

Figure 2.5. Structure and spectral data of pyrromethene 546 (1,3,5,7,8-pentamethylpyrromethene-difluoroborate complex): where $\lambda_{max,abs}$, $\lambda_{max,fl}$, ε_{493} and Φ_f are the absorption maximum, fluorescence emission maximum, molar extinction coefficient and quantum yield, respectively. Pyrromethene 546 is the same product as Bodipy 493/503 supplied by Molecular Probes Inc. The spectra data here is obtained from the manufacturers' websites: www.exciton.com and www.molecularprobes.com.

2.2. Experimental

Materials. The nematic fluid that was used in the studies reported in this thesis is TL205 (EM Industries), a mixture composed of chlorinated bi- and terphenyls with aliphatic tails of 2 to 5 carbons in the 4-position of the phenyl ring. This fluid displays a nematic phase over a wide temperature range from –20 °C to 87 °C. All the monofunctional acrylates and 1,1,1-trimethylol propane triacrylate (crosslinking agent) used in this study were obtained from Scientific Polymer Products Inc. All the monomers were used without further purification. The TL205, monofunctional acrylate monomers and the triacrylate crosslinker were mixed in an 80:18:2 weight ratio.[24] Darocur 1173 (Ciba Chemicals) was used as a photo-initiator. The mixture was placed by capillary action into a glass cell with thickness of 5, 10 or 15 μm controlled by the glass microbeads with a narrow diameter distribution of ±5% (Duke Scientific).

Photopolymerization-induced phase separation. The UV source we used is a Hg-arc lamp from Oriel (Model 68907) with adjustable output power up to 200 Watt and a narrow band filter of 360±5 nm. To make PDLC films with cellular morphology, a slow photopolymerization process was used. The photopolymerization was carried out in two stages: the pre-polymerization mixture in the glass cell was first exposed to UV irradiation of 360 nm with low intensity (e.g., 50 ~ 300 $\mu W/cm^2$) until the cellular morphology was formed.[24] The sample was then fully cured at much higher UV intensity (16 mW/cm^2). Any unreacted monomer left behind will be an impurity for the nematic phase and hence will lower the T_{NI}. Thus monitoring the T_{NI} on completion of photopolymerization serves as an indicator of conversion of the monomer to a polymer. The T_{NI} of 84 °C corresponds to about 1% of the unreacted monomer existing in the

finished film.[22] Moreover, initial UV illuminations with intensity of greater than 300 $\mu W/cm^2$ were also tested to see its effect on the morphology.

Optical microscopic imaging and confocal imaging. The resulting morphology was visualized by a polarized light microscope (Leica DMRX) and also by a laser scanning confocal microscope (Leica-TCS SP). The excitation and fluorescence light paths in the confocal microscope can be illustrated by Figure 2.4. For confocal imaging, about $2\sim3\cdot10^{-5}$ weight fraction of a fluorescent dye pyrromethene 546 (see structure and spectral data in Figure 2.5) was added to pre-polymerization mixtures to provide imaging contrast. The dye was excited at 488 nm by an Ar^+ laser, and the fluorescence was collected from 515 to 580 nm. Either a 40x oil immersion objective (NA=1.25) or a 100x oil immersion objective (NA=1.4) was used for confocal imaging. The refractive index of immersion oil is 1.518 to match the refractive index of the polymer. Excitation laser power reaching the objective varies from 100-200 $\mu W/cm^2$, measured by a powermeter (Newport model 1830-C) with removal of the objective from the light path. For optical sectioning along *z* axis (the optical axis of the microscope), the minimum step distance between 2 consecutive *xy* sections is chosen to be 0.203 μm.

The power of excitation laser can also be monitored by a built-in detector in the confocal system and read directly from the software (the intensity unit is arbitrary). This laser power reading is compared with the measurement using the powermeter. A good linear relationship between the two measurements is obtained as shown in Figure 2.6a.

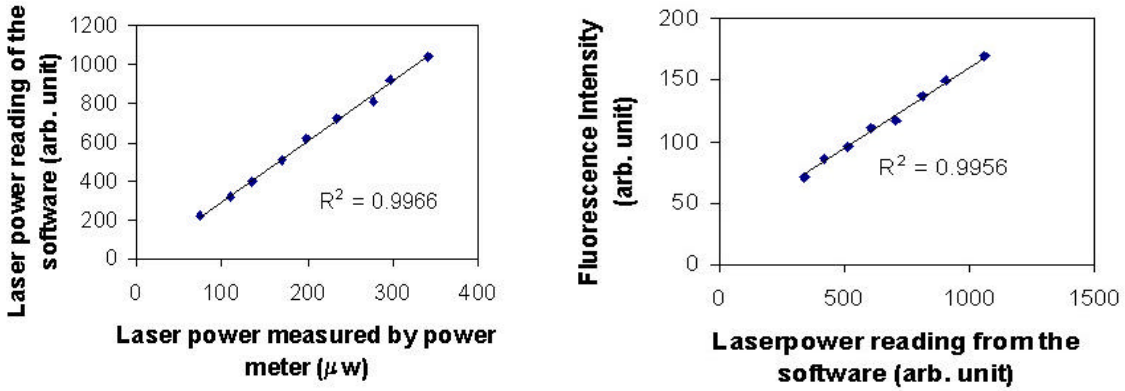

(a) **(b)**

Figure 2.6. Calibration of laser power reading of the confocal microscope and confirmation of linear fluorescence.

Under the experimental conditions we used, it was found that the fluorescence intensity is a linear function of the excitation intensity (Figure 2.6b). Thus, there was no fluorescence saturation in our experiments (note that fluorescence saturation occurs when the rate of the excitation is faster than that of the emission, appearing as a non-linear dependence of detected fluorescence signal versus the intensity of excitation).[33,34] In the regime of a linear fluorescence, the fluorescence intensity is also proportional to the concentration of the fluorophores,[35] which makes possible a good image contrast between the LC phase and the polymer phase in the PDLC films if the dye is preferentially dissolved into one of the two phases. Photobleaching of the dye by the laser excitation may happen in the confocal imaging.[36] But as long as we use a low power excitation and also avoid to scan the same sample region for too long a time, this problem is not serious.

Absorptions of the excitation light and the emission light by the dye molecules (the latter is due to overlap of the absorption spectrum and the fluorescence spectrum of pyrromethene 546) also affect the confocal imaging. Therefore, in the acquired images, the side of the film that is away from the incoming excitation (i.e., the bottom side of the

film in our case) usually appears darker than the other. To clearly view the features on the bottom side, one can flip over a film for confocal imaging.

2.3. Results and discussions

2.3.1. Characterization of cellular morphology

First, we optimized the photopolymerization conditions to obtain a cellular morphology of PDLCs. It was found that the size of the LC domains in the formed PDLC film decreases sensitively with increasing the UV intensity and concentration of photo-initiator, but increases with increasing the LC fraction in pre-polymerization mixtures. To form a cellular morphology, both low UV intensity and low concentration of photo-initiator are required. But the concentration of the photo-initiator can't be too low to overcome the inhibitor existing in the commercial acrylate monomers we used (these monomer were used directly without purification). The optimum concentration of the photoinitiator to form a cellular morphology under UV irradiation of 50~100 $\mu W/cm^2$ was found to be ca. 0.5 wt % of the total monomer.

As shown in Figure 2.7, the cellular morphology formed by a slow polymerization-induced phase separation process contains only one layer of close-packed polygonal LC cells between two glass substrates. Each LC cell is completely enclosed by polymeric matrix that extends through the film, with thin vertical polymer walls from the top substrate to the bottom. There are three different cases of cellular morphology in Figure 2.7.

Case (a): The UV irradiation was from the top side of the film during the photopolymerization. The film with thickness of 15 μm shows an asymmetry along

vertical direction (Figure 2.7a), i.e., the top polymer layer (~2 μm thick) is much thicker than the bottom layer. The bottom layer is hard to be observed even if the film was flipped over so that the thin "bottom" layer is close to the laser excitation during confocal imaging in order to avoid the effect of the light absorption on imaging this layer. The reasons for such an asymmetry is two fold:[37] (i) the density difference between the monomer (~0.9 g/cm^3) and LC (~1.2 g/cm^3) causes the monomer enriched at the top during PIPS because of gravity, and (ii) the absorption of the UV light by the LC film might create a gradient in UV intensity: the side of the film which was close to UV light source (i.e., the top side) has higher UV intensity than the other side (i.e., bottom side) so the polymerization occurs faster at the top side. The monomer hence diffuses from the bottom side to the top side, also leading to enriched polymer at the top side of the film.

To confirm the above rationale, photopolymerization was also carried out by irradiating the UV from the bottom, as shown in case (b) of Figure 2.7. The effect due to the density difference is compensated by the effect due to the gradient of UV intensity caused by absorption. The polymer layer at the two sides of the final film has approximately equal thickness. In case (c), the thickness of the LC cell is reduced to 5 μm with UV irradiation from the top. In this case, the top and bottom polymer layers are formed and appear to have the similar thickness.

The 3D reconstruction of the cellular morphology of case (a) is shown in Figure 2.8.

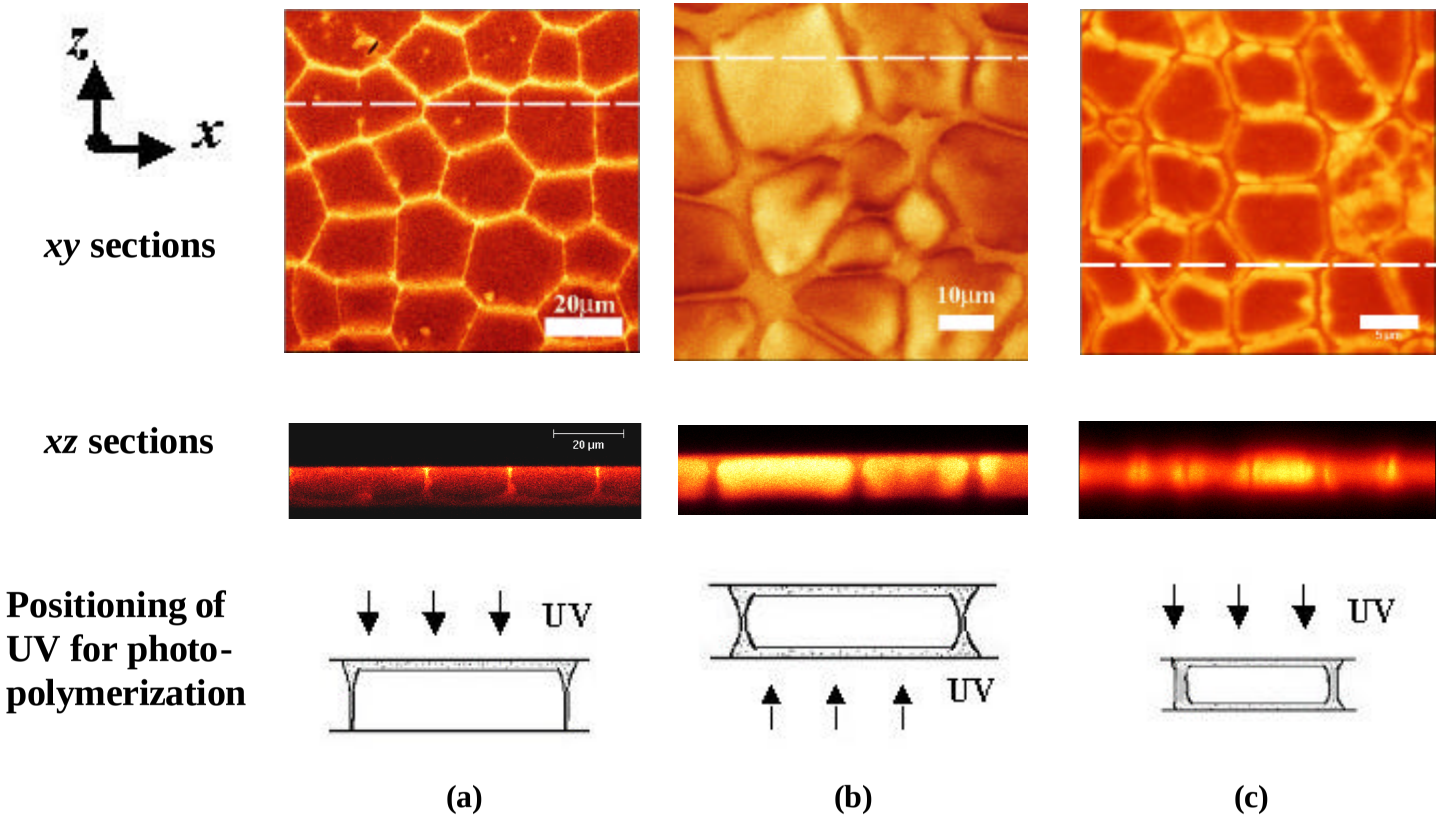

Figure 2.7. Confocal microscopic images: *xy* and *xz* sections of three PDLC films, (a) (b) and (c). The *xz* sections are taken along the dashed lines in the corresponding *xy* sections. Temperature is 25 °C. The scale bars in (a) (b) and (c) are 20, 10 and 5 µm respectively.

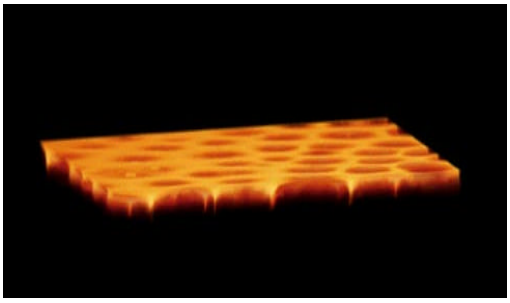

Figure 2.8. A 3D reconstruction of confocal imaging of cellular morphology. The long edge of the above film is 125 μm.

Figure 2.9. Polarized microscopic images of a polymer wall under (crossed polarizers as given by dark arrows). The sample is TL205/Poly(1-methylheptyl acrylate) system. The images were taken at 25 °C. The scale bar is 10 μm.

2.3.2. Isotropic or anisotropic polymer matrix ?

It is verified by polarized-light microscopy that polymer matrixes in PDLC films we made are isotropic. The polymer wall in Figure 2.9 appears dark under crossed polarizers and remains dark under rotation of the sample, indicating that the polymer wall is optically isotropic. No birefringence could be observed for polymer walls. On heating the film above T_{NI}, the film is completely dark under crossed polarizers, which also suggests that polymer walls are isotropic. Since the glass transition temperature of the

polymer matrix is far below room temperature,[38] should there have been stress-induced anisotropy in the process of phase separation, it would have relaxed

2.3.3. Shape of polymer wall boundary and polymer filaments

The surfaces of polymer wall boundary in many PDLC films appear "flat" (i.e., the wall projection in *xy* plane are linear) at room temperature as shown in Figure 2.7, Figure 2.9 and Figure 2.10a. But when a cellular PDLC film is heated close to or above T_{NI} of LC phase, the projections of the wall look very different from those at room temperature under an optical microscope, they have rough boundary (Figure 2.10b and Figure 2.11). It is very interesting to note that the boundary shape of polymer walls in Figure 2.10b is approximately sinusoidal, with the wavelength of about 10~15 μm. For many other PDLC films with larger LC cell than that in Figure 2.10 (e.g., the film in Figure 2.11), such regularly curved shape of polymer walls can also be found although it is not so dominant in the morphology. It is not clear to us now why such a regularly curved pattern forms at the polymer walls of a cellular PDLC. It is perhaps a pattern due to non-equilibrium process of phase separation, and frozen by crosslinking.[27]

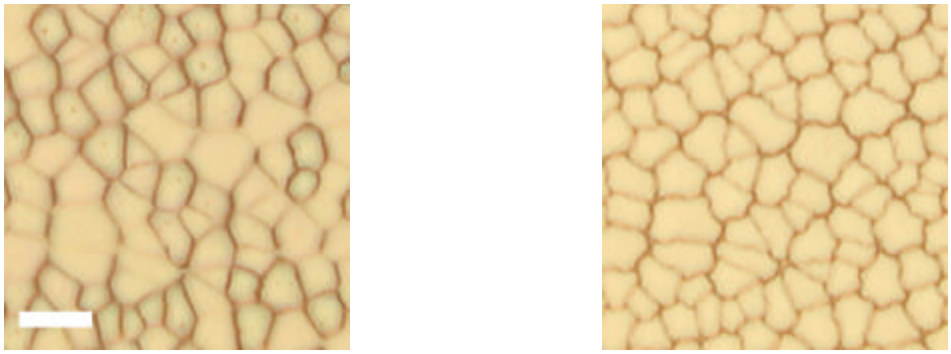

(a) 35 °C (b) 88 °C

Figure 2.10. Bright field microscopic pictures of a cellular PDLC film (without using analyzer). (a) and (b) are taken at temperatures below and above nematic-isotropic transition temperature respectively. The scale bar is 15 μm.

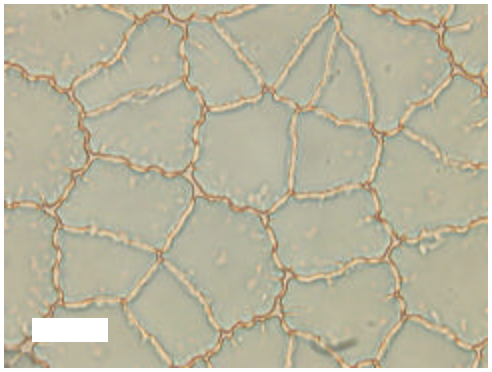

Figure 2.11. A bright field microscopic image of a typical cellular PDLC film. The image was taken at 90 °C (above T_{NI}). The scale bar is 20 μm.

The different appearance of the same polymer boundary at different temperature is reversible and reproducible (i.e., if the film is cooled back to room temperature, the projection of the walls looks linear again). We suggest that it is due to the existence of a thin layer of uncrosslinked polymer at interfacial region between solid-like polymer network and bulk LC phase when temperature is far below T_{NI} of LC. This is confirmed by observing the nematic-isotropic transition of the confined LC domains: T_{NI} of the nematic regions near polymer boundary is always 0.5~1°C lower than that of bulk nematic regions. That is because of that the uncrosslinked polymer molecules enriched at the interface acts as impurity to lower T_{NI} of the interfacial region with respect to bulk LC region when the temperature is increased close to T_{NI} of the bulk (it is not due to unreacted monomer since a small amount of monomer is able to dissolve into the LC phase and thereby uniformly distributed). At room temperature, these polymer molecules are not miscible with LC phase so that they stay at the interface of LC/polymer network. They are uncrosslinked and fluid-like because the glass transition temperature of poly(alkyl acrylates) we used is as low as -60°C.[38] The real LC/polymer interface at room temperature is actually between this fluid-like polymer thin layer and bulk LC and the shape of the interface is flat in order to reduce interfacial energy. The curved boundary of solid-like polymer network is hidden optically at room temperature due to no difference in the refractive index of the polymer network and the polymer thin layer. But when the film is heated close to T_{NI} of the bulk nematic region (84°C), the uncrosslinked polymer thin layer dissolve into bulk LC phase to disappear (so it lowers T_{NI} of the interfacial region). The surface curvature of polymer network is then observed by optical microscopy due to the refractive index contrast between polymer network and LC phase.

The above observation provides us a picture of interfacial region between polymer network and bulk nematic phase in the PDLC system we studied. The existence of a fluid-like polymer thin layer at the interface plays an important role in determining the anchoring behavior of the confined bulk nematic phase.

It should be noted that a lot of polymer filaments are also observed attached to polymer walls or the substrates at the central regions of LC cells. These features are more prevalent in larger LC cells. They are crosslinked polymer since they don't dissolve into isotropic liquid crystal domains even if the temperature is far above T_{NI}. As suggested by Amundson,[22] these filaments form when the less viscous LC displaces the more viscous polymer phase during the phase separation and drop growth; and these filaments are sufficiently solid and left behind by the advancing LC front.

2.4. Conclusions

(1) A slow photopolymerization process is successfully used to prepare the PDLC film with cellular morphology, which is characterized by both polarized light microscopy and laser scanning confocal microscopy.

(2) There is no noticeable anisotropy in the polymer matrix of PDLC films we studied.

(3) The crosslinked part of polymer walls in a cellular PDLC was found to be very rough surface and show a regularly curved pattern in many cases.

(4) At temperatures far below T_{NI} of the bulk nematic phase of a PDLC film, a thin layer of fluid-like polymer at interfacial region acts the real polymer boundary to interact with the nematic phase in contact with it. It flattens out the rough solid polymer boundary.

REFERENCES

[1] Churchill, D.; Cartmell, J.V. "Display device containing minute droplets of cholesteric liquid crystals in a substantially continuous polymeric matrix," US patent 3,600,060; **1971**.

[2] Fergason, J.L. "Encapsulated liquid crystals for displays,," US patent 4,435,047; **1984**.

[3] Doane, J.W.; Vaz, N.A.; Wu, B.G.; Zumer, S. "Field controlled light scattering from nematic microdroplets,," *Appl Phys Lett* **1986**, *48*, 269–71.

[4] Drzaic, P.S. "Polymer dispersed nematic liquid crystal for large area displays and light valves,," *J. Appl. Phys.* **1986**, *60*, 2142-8.

[5] Doane, J. W. in *Liquid Crystals: Applications and Uses* Vol. 3; Bahadur B., Ed.; World Scientific: Singapore, 1992; p.361.

[6] *Liquid Crystals In Complex Geometry*; Crawford, G. P.; Zumer S., Eds; Taylor & Francis: London, 1996.

[7] Drzaic, P. S. *Liquid Crystal Dispersions*; World Scientific: Singapore, 1995.

[8] Bouteiller, L.; LeBarny, P. "Polymer-dispersed liquid crystals: Preparation, operation and application," *Liq. Cryst.* **1996**, *21*, 157-74 and literatures within.

[9] Crawford, G. P.; Doane, J. W.; Zumer, S. in *Handbook of Liquid Crystal Research*; Collings, P. J.; Patel, J. S., Eds.; Oxford University Press: New York, 1997, p.347.

[10] Higgins, D.A. "Probing the mesoscopic chemical and physical properties of polymer-dispersed liquid crystals," *Adv. Mat.* **2000**, *12*, 251-64.

[11] Mucha, M. "Polymer as an important component of blends and composites with liquid crystals," *Prog. Polym. Sci.* **2003**, *28*, 837-73 and literatures within.

[12] Rajaram, C.V.; Hudson, S. D., Chien, L.C. "Morphology of polymer-stabilized liquid crystals," *Chem. Mater.* **1995**, *7*, 2300-2308.

[13] Nomura, H.; Suzuki, S. Atarashi, Y. "Electrooptical properties of polymer films containing nematic liquid crystal microdroplets," *Jpn. J. Appl. Phys.* **1990**, *29*, 522-8.

[14] Jain, S.C.; Rout, D. K.; Chandra, S. "Electrooptic studies on polymer dispersed liquid crystal films prepared by solvent-induced phase separation technique," *Mol. Cryst. Liq. Cryst*. 1990, *188*, 251-9.

[15] West, J.L. "Phase separation of liquid crystals in polymers," *Mol. Cryst. Liq. Cryst.* **1988**, *157*, 427-41.

[16] Rajaram, C.V.; Hudson, S. D., Chien, L.C. "Effect of polymerization temperature on the morphology and electrooptic properties of polymer-stabilized liquid crystals," *Chem. Mater*. **1996**, *8*, 2451-60.

[17] Roussel, F.; Buisine, J.M.; Maschke, U.; Coqueret, X. "Photopolymerization kinetics and phase behavior of acrylate based polymer dispersed liquid crystals," *Liq Cryst* **1998**, **24**, 555–61.

[18] Serbutoviez, C.; Kloosterboer, J.G.; Boots, M.J.; Touwslager, F.J. "Polymerization-induced phase separation .2. Morphology of polymer-dispersed liquid crystal thin films," *Macromolecules* **1996,** *29*, 7690-8.

[19] Amundson, K. "Electro-optic properties of a polymer-dispersed liquid-crystal film: Temperature dependence and phase behavior," *Phys. Rev. E.* **1996**, *53*, 2412-22.

[20] Pogue, R.T.; Natarajan, L.V.; Siwecki, S.A.; Todiglia, V.P.; Sutherland, R.L.; Bunning, T.J. "Monomer functionality effects in the anisotropic phase separation of liquid crystals," *Polymer* **1999**, *41*, 733–41.

[21] Nwabunma, D.; Chiu, H. W.; Kyu, T. "Morphology development and dynamics of photopolymerization-induced phase separation in mixtures of a nematic liquid crystal and photocuratives," *Macromolecules* **2000,** *33*, 1416-24.

[22] Amundson, K.; Van Blaaderen, A.; Wiltzius, P. "Morphology and electro-optic properties of polymer-dispersed liquid-crystal films," *Phys. Rev. E.* **1997**, *55*, 1646-54.

[23] Flory, P.J. *Principles of polymer chemistry*; Cornell University Press: Ithaca, 1953.

[24] Amundson, K. R.; Srinivasarao, M. "Liquid-crystal-anchoring transitions at surfaces created by polymerization-induced phase separation," *Phys. Rev. E.* **1998**, *58*, R1211-4.

[25] Cheng, S.X.; Bai, R.K.; Zou, Y.F.; Pan, C.Y. "Electro-optical properties of polymer dispersed liquid crystal materials," *J. Appl. Phys.* **1996**, *80*, 1991-5.

[26] Gunton, J.D.; San Miguel, M.; Sahni, P. *Phase Transitions and Critical Phenomena*; vol 8, Domb, C; Lebowitz, J. L., Eds, Academic Press: New York, 1983.

[27] Tanaka, H. "Viscoelastic phase separation," *J. Phys.: Condens. Matter* **2000**, *12*, R207-64.

[28] Kalman, E.; Nagy P.; Csanady, A.; Papp, K.; Csorbai, H.K.; Hunyadi, C.; Telegdi, J. "AFM and SEM: competing or complementary techniques?," *Mater. Sci. Forum*, 2003, 414-4, 241-51.

[29] Wilson, T. in *Confocal Microscopy*; Wilson, T., Eds; Academic Press: London, 1990.

[30] Carter, S.A.; LeGrange, J.D.; White. W.; Boo, J.; Wiltzius, P. "Dependence of the morphology of polymer dispersed liquid crystals on the UV polymerization process," *J. Appl. Phys.* **1997**, *81*, 5992-9.

[31] Smalyukh, I. I.; Shiyanovskii, S.V.; Lavrentovich, O. D. "Three-dimensional imaging of orientational order by fluorescence confocal polarizing microscopy," *Chem. Phys. Lett.* **2001**, *336*, 88-96.

[32] Voloschenko, D.; Lavrentovich, O. D. "Optical vortices generated by dislocations in a cholesteric liquid crystal," *Opt. Lett.* **2000**, *25*, 317-9.

[33] Patsayeva, S.; Yuzhakov, V.; Varlamov V. "Laser induced fluorescence saturation for binary mixtures of organic luminophores", *Proc. SPIE* **1999**, *3732*, 147-56.

[34] Hellen, E.H.; Burghardt, T.P. "Saturation effects in polarized fluorescence photobleaching recovery and steady-state fluorescence polarization," *Biophys. J.* **1994**, *66*, 891-897.

[35] Rost, F.W.D. *Fluorescence microscopy Vol 1* Cambridge University Press: Cambridge, 1992; p177.

[36] Song, Y. "Study of dye diffusion in fibers by laser scanning confocal microscopy," *Ph.D. Thesis*; North Carolina State University, 1999.

[37] Vorflusev, V.; Kumar, S. "Phase-separated composite films for liquid crystal displays," *Science* **1999**, *283*, 1903-5.

[38] Andrews, R.J.; Grulke, E.A. in *Polymer Handbook*; Brandrub, J., Immergut, E.H. Eds.; John Wiley and Sons: New York, 1999; VI-200.

CHAPTER 3

STUDY OF ANCHORING BEHAVIOR AND ANCHORING TRANSITIONS AT POLYACRYLATES SURFACES

3.1. Introduction

Preferential alignment of liquid crystals (LC) at interfaces is referred to as anchoring. In absence of external fields (electrical, magnetic, shear flow, etc), the anchoring determines the bulk LC alignment through the elasticity of LC phases. Nematic molecules in contact with a surface may have this preferential alignment parallel, perpendicular, or tilted at an intermediate angle to the surface. They are referred to as planar anchoring (P), homeotropic anchoring (H) and tilted anchoring respectively. Anchoring plays an important role in determining the bulk alignment of liquid crystalline phases, and thereby the electro-optical properties of LC-based devices.

Rubbing polymer layers is the dominant method being used in modern LC displays (LCD) to provide unidirectional anchoring with a slight or high pretilt angle with respect to the substrates. However, it is well known that mechanical rubbing has disadvantages such as generation of static charges and dust particles, and also cause damages to the underlying thin film transistors, giving rise to low yield and high cost of this process. Many other techniques have been developed to substitute this technique. They will be briefly summarized in the following section.

3.1.1. Anchoring of nematics and surface alignment techniques

The early study of anchoring effect before the invention of liquid crystal displays include studying anchoring of nematics on crystal surfaces, the influence of unidirectional rubbing of glass substrates on LC alignment and homeotropic anchoring on

surfactant-coated surfaces.[1,2,3,4] These studies, although not too many, constitute the foundation of many of the alignment techniques in use today. Since the end of 1960s, the importance of having a precise and reliable control of LC alignment on the surfaces of LCD has accelerated studies of anchoring phenomena and resulted in many new alignment techniques; at the same time, a general interest in the physics of surface and interfacial phenomena has also risen.[1,5]

3.1.1.1. Rubbing polymer layers, twisted nematic devices and pretilt

Rubbing polyimide layers coated on glass substrates provides a strong and unidirectional planar anchoring with a pretilt angle, which is required by twisted nematic (TN) devices, a traditional mode of LCD. This method is superior to the weak alignment that is produced by rubbing uncoated surfaces, studied long before.[6] The working principle of a TN device and pretilt angle is briefly described below.

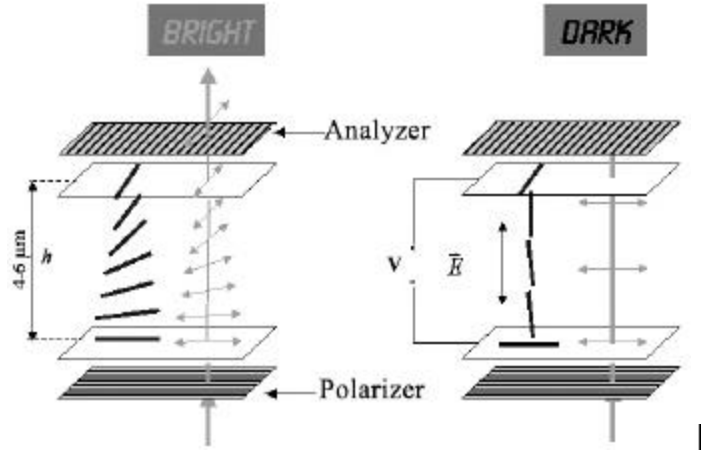

Figure 3.1. Schematics of a twisted nematic device (redrawn after Dr. Rainer Macdonald's website at http://moebius.physik.tu-berlin.de/lc/lcd.html).

A TN device is illustrated in Figure 3.1. A nematic LC is confined between two rubbed polymer layers (coated on transparent electrodes) with their rubbing directions

perpendicular to each other. The confined nematics adopts a 90° twisting deformation from the bottom to top substrate. When there is no electric field, due to the wave-guiding effect if the Mauguin limit (equation 3.1) is satisfied, the polarization of a linearly polarized light traveling through the LC cell follows the local twist of nematic director. Thus the light is able to pass the crossed analyzer at the other side of the TN device and the cell looks bright.

$$\Delta n \cdot h \geq \lambda / 2 \tag{3.1}$$

here Δn is the birefringence of nematics, h the thickness of the cell and λ the wavelength of the light.

When an electric field of sufficient strength is applied across the thickness of the LC cell, the director of the bulk nematics (with positive dielectric anisotropy) aligns parallel to the field direction. In this case, the polarization of a normally incident light is not affected by the nematics in the LC cell. The light is thus extinguished by the analyzer and the cell appears dark.

Pretilt angle is the angle adopted by the nematic director near the alignment layer with respect to the surface. A non-zero pretilt angle (not shown in Figure 3.1) is necessary for TN devices, which ensures that the reorientations of nematic molecules throughout the LC cell are along the same direction when the electric field is off. Otherwise the wall defects due to opposite twist of neighboring domains may occur and deteriorate the display quality. A high pretilt angle also helps to reduce the switching voltage in TN devices.

3.1.1.2. Photo-alignment techniques

Photo-alignment as an alternate to mechanical rubbing alignment has been a subject of extensive research since the demonstration of the effect of reversible *cis-trans*-isomerization (*E/Z*) of surface-attached azobenzene unit on control of the alignment of nematics.[7,8] Two main types of materials developed for LC alignment using a polarized UV illumination are as follows:[7,9]

One of them is for reversible process based on either *E/Z* photoisomerization of azobenzene, stilbene, or cinnamate derivatives or electrocyclic reaction of spiropyran derivatives. These structures can be incorporated into the aligning substrates of LC cells in various ways via: dye doped polymer layers,[10] surface tethered,[11,12] or the side chain of polymers.[13] The azo dye can also be directly added into bulk LC phase to serve as photo-aligning agent.[14] In most cases of this type of process, an in-plane alignment (i.e., parallel to the surface) of nematic molecules that is perpendicular to the polarization of linearly polarized illumination is obtained after UV exposure. The substrates containing the above photoactive structures is also called "command" surface as the alignment of LC can be reversibly controlled by changing polarization or wavelength of incident illuminations.

The other is for irreversible process based on photochemical reactions such as cross-linking or decomposition of polymers. The crosslinking of the side chains of polyvinyl cinnamate by linearly polarized UV light to control LC alignment was first demonstrated by Schadt *et al.*[15] The nematic molecules were found to align in-plane and perpendicular to the polarization of linearly polarized illumination. Following this work, many similar materials and techniques have been developed. The quality of the photoaligned LC cells based on this type of method proves to be high. The orientation

order parameters of crosslinked polymer film and anchoring energy depend on the energy of UV illumination.[9] In addition, it has also been demonstrated that photodecomposition of a few polyimides by linearly polarized UV light aligns nematic phases in contact with these substrates.[16,17]

3.1.1.3. Depositions of inorganic materials

Depositions of inorganic materials were also used extensively to achieve a unidirectional planar or tilted alignment of LC. Among these techniques, obliquely evaporated metal (e.g., gold[18]) or oxides (S_iO_x) can give reproducible results. The surfaces of these deposited inorganic materials usually have groove-like topography, which aligns nematic molecules parallel to the groove to achieve the minimum free energy of elastic deformation. The details of this type of method can be found in the review by Cognard.[19] Researchers in IBM recently showed that deposition of amorphous carbon layer followed by low energy ion beam impinging is able to achieve alignment properties similar to those of rubbed polyimides technique, but with advantages of non-contact way of alignment and lower manufacturing cost. A prototype of laptop computer based on this technique was also demonstrated.[20,21]

3.1.1.4. Deposition of surface active molecules

Surface active molecules (e.g., Lecithin molecules) coated on glass substrates is generally used to achieve homeotropic alignment of nematic fluids.[19] Porte has shown that the LC alignment on alkyl chain surfactant layers depends on the length of alkyl chains: long chain gives homeotropic anchoring while shorter chain yields tilted alignment of nematic fluids.[22]

3.1.1.5. Self-assembled monolayers (SAMs)

Self-assembled monolayers (SAMs), especially those formed by chemisorption of alkanethiols on gold surfaces, have been well studied to control the alignment of nematic fluids.[23,24,25,26] The advantage of this method over the above methods is that the structure of these SAMs is well defined and can also be easily tuned by varying molecular structures,[27,28] and thereby allows the relationships between the alignment of LC and the structure of underlying substrate at molecular scale to be explored. This method is often used together with gold substrates with nanometer topography to align nematics.[18] The molecular parameters that can be adjusted include the length and end functional groups of alkanethiols (a lot of choices of the end groups are available like, CH_3, COOH, OH, OCH_3, ferrocene, azobenzene, etc.), fluorinated or hydrocarbon thiols,[25] and mixed SAMs formed from long and short alkanethiols, etc.[29] Both unidirectional planar anchoring and homeotropic anchoring of nematic LCs on these surfaces can be obtained by choosing different molecular structures. These surfaces can also be easily patterned by micro-contact printing techniques to fabricate optical devices from the LC in contact with them.[24] Moreover, if the end functional groups of the alkanethiols are coupled with metal ions, protein (or receptor) molecules, or redox-active groups (e.g., ferrocene), which is responsive to external chemical or electrical stimulus, the change in structure of monolayer due to the external stimulus can cause an anchoring transition of the bulk nematic phase in contact with the monolayer, and thus be identified by the change in optical appearance of the nematics. Based on this, highly sensitive and selective chemical sensors, and potential for novel LCD using electrochemically-controlled surfaces have been demonstrated. [26,30]

3.1.1.6. Micro-patterned surfaces

Micro-patterned surfaces may be constructed with either inorganic or organic materials. One example of using this type of surfaces to align LC phases is to create periodical surface topography (grooves) from polymers or inorganic materials. The nematics at such surfaces adopts a unidirectional in-plane alignment parallel to the grooves.[31] It has been reported that such grooves can be created in a non-contact way, e.g., photo-ablating polymer layers by exposure to patterned UV light.[32] Moreover, Lee and Clark have shown that SAMs formed by octadecyltriethoxysilane on glass, which itself is isotropic, is able to align nematic molecules along a uniform in-plane direction if the SAMs are micro-printed into parallel stripes on the glass substrate.[33] In this case, neither anisotropic substrates, nor surface topography is responsible for the alignment. The observed in-plane uniform LC alignment is due to the anisotropy of elastic constants of nematics, namely, with twisting elastic constant (K_{22}) smaller than the two others (K_{11} and K_{33}).

Another application of micropatterned surfaces is to create multistable anchoring. The multistable anchoring has applications in fabrication of low power-consumption LCDs since only electric pulses are needed to switch bulk nematic LC between different orientation states for display purpose. For example, it has been recently reported that by utilizing an atomic force microscope, one can pattern small domains with different orientations of easy axis on a polyimide substrate.[34,35] The polyimide layer underlying every display pixel has several of such small domains arranged in a four-fold or six-fold rotational symmetry. Due to the competition of anchoring between neighboring domains and the pixel symmetry, only the diagonal axes of these square or hexagonal pixels

become equally stable directions for macroscopic LC alignment. A bistable or tristable anchoring can thus be achieved and the LC alignment is switched between the states by an in-plane electric field.

3.1.1.7. Techniques for highly tilted alignment

As we mentioned above, the pretilt angle is important in TN devices. In addition, high pretilt is also a prerequisite for operation of novel LCDs based on super-twisted nematics (STN).[36] But, highly tilted alignment is not easily obtained by typical rubbing technique and traditional polyimides. Some other approaches have been proposed. One type of these methods is for unidirectional tilted alignment; the other type is for degenerate tilted alignment (also referred to as conical anchoring[5]).

(i) Unidirectional highly tilted alignment can be achieved by tangential evaporation of SiO_x material to glass,[19] slantwise UV irradiation of photochromic molecules attached to the surfaces, rubbing some special polyimides,[37,38] or by combining rubbing with solvent dipping of polymers.[39] (ii) The methods that obtain conical anchoring include deposition of two chemicals (polymers or small molecules) with competing anchoring tendencies[40,41,42] (i.e., one favors homeotropic and the other in-plane alignment), using inhomogeneous surfaces,[43] grafting of polymer brushes to the surfaces,[44] or utilizing a continuous homeotropic-to-planar transition.[45]

3.1.2. Anchoring mechanism

Although tremendous efforts have been directed to elucidate anchoring mechanism, anchoring phenomena (especially those on solid substrates) are still far from being well understood. The mechanisms responsible for many of the above mentioned alignment techniques are still in controversy. This is partially due to the diversity of

anchoring phenomena and underlying substrates, and difficulty in charactering LC-solids interface structure. Nevertheless, some progress has been made which can be divided into two approaches: macroscopic approach (phenomenological) and microscopic approach (molecular interactions).[1,5]

3.1.2.1. Phenomenological approaches

First, as indicated by Jerome,[5] the symmetry of anchoring directions adopted by LC molecules must be consistent with the symmetry of underlying substrates. For example, nematic LC adopts a unidirectional planar anchoring on mica surface which was discovered by Mauguin.[46] In this case, the mica surface has a mirror symmetry, the anchoring direction of nematics is located right in the mirror plane, satisfying this symmetry.[5]

Creagh and Kmetz proposed a phenomenological rule to explain anchoring observations at solid substrates, trying to relate anchoring phenomena to wetting properties of LC fluids: [19, 47]

If $\gamma_s<\gamma_{LC,}$ homeotropic alignment;

If $\gamma_s>\gamma_{LC,}$ parallel alignment.

Here γ_s and γ_{LC} are the surface tensions of solid substrate and liquid crystal, respectively. Naemura further extended this rule to consider the effects of both the polar and nonpolar compositions of the surface energy of a few surfactant-treated surfaces on the alignment of nematics.[48] Although this approach based on surface tension is sometimes useful (e.g., to explain the homeotropic alignment of nematics on surfactant-coated surfaces), it oversimplifies the problem in many cases. For example, γ_s may be affected by adsorption of impurities dissolved in LC in practical cases; also the first monolayer of nematic

molecules adsorbed to a solid substrate whose properties are different from bulk LC molecules may change the surface tension of the underlying substrate, making original γ_s ill-defined. Moreover, this rule cannot explain azimuthal (in-plane) anchoring transitions.

Observations of anchoring transitions help to understand anchoring mechanism, establish the relationship between the anchoring and the parameters characterizing the surface, as shall be discussed in the section 3.1.3.

3.1.2.2. Microscopic mechanism

The microscopic mechanisms of anchoring of nematics on solid substrates suggested in literature can be classified into two groups as follows:

(I) Surface topography

It has been long known that rubbing a glass surface with a dry cloth or tissue may induce parallel alignment of nematic molecules to the glass surface. Barreman has shown that geometric factors play an important role in such an alignment.[31] Mechanical rubbing can corrugate the surface. If the both ends of the nematic molecules have equal affinity for the surface material so that they lie flat against the surface, it is obvious that the molecules lie normal to the rubbed direction cost more elastic energy than those aligning parallel to it. The same mechanism also plays a role in the rubbed polymer layers used in traditional LCDs since rubbing can scratch polymer surface to create a grooved surface.

(II) Physico-chemical interactions between nematic molecules and underlying surfaces

In the case of the rubbed polymer layers, some researchers proposed that rubbing orients polymer chains in the film along the direction of rubbing. Geary *et al.*, based on the observation of birefringence, suggested that a liquid crystal phase on the crystalline,

oriented polymer surfaces is analogous to the epitaxial growth of conventional solid crystals.[6] Further, Shen and coworkers have shown by sum frequency generation technique (SFG) that the first monolayer of nematic molecules in contact with rubbed polymer substrate has an anisotropic distribution of the molecules with maxima along the rubbing direction.[49] This indicates that the bulk orientation of nematic molecules on rubbed polymer layers arises from the molecular interaction with anisotropic polymer chains. X-ray scattering measurements by Toney *et al.* have unambiguously shown that rubbing a polyimide film causes near surface alignment of the polymer molecules (polymer chains within several nanometers deep below the surface are oriented).[50] Other techniques like polarized infrared absorption spectroscopy has also verified that a very thin LC film and underlying rubbed polyimide film are both oriented along the rubbing direction.[51] Besides that rubbing aligns the backbone of polymers, it can also align the liquid crystalline side chain of polymers, resulting in an alignment of nematics with high pretilt.[38] The high pretilt in this case is likely due to dipolar interactions between nematics and liquid crystalline side chain.

In the case of many surfactant-treated surfaces that induce homeotropic or highly tilted anchoring of nematic phases, a possible mechanism is that the nematic molecules penetrate the layers formed by the alkyl chains of the surfactant. They can adopt the orientation of these chains, which leads to a homeotropic or conical anchoring, depending on the chain's orientation.[5,22,52] This hypothesis is consistent with Porte's result,[22] and also has been confirmed by SFG measurement of 8CB (i.e., 4'-*n*-octyl-4-cynobipenyl) monolayers deposited on a surfactant-coated surface.[53] However, sometimes, surfactant molecules may carry large head groups with ions, e.g., the case of nematics in contact

with a Langmuir-Blodgett (LB) monolayer formed by amphiphilic surfactants. In this case, one has to consider the alignment effects due to dielectric interactions between surface electric field and dipolar LC, flexoelectric and surface polarization coupling mechanisms, in addition to steric interaction.[54]

In the case of SAM formed by alkanethiols on gold, the situation is different from that of typical surfactant-coated surfaces. Planar anchoring of nematics is generally observed except in the case of using mixed SAMs from long and short alkanethiols. Abbott *et al* suggested that a strong anisotropic dispersive force exists between gold substrate and nematics to align nematic molecules parallel to the surface.[25] Moreover, the observed odd and even effect of the length of the alkanethiol on the in-plane switching of anchoring direction of nematic molecules is attributed to the different orientation of the end CH_3 group in densely packed thiol monolayers.[55]

Photoalignment by "command" surfaces is another good system for understanding the relationships between anchoring and the molecular interaction between LC and underlying surfaces. For example, photoisomerization of azobenzene group causes the alteration of the molecular axis of surface-tethered molecules, which may in turn induce an anchoring transition between homeotropic state and planar state or a 90° in-plane rotation of nematic molecules at the surface, depending on the molecular structure of azobenzene derivatives being used. Such a cooperative reorientation of photoactive surface unit and non-photoactive nematic molecules is driven by either their dipolar interactions, steric interactions, or the combination of both.[7]

The mechanism for the techniques realizing highly tiled alignment is generally due to the competition between two different alignment tendencies arising from depositing two different chemicals on the surface[40] or inhomogeneous substrates.[43]

3.1.3. Anchoring transitions

When the parameters characterizing the interface structure change, anchoring of nematic fluid may transit from one state to another state, which is called anchoring transition. Anchoring transitions can be induced by change in temperature, surface adsorption, surface strain, molecular conformation of surface units etc.[5]

The early observations of anchoring transitions induced by molecular adsorption at interfaces include those reported by Pieranski and coworkers and Kitzerow *et al.*[56,57] They found that the anchoring state of LCs supported on inorganic substrate (gypsum, mica, calcite, etc.) changes upon exposure to vapors of water, alcohol, and acid. In recent examples reported by Abbott *et al*, anchoring transitions induced by competitive binding of small molecular analytes[26] (e.g., amine or organophosphorous compounds) or macromolecular analyte[58] (protein) to functionalized SAMs substrates are highly selective to targeted analytes. Very low concentration of analyte (in the order of ppb by volume) can dramatically change the optical appearance of LC films due to the anchoring transition.

Kitzerow *et al* analyzed strain-induced anchoring transitions observed on mica surfaces. They interpreted such anchoring transitions using an anchoring diagram (a plot of anchoring condition as function of surface parameters), which is similar to phase diagram in some aspects.[57]

As mentioned above, the change in molecular conformation of surface-attached units induced by photoisomerization can drive anchoring transitions. An anchoring transition between homeotropic and planar state was also observed at surfactant-coated substrates when the packing density of the surfactant monolayer was varied.[52] The authors explained this transition by change in steric interactions between LC and surfactant molecules. Similarly, Zhu *et al.* reported that a homeotropic–to-planar anchoring transition was observed at the interface of LC/double-armed crown ether monolayer when the packing density of the monolayer was increased.[59] They attributed the anchoring transition to conformation change of the alkyl chains of the double-armed crown ether caused by change of surface pressure in making LB monolayer.

A few of experimental observations of temperature-driven anchoring transitions are as follows. Ryschenkow and Kleman reported that the transitions between conical or planar anchoring and homeotropic anchoring of the nematic phase of MBBA (methoxy benzylidene butylaniline) on a carbon black substrate occurred twice when the LC sample is continuously heated toward the bulk isotropic-nematic transition temperature, T_{NI}.[60] The first anchoring transition at low temperature is conical-to-homeotropic, occurring within a relatively broad temperature window while the second one is homeotropic-to-planar at a temperature very close to T_{NI}. Patel and Yokoyama also reported a similar continuous planar-to-homeotropic anchoring transition of E7 at the surface of fluoropolymers.[45] Dilisi *et al.* reported a sharp tilted-to-homeotropic anchoring transition of a nematic fluid at the surface treated by a phospholipid surfactant if the temperature is increased to 7°C below T_{NI}.[61] Most of temperature-driven anchoring transitions reported in literature occur at temperatures near the bulk isotropic-nematic transition temperature

T_{NI}. However, Amundson and Srinivasarao reported a unique temperature-driven anchoring transition that occurs far below T_{NI} of bulk nematic phase of TL205 in contact with poly (alkyl acrylate) substrates.[62] It was found that the anchoring transition temperature is sensitive to the side chain length of polyacrylates. It was also proposed that nematic molecules likely interdigitate into the alkyl side chains of polymer protruding out of the surface, which leads to a homeotropic alignment favored by interfacial enthalpy. The entropy of the interface, on the other hand, favors parallel alignment. So these two terms reach a balance at the anchoring transition temperature T_t. However, the microscopic mechanism for anchoring transitions observed in such a system is still far from being well understood. It deserves to be further explored.

3.1.4. Measurement of tilt angles

The anchoring condition of a nematic fluid at substrate surfaces is characterized by both anchoring direction (tilt and azimuthal angle of nematic director at the surface) and anchoring energy. In the system under study in this thesis, only tilt angle q needs to be considered to distinguish different anchoring states since the anchoring is symmetric with respect to azimuthal direction, i.e., either a degenerate anchoring or homeotropic one. Measurement of the tilt angle as a function of temperature during a temperature-driven anchoring transition may provide us with the useful information about anchoring mechanism. Two possible cases are illustrated in Figure 3.2, where a sharp anchoring transition (case 1) occurs within a narrow temperature window (e.g., $T_t \pm 0.1°C$) while a broad one (case 2) takes place over a wide temperature range.

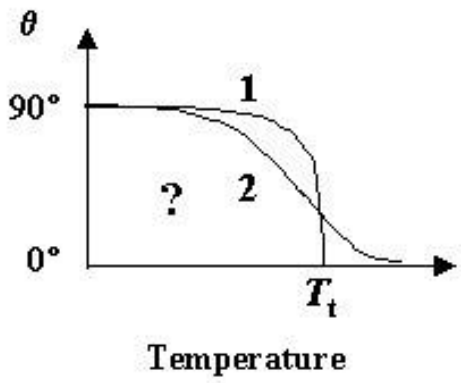

Figure 3.2. Schematic of tilt angle q as a function of temperature during a temperature-driven anchoring transition.

The tilt or pretilt angle of nematic fluids in contact with a boundary surface can be measured in a number of ways: crystal rotation method,[63,64] capacitive methods,[48,65] magnetic null method,[65] half-leaky wave guide method[66] and conoscopy, etc.[67,68] However, since the size of uniaxial alignment region in PDLC cells is usually not big enough, it is difficult to apply any of the above methods directly. In our PDLC sample, the birefringence color is a good indication of the effective retardation due to the anisotropy of the sample.[60,68,69] If the tilt angle is assumed to be uniform through the thickness of the sample, and both extraordinary and ordinary refractive indices of the nematic fluid at different temperatures are known, we can estimate the tilt angle from the birefringence color observed.[60] In other words, the color variation with change in the temperature can be converted to the tilt angle as a function of the temperature.

3.1.5. Measurement of anchoring energy

The anchoring energy, W_s (q, f), represents the work that is needed to rotate the director away from the easy axis of the surface and is a function of the tilt angle, q and the azimuthal angle (in-plane), f. In the case of a degenerate anchoring as is the case in

the system we study, anchoring energy is a function of q only (i.e., independent of f), as referred to as polar anchoring energy $W_p(q)$. The angular dependence of $W_p(q)$ is usually described by a phenomenological formalism by Rapini-Papoular.[70,71]

$$W_p(q)=W_p \sin^2(q - q_0) \qquad (3.2)$$

Where W_p is the polar anchoring strength and q_0 is the tilt angle of the easy axis. The azimuthal anchoring energy, $W_a(\theta)$, can also be defined in a Rapini-Papoular form.

The knowledge of anchoring energy strength is important because the equilibrium configuration of a bulk nematic domain confined in the boundary surfaces is the state minimizing the total free energy given by the sum of the elastic free energy and anchoring energy. Many different methods to measure the anchoring energy are reported in literature, including (a) measurement of surface tension (indirect way);[70] (b) using wall or line defects;[60] (c) wedge cell method; (d) conflicting surface alignment;[72] (f) Freedericksz transitions;[48,61] (g) high-electric-field techniques;[73,74] (h) torque measurement;[75] (i) dynamic light scattering,[76] etc.

The first method is an indirect method based on a phenomenological approach. All the other methods are direct methods. Most of these direct methods require a surface distortion of nematic phase which can be created by either a surface defect (method b), conflicting boundary conditions (methods c and d) or external fields (methods f through h). Such a director distortion can be characterized by optical techniques such as microscopic observation, measurement of optical retardation of LC cell using a polarized light or monitoring interference patterns, etc. The experimental data are fitted to the calculated or predicted results based on the continuum theory of nematics to obtain anchoring energy strength. More details are available in the review by Yokoyama.[70] It

should be noted that the range of anchoring energy measurable by a method is usually limited by the principle of that method. The method based on dynamic light scattering is a unique method in that it measures the fluctuation relaxation time of nematics, which depends on surface anchoring energy. It doesn't require the surface distortion and can be carried out without using any external field.[76]

One of the earliest methods of estimating the polar anchoring energy is through microscopic observation of Bloch wall defects. According to Ryschenkow and Kleman,[60] the anchoring energy can be estimated from the geometry of the wall defect. The director field of an ideal 180° rotation wall is illustrated in Figure 3.3a, which has pure twist deformation. The polar anchoring strength, W_p, can be estimated from the geometry of such a pure twisting wall using the equation below:[60]

$$W_p\left(1+\frac{\sin(4\theta_0)}{2(\pi-2\theta_0)}\right)=\frac{(\pi-2\theta_0)^2}{2}\frac{h\cdot K_{22}}{d^2} \qquad (3.3)$$

Here q_0 represents tilt angle at the edge of the wall (i.e., tilt of the easy axis), h the sample thickness, K_{22} the elastic constant for twisting deformation and d the width of the wall.

In the case of homeotropic anchoring where q_0 is 0, equation (3.3) is rewritten as:

$$W_p=\frac{\pi^2}{2}\frac{h\cdot K_{22}}{d^2} \qquad (3.4)$$

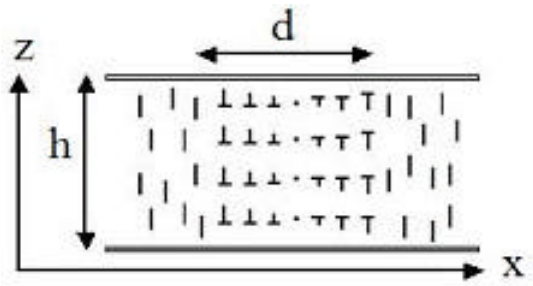

Figure 3.3. Schematics of director configuration of a 180° pure twisting Bloch wall. The head of nail sign "⊥" is behind the paper plane (redrawn after Kleman[77]).

However, the ideal wall structure exists only when the extrapolation length, b (defined as $2K/W_{s;}$ for this case, it is K_{22}/W_p), is larger than the dimension of the sample h. If b<h, the diffused walls or surface lines instead of pure twisting wall are favored.[60] We will address this topic in more details in Chapter 6 of this thesis. In addition, this method is only appropriate for measuring weak anchoring regime (10^{-5}~10^{-6} J/m^2) which allows wall defects to exist or be measurable by optical microscopy. The system under our study belongs to this anchoring regime as we shall discuss in section 3.3.4.

3.1.6. Outline of our study in this chapter

A systematic study of anchoring properties and anchoring transitions of nematic fluids at polyacrylate surfaces is the focus of this thesis. It is hoped that it will contribute to a better understanding of microscopic (and macroscopic) mechanism that are responsible for anchoring of nematic fluids at polymer surfaces, and also learning how to control the surface anchoring at the molecular level. The following aspects will be addressed in this chapter:

(i) Study the effect of chemical modifications of polymer substrates on anchoring behavior. Such modifications include varying the branching structure of the side chains

of the homopolymers of alkyl acrylates, varying the composition of the copolymer of two acrylates.

(ii) Investigate possible microscopic mechanisms for observed anchoring and anchoring transitions in such systems by measuring both tilt angle and polar anchoring energy as a function of temperature

(iii) Examine the effects of using different nematic fluids or different phase separation methods to make LC-polymer composite films on the anchoring properties.

3.2. Experimental

Materials. The nematic fluids used are TL205, TL213, and 5CB (EM Industries). TL 205 is a eutectic mixture of chlorinated bi- and terphenyls with aliphatic tails of 2 to 5 carbons. TL 213 is a mixture having a similar composition as TL 205. 5CB, i.e., 4'-pentyl-4-cynobiphenyl, is a single component nematic fluid. 2-Ethylhexyl acrylate (2-EHxA), *n*-hexyl acrylate (C6A), *n*-octyl acrylate (C8A), *n*-decyl acrylate (C10A) and 1,1,1-trimethylol propane triacrylate were obtained from Scientific Polymer Products Inc. and *n*-heptyl acrylate (C7A) was provided by Lancaster Inc. The purity of all of the commercial monomers is greater than 98 mol% and they were used as received. The TL205, monofunctional acrylate monomers and the triacrylate crosslinker were mixed in an 80:18:2 (w/w). The monomer mixtures used for copolymerization are composed two acrylates, in which the mole fraction of one acrylate was varied from 0 to l00%. Approx. 0.5 wt % of Darocur 1173 (Ciba Inc) was used as a photoinitiator. All of the chemicals and solvents used for synthesis of the following alkyl acrylates were at least 97 mol % pure and obtained from Aldrich.

Synthesis of alkyl acrylates. Methylheptyl acrylates (MHA) and dimethylhexyl acryaltes (DMH_xA) were synthesized from their corresponding alcohols and acryloyl chloride. The synthesis is illustrated here by the preparation of 1-methylheptyl acrylate (1-MHA). The other MHA and DMH_xA were synthesized by the same procedure. The ^1H NMR and ^{13}C NMR spectra of all of these synthesized acrylates are listed in Appendix B, which confirm that they have the structures as named. The final purities of all of the synthesized acrylates are greater than 97 mol%.

A mixture of anhydrous triethylamine (4.3 ml, 0.031 mmol), 2-octanol (2.5 g, 0.0194 mmol) and methylene chloride (65 ml) was cooled to 0°C and acryloyl chloride (2.2 g, 0.023 mmol) was slowly added into the mixture, giving a yellow solution. The reaction mixture was stirred at 0-10°C for 2 h. The reaction mixture was allowed to warm to room temperature and washed with water twice (2x50 ml). The resulting aqueous phase was extracted with methylene chloride three times (3x75 ml) and the combined organic extracts were washed with saturated sodium bicarbonate and brine twice (2x 75 ml). The organic extracts were then dried over anhydrous magnesium sulfate and the solvent was removed under reduced pressure. The resulting yellow oil was purified by flash chromatography (30-60 μm silica gel, methylene chloride) to give 2.8 g of a light yellow clear liquid (78% yield). ^{1}H NMR (300 MHz, $CDCl_3$): δ 6.30 (dt, J=17.4, 1.5 Hz, 1H), 6.0 (dd, J=17.4, 10.5 Hz, 1H), 5.73 (dd, J=10.5, 1.5 Hz, 1H), 4.90 (m, 1H), 1.59 (m, 1H), 1.50 (m, 1H), 1.24 (m, 8H), 1.2 (d, J= 6.3 Hz, 3H), 0.84 (t, J= 6.6 Hz, 3H). ^{13}C NMR (75 MHz, $CDCl_3$): δ165.9, 130.1, 129.2, 71.3, 36.1, 31.8, 29.2, 25.5, 22.7, 20.0, 14.1.

Preparation of homopolymers of acrylates by free radical polymerization in solution. Homopolymerization of each synthesized acrylate with azobisisobutyronitrile (AIBN) as initiator was carried out in toluene at 60 °C under nitrogen flow.[78] After the polymerization, the solution was diluted by ethyl ether (1:1 v/v) and polymer was precipitated by pouring the solution into methanol bath. The polymer was then collected and dried under vacuum to remove the solvent. The resulting polymer, which appears like a fluid with very high viscosity at room temperature, was characterized by gel permeation chromatography (GPC), differential scanning calorimetry (DSC), and ^{1}H and ^{13}C-NMR.

The results of GPC and DSC are listed below while the NMR results are listed in Appendix B.

Glass transition temperatures (T_g) of poly(x-methylheptyl acrylates). T_g was measured by DSC (Seiko 220 with liquid nitrogen cooling unit). A sample of ~5 mg was first quenched to –100°C and heated to 40°C by 10 °C /min (1st heating). The temperature was held at 40°C for 3 minutes and cooled down to –100°C again by 10 °C /min, held at –100°C for ~1 min, heated to 40°C by 10 °C /min again (2nd heating), and then cooled back to room temperature. The T_g was measured from the heating cycles and the results are listed in Table 3.1.

Molecular weights of poly(x-methylheptyl acrylates). M_w and M_n were measured by GPC. Tetrahydrofuran (THF) was used as elution solvent. The concentration of the polymer solution was ~10 wt %. The flow rate of 1 ml/min was used. The measured molecular weights of poly(x-methylheptyl acrylates) have similar values: M_w = 75,000 to 90,000 g mol^{-1} and M_w/M_n = 3.0 to 4.0.

Photopolymerization and PDLC film morphology. All of the PDLC films made for study of anchoring properties have a cellular morphology created by a slow photopolymerization process, as discussed in Chapter 2. Such a cellular morphology facilitates identifying the anchoring present in the PDLC films. The size of the LC cells can be varied from 5 to 70 μm by changing the conditions of the polymerization (mainly by changing intensity of UV irradiation). As verified by confocal microscopy (see Chapter 2), each LC cell in such a morphology is completely enclosed by the polymeric matrix, with thin vertical polymer walls extending from the top substrate to the bottom.

Measurement of anchoring transition temperatures. The anchoring behavior of PDLC films was evaluated by observations using a polarized light microscope (Leica DMRX) equipped with a hotstage (Linkam TMS 90, with the accuracy of temperature up to 0.1°C) and crossed polarizers. For the observation of a sharp transition (i.e., anchoring transition occurring within a narrow temperature window of less than 1°C), the samples were heated at 2°C/min from room temperature, and then in 0.1°C steps when the temperature was close to the anchoring transition T_t, holding the temperature constant for 5 minutes between each step. For the observation of a broad transition (i.e., occurring within a temperature window of greater than 1°C), the samples were heated at 2°C/min from room temperature, and then in 0.3°C steps when the temperature was close to the point where the anchoring transition starts until the transition is over, holding the temperature constant for 5 minutes between each step. The measurement of T_t was repeated with at least two films made using the same conditions. Since the value of T_t depends on the nematic-to-isotropic clearing temperature T_{NI} of the liquid crystal phase (Figure 3.4), which in turn depends on the amount of impurity (uncrosslinked polymer or unreacted monomer) dissolved in LC phase of the film, the PDLC films were cured to such a extent to achieve a constant T_{NI} of 84±0.5°C in order to provide a valid comparison of T_t data between different films.

Thermally-induced phase separation. A homogeneous solution containing chloroform, TL205 and the polyacrylate (in 90:7:3 weight ratio) was prepared. A thin film was cast on the glass slide using a drop of this solution at room temperature and the remaining chloroform was removed by vacuum. The film containing TL205 and the polymer was heated above T_{NI} of TL205 (87°C) to make a single isotropic phase, and

then *slowly* cooled back to room temperature. The LC droplets with size varying from 2~3 μm up to 15 μm, dispersed in the polymer matrix, were obtained. This method is actually a combination of solvent-induced and thermally-induced phase separation methods (refer to the work by Mcfarland *et al*[79]).

3.3. Result and discussion

3.3.1. The relationship between T_t and T_{NI}

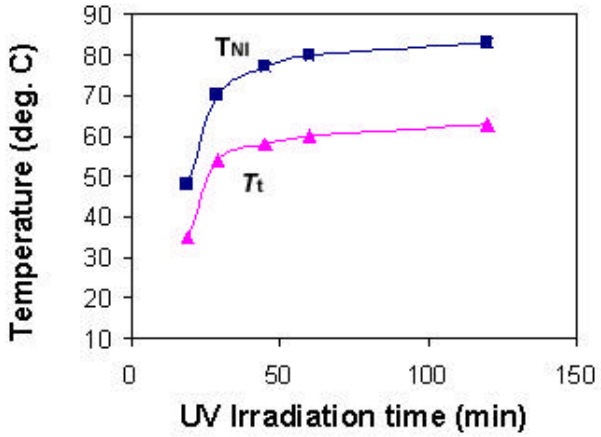

Figure 3.4. T_{NI} and T_t as a function of UV irradiation time. The PDLC films are made from the same solution of TL205/(n-hexyl acrylate) system with UV intensity of 300 μWatts/cm^2.

As shown in Figure 3.4, the longer the irradiation time at a low UV intensity, the higher the T_{NI}. It is because of that the unreacted monomer after photo-polymerization works as impurity in bulk LC and decreases T_{NI}. The more complete the photo-polymeriazation, the lesser the amount of the unreacted monomer in LC domain, the higher the T_{NI}. T_{NI} is hence an indicator of the amount of the unreacted monomer left in LC domain.

It is also shown in Figure 3.4 that T_t increases with the T_{NI} by almost the same extent. In fact, all of the factors that affect T_{NI} of PDLC film also affect T_t of the film. These factors include the intensity of UV irradiation, irradiation time, and initiator concentration. In order to compare the different T_t data from different polyacrylate systems, the same T_{NI} is required for all PDLC films. One method of doing this is to keep all the factors above mentioned as constant for making the PDLC films, and achieve as

high T_{NI} as possible, which is ca. 84±0.5°C for the PDLC films with a cellular morphology. So there is ~1 wt% unreacted monomer left in the bulk LC phases of these PDLC films according to reference [80], which reported that 1 wt% unreacted monomer causes approximately 3 °C drop of T_{NI} in a similar system (TL205/polyacrylates).

A couple of degree higher T_{NI} than 84°C can be obtained if a higher amount of initiator is used for photo-polymerization; but that typically does not yield a cellular morphology. For ease of observation of anchoring transitions, we keep using the cellular morphology of PDLC film.

3.3.2. Effect of branching of alkyl side chain on anchoring behavior of NLC [81]

3.3.2.1. Effect of methyl branching

The effect of incorporating a methyl branch into the alkyl side chain of polyacrylates on control of anchoring behavior of polymer dispersed liquid crystal (PDLC) films is studied. A series of poly(methylheptyl acrylates) (MHA) were used as polymer matrices of the PDLC films.

An example of a homeotropic–to-planar transition (H-to-P) is shown in Figure 3.5. For a PDLC film made from 2-MHA/TL205, a uniform homeotropic anchoring is observed at temperatures below T_t (~ 78^{o}C). The centers of the LC cells are dark under crossed-polarizers, indicating that the optical axis of the LC is along the propagation direction of the light. The edges of the polymer walls appear the brightest if the projection of the wall is aligned at about ±45° to the polarizer or analyzer, consistent with homeotropic anchoring at the polymer walls. One of the possible director configurations in a LC cell with homeotropic anchoring is shown in Figure 3.5e. When the temperature is increased to T_t, the appearance of the film changes dramatically such that in-plane

birefringence dominates the texture (Figure 3.5c). When the temperature is 3 °C above T_t (Figure 3.5d), anchoring with a tilt angle less than 20° (close to planar anchoring) is estimated from the orientation of the dark brushes of the nematic texture near the polymer walls. Weak anchoring condition is observed when the temperature is close to T_t, as shown by very uniform alignment of the nematic molecules within each LC cell in both Figure 3.5b and c. This is consistent with the results of electro-optical measurement of the previous report, in which switching-on voltage and switching-off time as functions of temperature were found to show a valley and a peak around T_t, respectively.[62]

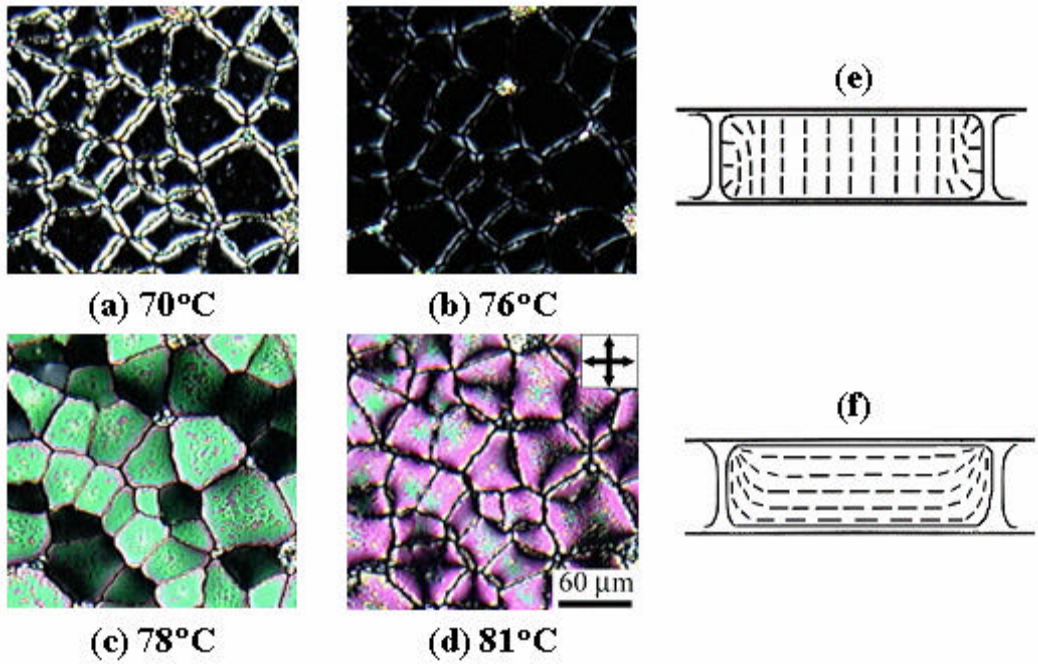

Figure 3.5. Polarized light micrographs of homeotropic-to-planar anchoring transition of a PDLC film made from 2-MHA/TL205. (a) and (b) are for homeotropic anchoring and (c) and (d) are for planar anchoring. The schematics, (e) and (f), represent possible director fields within a LC cell with homeotropic and planar anchoring, respectively.

The values of anchoring transition temperature, T_t, in the PDLCs made from all other MHA and TL205 are also measured and shown in Table 3.1. It is noted that nematic

anchoring at the interface of poly(1-methylheptyl acrylate) is dramatically different from that of the other polyacrylates with the methyl branch further removed from the polymer backbone: poly(1-MHA) induces only planar anchoring at temperatures above –14 ^{o}C, while all other poly(MHAs) show homeotropic-to-planar anchoring transition at 71-78 ^{o}C. The polarized light microscopic pictures of PDLC made from TL205 and 1-MHA are shown in Figure 3.7.

Since T_t is far above T_g of the polyacrylates (Table 3.1), and insensitive to the amount of the crosslinking agent (and thereby to the average length of the polymer chains between the crosslinking points) within the range studied (Figure 3.6), mobility of the polymer backbone is ruled out as the origin of the anchoring transitions. T_t is also insensitive to the size of the LC domains (droplets or polygonal cell) within the range of 2 to 70 μm (LC cell of ~2 μm was obtained by making PDLC with typical droplet-like morphology, see chapter 2). By contrast, T_t is very sensitive to the variation of the structure of the side chain.

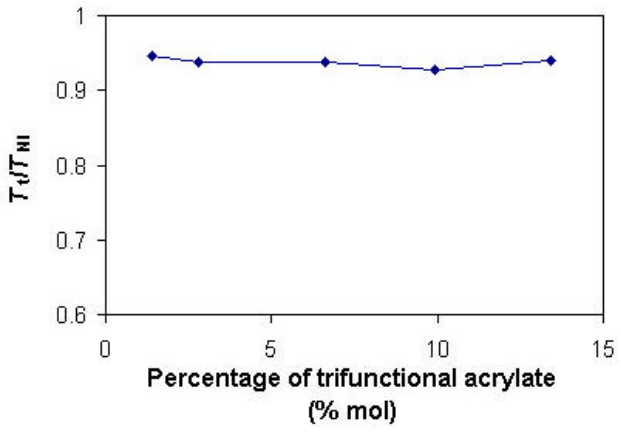

Figure 3.6. Effect of amount of crosslinking agent on anchoring transition temperature, where the reduced T_t, T_t /$T_{NI,}$ is used.

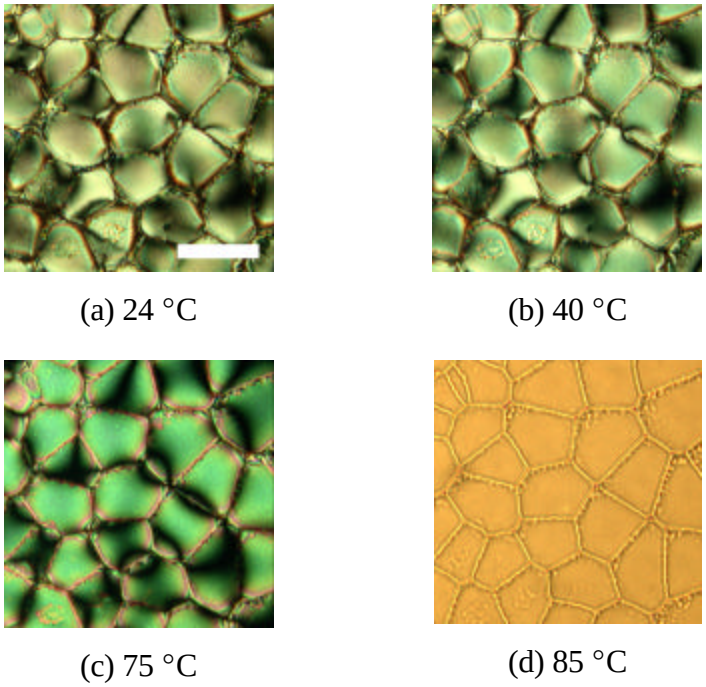

(a) 24 °C (b) 40 °C

(c) 75 °C (d) 85 °C

Figure 3.7. Polarized light microscopic images showing planar anchoring for the film made from 1-methylheptyl acrylate. (a)-(c): taken under crossed polarizers; (d): taken without polarizers. The scale bar is 40 μm.

Table 3.1. Anchoring transition temperatures (T_t) of TL205 in PDLC and glass transition temperatures (T_g) of homopolymers.

Acrylates	Monomer structure	T_t (°C)	Homopolymer T_g (°C)
n-heptyl acrylate	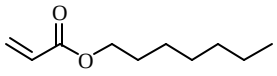	78	-60[a]
1-MHA	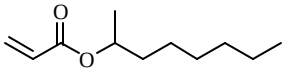	—[b]	-46[a]
2-MHA	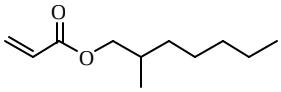	78	-60
3-MHA	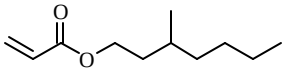	71	-65
4-MHA	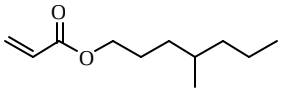	73	-62
5-MHA	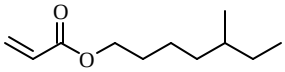	71	-58

[a] compare to reference [82]. [b] Only planar anchoring was observed down to –14°C, see text.

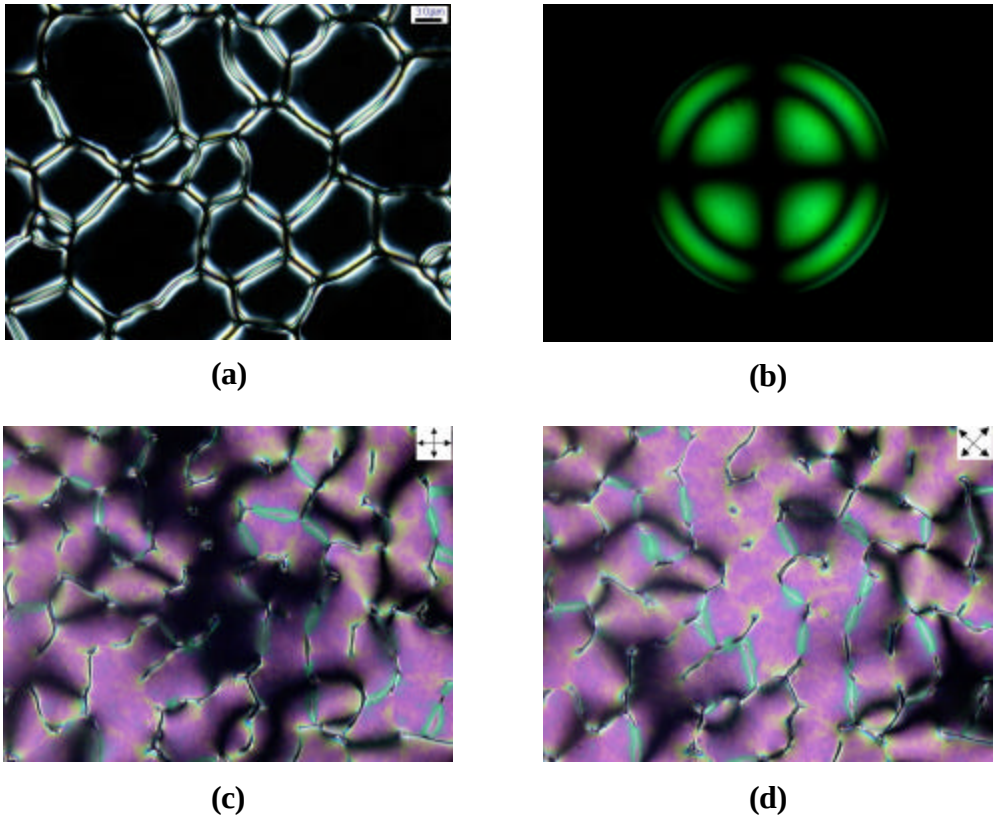

Figure 3.8. Polarized micrographs (crossed polarizers) of PDLC films made from 5CB/2-MHA (a) and (b), and 5CB/1-MHA (c) and (d). (b) is the conoscopic image of the central region of a LC cell in (a). All the pictures here are taken at 25 °C and with the same magnification. The scale bar in (a) is 30 μm.

PDLC films from a single component nematic fluid, 4-pentyl cynobiphenyl (5CB) and the acrylates used in Table 3.1 were also made. The mass ratio of 5CB/acylate in the pre-polymerization mixture is 90/10 according to reference [83]. The photopolymerization procedure for making cellular PDLC films is the same as that of TL205/acyatle system. As shown in Figure 3.8, the anchoring of the nematic phase of 5CB at room temperature is consistent with the result for TL205. At poly(2-MHA) surface, homeotropic anchoring of 5CB is observed as verified by conoscopic technique, while at poly(1-MHA) surface, planar anchoring of 5CB is observed.

In order to explain the above observations, the following interfacial model is considered. van der Waal's interaction between the side chains of polyacrylates and the alkyl tails of LC molecules provides the enthalpic drive for homeotropic anchoring.[22,52] NMR investigation has shown that the alkyl side chains of polyacrylate in contact with the nematic molecules at the interface are partially ordered under homeotropic anchoring condition.[84] On the other hand, planar anchoring is driven by the entropy of the interfacial free energy, which is contributed by both the entropy-favored planar packing of the rod-like molecules on the surface[85] and a possible order-disorder transition of the side chains of polyacrylate in contact with nematic fluid.[86] These two driving forces are competitive and reach a balance at T_t. We suggest that the unique behavior of 1-methylheptyl side chain in control of anchoring of nematic fluids is in that its side chain conformation is dramatically different from those of the other poly(MHA). For poly(1-MHA), where the methyl substituent is the closest to the polymer backbone, the side chains is likely to adopt a randomly "tilted" conformation with respect to the interface normal such that an ordered packing of the side chains at the interface is impossible. Planar anchoring is thus

preferred even at temperatures as low as –14 °C. This suggestion of the side chain conformation is consistent with the observation that the T_g of poly(1-MHA) is ~ 15°C higher than those of the other polyacrylates (although the glass transition of the polymer matrix is not the reason for the anchoring transition discussed here). It is also very interesting to note that 1-methylheptyl as a substituent in LC molecules usually has a strong effect on the packing of the molecules in the mesophases.[87,88] For example, in the reference 87, the 1-methylhelptyl tail of the banana-shape LC molecule gives rises to a anti-parallel relationship in the tilt directions of the director between two consecutive layers of the smectic C phase.

3.3.2.2. Effect of dimethyl branching

The effects of dimethyl branching modification of the side chain of polyalkylacrylates on the anchoring were also examined. The anchoring behavior of TL205 in the PDLC films is shown in Table 3.2. The result is consistent with our prediction: the surface of poly(1,1-dimethylhexyl acrylate) (P(1,1-DMH$_x$A)) favors only planar anchoring of nematic molecules. However, P(2,2-DMH$_x$A) behaves like straight side chain analog, *n*-hexyl acrylate, showing T_t of H-to-P transition at 65°C. The reason for the planar anchoring of P(1,1-DMH$_x$A) is similar to the case of P(1-MHA).

Table 3.2. Anchoring transition temperatures (T_t) of PDLCs made from TL205 and dimethylhexyl acrylate.

Acrylate	Monomer structure	T_t (°C)
n-hexyl	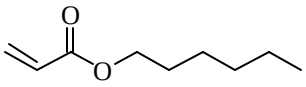	65
1,1-DMH$_x$A	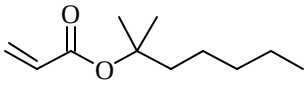	— [a]
2,2-DMH$_x$A	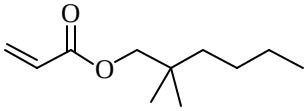	65

[a] Only planar anchoring was observed.

3.3.2.3. Anchoring in the PDLC films made by thermally-induced phase separation

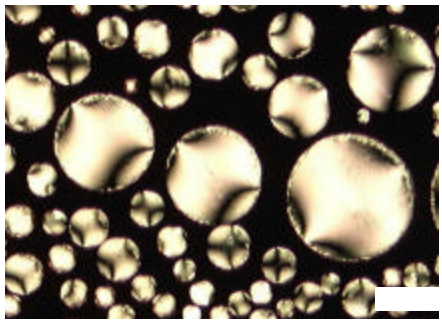

(a) Poly(1-MHA)/TL205
25°C, planar anchoring

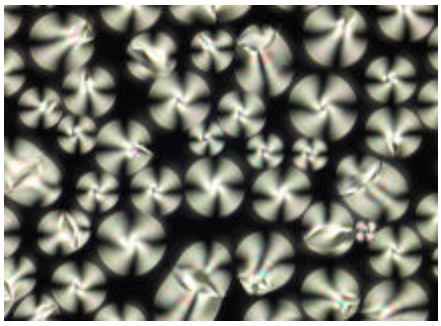

(b) Poly(2-MHA)/TL205
25°C, homeotropic anchoring

Figure 3.9. Polarized light micrographs of PDLC film made by thermally-induced phase separation. The scale bar is 10 μm.

As shown in Figure 3.9, the anchoring behavior of PDLC made by a thermally-induced phase separation of TL205 and polyacrylates is consistent with those made from polymerization-induced phase separation: the bipolar texture in (a) corresponds to planar anchoring while the radial texture in (b) corresponds to homeotropic anchoring (refer to Figure 1.10).

In addition, the samples were also prepared by inserting the TL205 under isotropic state (heated above T_{NI} of 87°C) between the two glass substrates coated with polyalkyl acrylate thin films (film was coated by casting process) and slowly cooling the sample to room temperature. The consistent results were also obtained: the TL205 adopts a homeotropic anchoring at the surface of poly (2-methylheptyl acrylate) while showing a planar anchoring at the surface of poly (1-methylheptyl acrylate).

3.3.3. Effect of copolymerization of two monomers with different side chains

3.3.3.1. Copolymerization of linear alkyl acrylates with 2-ethylhexyl acrylate

In order to further establish the link between the molecular structure of polymer surfaces and anchoring properties of the nematic fluids in the LC-polymer composite films, we have varied the structure of the polymers by copolymerization of branched (2-ethylhexyl acrylate (2-EH_xA)) and linear acrylates (*n*-decyl acrylate (C10A), *n*-octyl acrylate (C8A), *n*-heptyl acrylate (C7A) and *n*-hexyl acrylate (C6A)). Here we show that the T_t of TL205 at a copolymer surface can be adjusted over the temperature range between the anchoring transition temperatures[22] (T_{t1} and T_{t2}) prepared from the individual homopolymers.

Values of T_t were normalized such that $T_t^* = (T_t - T_{t2})/(T_{t1} - T_{t2})$, where T_{t1} and T_{t2} are the anchoring transition temperatures of the individual homopolymers. The normalization offers good comparison between different monomer pairs. Figure 3.10 is a plot of T_t^* against the mole percentage of 2-EH_xA in the copolymerization mixture of four monomer pairs, 2-EH_xA with C10A, C8A, C7A and C6A, respectively. All of the curves show nonlinear behavior, with a strong dependence on the length of the linear alkyl side chain. In the case of the films made from copolymers of 2-EH_xA and C7A, C8A and C10A, T_t remains similar to that of the film made from the homopolymer of acrylate with a linear side chain up to ca. 40-60 mol % 2-EH_xA. T_t drops substantially when the fraction of 2-EHA exceeds 40-60 mol%. However, in the case of film prepared from 2-EHxA and the shortest linear homolog studied, C6A, even a small amount of 2-EH_xA results in a lower T_t, and the anchoring transition occurred over wide temperature ranges as indicated by the vertical bars in Figure 3.10.

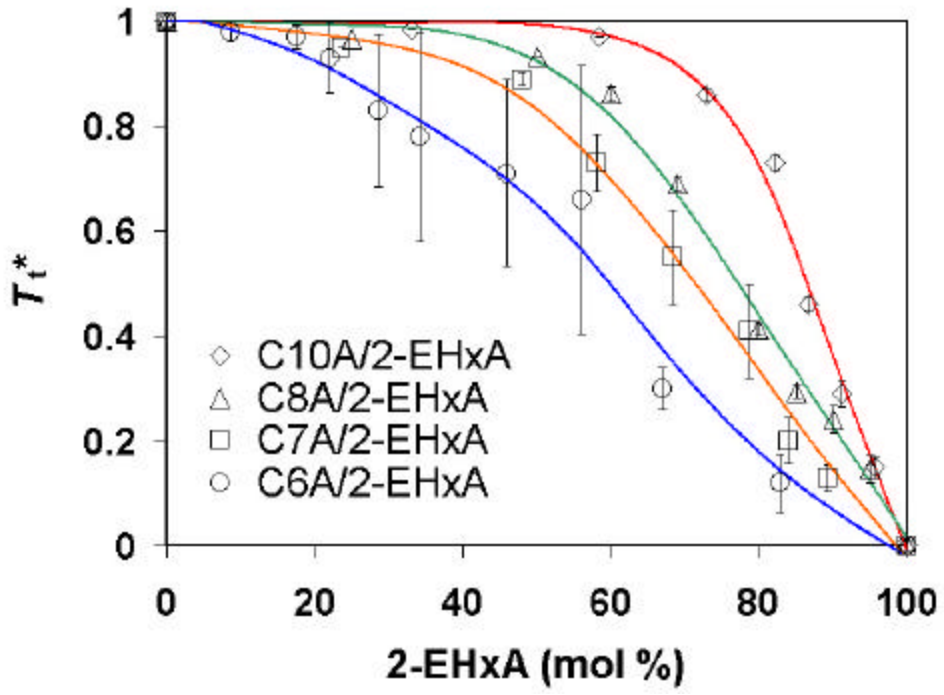

Figure 3.10. A plot of normalized anchoring transition temperature, $T_t^* = (T_t - T_{t2})/(T_{t1} - T_{t2})$, against the molar composition of the comonomer mixtures. The monomer mixtures consist of 2-EH_xA and one of the acrylates with linear alkyl side-chain, C10A, C8A, C7A and C6A. The vertical bar on each data point represents the range of temperature over which the anchoring transition occurs, instead of error bar.

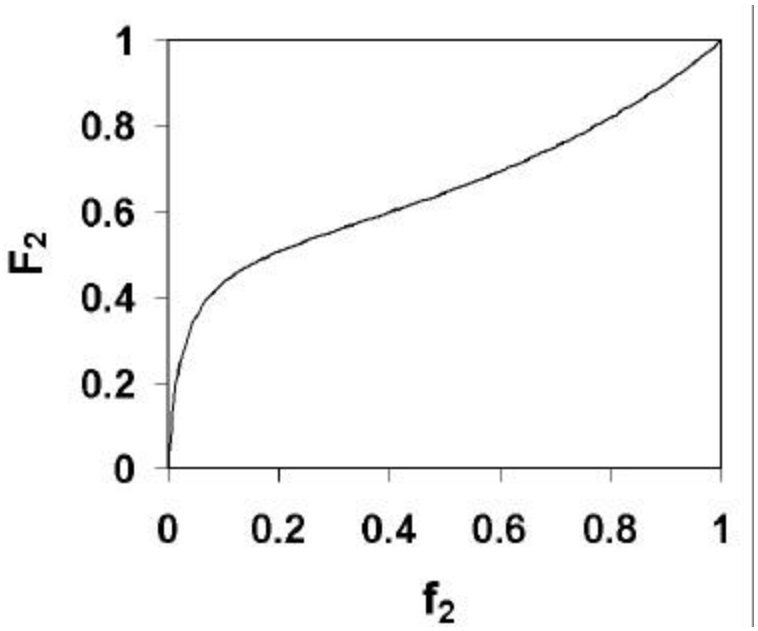

Figure 3.11. Plot of the calculated composition of copolymer versus the composition of monomer mixture for free radical copolymerization of *n*-octyl acrylate and 2-ethylhexyl acrylate (2-EH_xA). F_2 and f_2 are the mole fractions of $2EH_xA$ in the copolymer and the monomer mixture, respectively.

The influence of copolymerization of acrylates on T_t can also be understood in terms of the interfacial model for nematic orientation suggested above. In the present system, the long linear alkyl chains at the interface may be considered to form ordered domains that favor homeotropic packing of nematic molecules. The incorporation of 2-EHxA into the interface through the random copolymerization presumably disturbs the order of these domains, which is due to the different side chain conformation of the branched side chain with respect to that of linear one.[81] This reduces the tendency of the nematic molecules to align homeotropically, and hence lowers T_t.

On the other hand, the feed ratio of the monomers in the copolymerization does not necessarily represent the composition of the copolymer at the polymer-LC interface. Based on the Q-e scheme for free radical copolymerization,[89] the reactivity ratios of C8A (M_1) and 2-EH_xA (M_2) are estimated to be 0.05 (r_1) and 0.90 (r_2), respectively. Therefore, the plateaus (of T_t^*) in Figure 3.10 might be explained by the kinetics of copolymerization. The relation between the global composition of the copolymer and the composition of the monomer mixture is shown in Figure 3.11. During the process of polymerization-induced phase separation, 2-EH_xA reacts faster and is depleted from the comonomer mixture during the early stages of the polymerization. The mixture becomes enriched in the less reactive monomer, C8A. As the polymerization is continued to high conversion, the less reactive monomer is over-represented in the interfacial region that is formed at the end of polymerization. A concentration gradient of comonomers in the polymer wall must be established in which the amount of 2-EH_xA decreases upon proceeding from the interior of the wall out to the interface with the LC. Thus, the linear side chains can still predominate in the interface even if the fraction of 2-EH_xA in the

comonomer mixture is as large as 40 mol %, as seems to be the case based on T_t^* data. The same argument may be applied for all the copolymers, where, as the side chain decreases from C10A to C6A, the reactivity ratio difference also decreases and hence the polymer wall has less steep concentration gradient, which results in shorter T_t plateau.

If the composition of the copolymer at the interface is predominantly high in either type of side chain (linear or branched), the H-to-P transition occurs over a very narrow temperature range (≤0.1°C). However, if the ratio of the comonomer is within an intermediate range over which there is a sharp decease in T_t, when the interface has appreciable amount of both comonomer side chains which prefer opposite anchoring conditions, their competition results in a broad anchoring transition (with a temperature range of 3 °C up to 22 °C), as indicated by the bars on the data points in Figure 3.10. The birefringence color within the center of the LC cells under crossed polarizers is sensitive to the temperature during the broad transition as shown in Figure 3.12, changing gradually upon heating from low-order white to the third- or fourth-order color in accordance with the Michel-Levy chart.[90] The tilt angle q (q is 0° if the nematic director is parallel to the substrate normal) can be derived from the total retardation, R,[60] which is estimated from the birefringence color using Michel-Levy chart:

$$\cos^2\theta = \frac{n_o^2\left(\frac{n_e^2}{n_{eff}^2}-1\right)}{(n_e^2-n_o^2)} \qquad (3.5a)$$

$$n_{eff} = n_o + R/d \qquad (3.5b)$$

Such an estimation is based on the assumption of θ being constant through the thickness of the film (i.e., $\partial q/\partial z$ is a constant, which is reasonable since weak anchoring

condition exists around the anchoring transition temperature), knowledge of film thickness (measured by confocal microscopy), and availability of the refractive indices (n_e and n_o) of LC as a function of temperature (measured by polarized Abbe refractometry,[91] see Appendix C for more details). The plot of estimated tilt angle, q, against the temperature is shown in Figure 3.13. The result of Figure 3.13 is reminiscent of the continuous anchoring transitions previously reported,[45,60] during which the tilt angle of the LC phase gradually changes upon heating or cooling. The origins of the continuous anchoring transitions are not clear in these previous studies. Here, we attribute the nature of the broad anchoring transition to the coexistence of, and competition between, two anchoring forces arising from the two different side chains at the interfaces: one favors homeotropic anchoring and the other planar anchoring. It is also noticed in Figure 3.10 that such broad anchoring transition is more obvious in the films made by the copolymerization of C6A and 2-EHxA than in the other cases, which is consistent with the suggestion of the similarity in the reactivity ratios of C6A and 2-EHxA. In other words, the pair of C6A and 2-EHxA having similar reactivity forms the interfacial structure with comparable amount of both linear and branched side chains, thus showing broad transition within a wide range of comonomer composition.

The variations of T_t^* as a function of the composition of the comonomer mixtures consisting of two linear acrylates were also investigated. The result is shown in Figure 3.14. For the case of the two comonomers having similar side chain lengths (e.g., C10A and C8A), T_t is almost constant across the entire composition range. However, for the monomer pair of C10A and C6A, which has a larger side chain length difference, hence a

larger reactivity ratio difference, the T_t curve shows similar pattern to those in Figure 3.10.

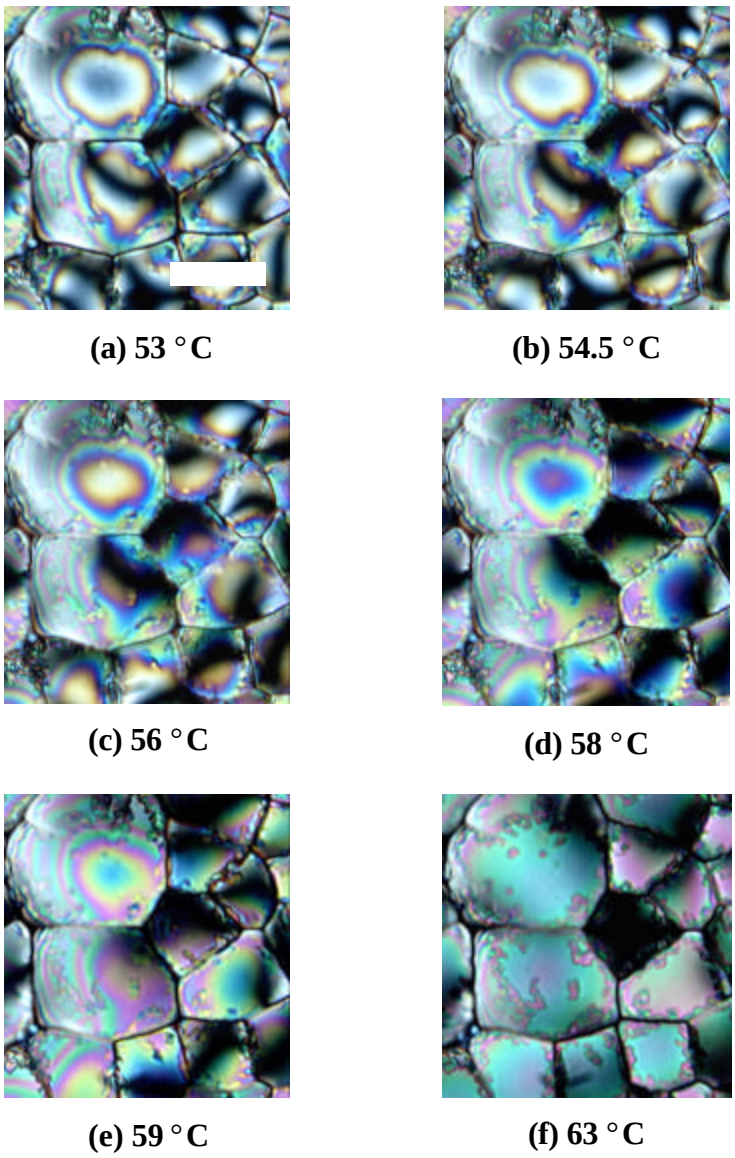

(a) 53 °C **(b) 54.5 °C**

(c) 56 °C **(d) 58 °C**

(e) 59 °C **(f) 63 °C**

Figure 3.12. Polarized light microscopic images showing broad homeotropic-to-planar transition (all of the images are taken under crossed polarizers). The film is made from C6A and 2-EHxA (C6A/2-EHxA = 72/28 (mol/mol), T_t = 53-66°C). The scale bar in (a) is 20 μm.

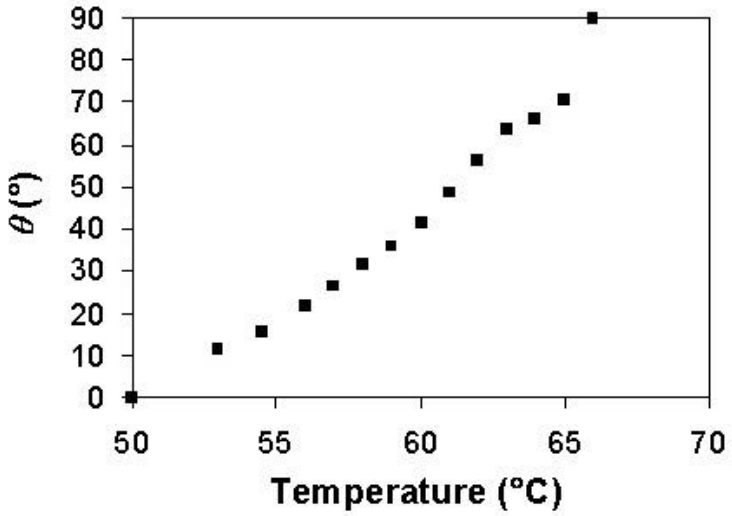

Figure 3.13. Tilt angle *q* as a function of temperature for the sample in Figure 3.12.

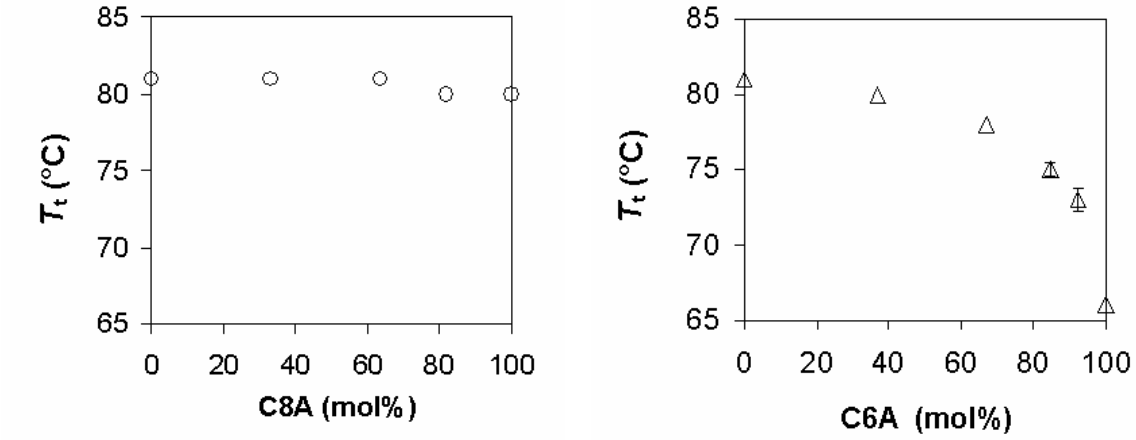

(a) **(b)**

Figure 3.14. Plots of anchoring transition temperature, T_t, against the composition of the comonomer mixtures for two monomer pairs: (a) C10A with C6A; (b) C10A with C8A.

3.3.3.2. Copolymerization of 1-methylheptyl acrylate with a linear alkyl acrylate

The PDLC films were also made from the monomer mixture of 1-MHA with *n*-decyl acrylate, a linear alkyl acrylate. T_t versus the mole percentage of 1-MHA in the monomer mixture is shown in Figure 3.15 and Table 3.3. At low composition of 1-MHA, the system behaves like that made by copolymerization of 2-EHA and linear side chain acrylates, ie., there is a plateau in T_t when the percentage of 1-MHA< 65 mol% and the anchoring at room temperature is homeotropic. However, it is very interesting that when the percentage of 1-MHA is between 68 mol% and 77 mol%, the textures of PDLC films is dramatically different, showing a highly tilted anchoring (conical anchoring) at the room temperature. These films have two temperature-driven anchoring transitions when heated: conical-to-homeotropic (C-to-H) transition at lower temperature, and homeotropic-to-planar (H-to-P) at higher temperature. The C-to-H transition is a broad anchoring transition, occurring in the temperature range of ~10 °C wide while the H-to-P transition at higher temperature is a sharp transition occurring within 0.1~0.2 °C.

One example of C-to-H transition process is shown in Figure 3.16 in which several Bloch walls are utilized to show this transition more clearly. As shown in Figure 3.16, the birefringence color is very sensitive to the temperature in the range from 20 to 30°C. The retardation decreases continuously and symmetrically near the Bloch walls as the temperature increases. The plot of tilt angle at a fixed point within a LC cell as a function of temperature during the C-to-H transition is shown in Figure 3.17, where the tilt angle was obtained based on birefringence color, knowledge of refractive indices of TL205 (Appendix C) and sample thickness. Such a transition process is very similar to those reported by Ryschenkow and Kleman,[60] as well as Patel and Yokoyama.[45,] But the

difference is that the C-to-H transition observed here occurs far below the bulk nematic-isotropic transition temperature. Also in these previous studies, little is known about the chemical nature of the interfaces. Here, we know that the polymer interface is composed of two different acrylates, one of which favors planar anchoring and the other favors the homeotropic anchoring. The competition of two opposite anchoring forces plays a key role. The anchoring strengths of both two competing surface interactions are temperature dependent, which may induce a temperature–driven anchoring transition. Moreover, a theoretical model proposed by Dubois-Violette and de Gennes has some bearing on understanding the mechanism of this continuous transition, which also suggested that two competitive alignment tendencies likely cause a temperature-driven anchoring transition.[92]

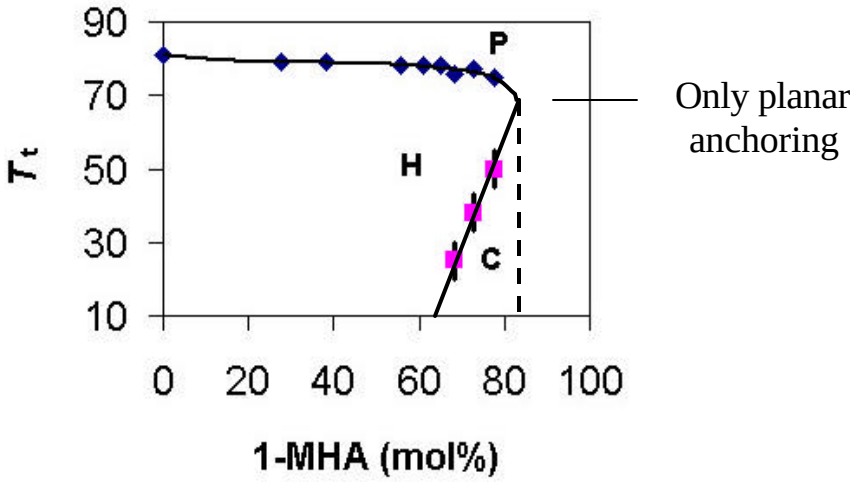

Figure 3.15. Anchoring transition versus mole percentage of 1-MHA in the monomer mixtures making PDLC by copolymerization of 1-MHA and *n*-decyl acrylate. Diamond point represents H-to-P transition; and square point C-to-H transition. The vertical bars on the data point represent the temperature range over which the transition occurs. H: homeotropic; P: planar and C: conical.

Table 3.3. Anchoring transition temperatures of PDLC films made by copolymerization of 1-methylheptyl acrylate (1-MHA) and n-decyl acrylate.[a]

Percentage of 1-MHA (mo%)	T_{t1}(°C)] conical-to-homeotropic	T_{t2}(°C) homeotropic-to-planar
0	—[b]	81
28	—	79
38	—	79
55	—	78
61	—	78
65	—	78
68	20 ~ 30	76
72.5	34 ~ 43	77
77	45 ~ 55	75
82	Planar anchoring	Planar anchoring
100	Planar anchoring	Planar anchoring

[a] T_{NI} of all films is 84 °C. [b] "—" means no first anchoring transition.

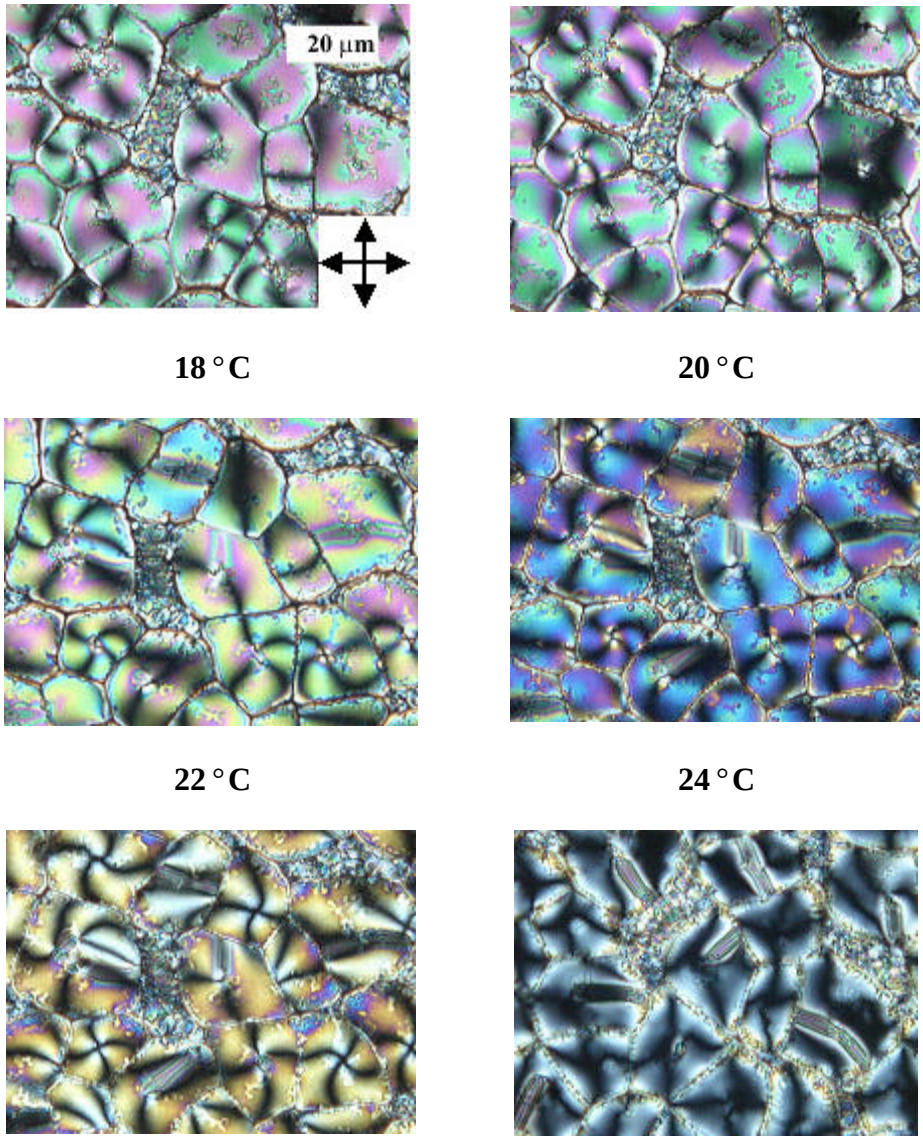

Figure 3.16. Polarized microscopic graphs (under crossed polarizers) showing a broad conical-to-homeotropic anchoring transition which occurred from 18 to 29 °C (note that the sample was rotated by a few of degrees in these images).

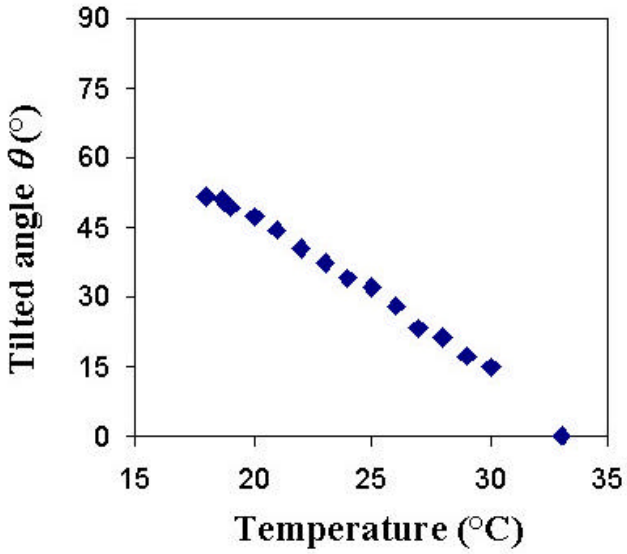

Figure 3.17. Plot of tilt angle against temperature during a conical-to-homeotropic anchoring transition in Figure 3.16.

3.3.4. Anchoring of TL205 in contact with polymethacrylate matrices

PDLC films were also made from the TL205 and methacrylates using the photopolymerization-induced phase separation. It is found that the anchoring conditions become dramatically different only due to introduction of α-methyl group into the polymer backbone (Table 3.4). For example, poly (*n*-octyl methacrylate) provides planar anchoring of TL205 instead of homeotropic anchoring as we predicted, based on the effect of the side chain length on the anchoring in the nematic fluids/polyacrylate system. TL205 in contact with poly(*n*-decyl methacrylate) even shows two anchoring transitions, a C-to-H transition at lower temperature and a H-to-P at higher temperature close to T_{NI}. The possible reason is still unknown.

Table 3.4. Anchoring behavior of the PDLCs made from TL205 and methacrylates with different side chains.

Side chain of methacrylate	monomer structure	T_t (°C)
n-pentyl	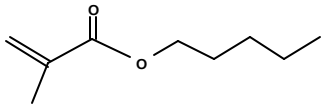	planar from 10°C to 84°C (T_{NI})
n-hexyl	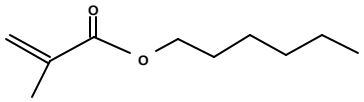	82
n-octyl	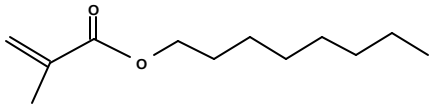	planar from 10°C to 84°C
n-decyl	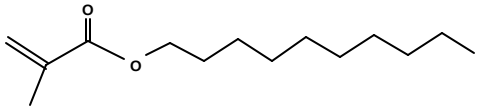	C-to–H, T_{t1} =36; H-to-P, T_{t2}=79

3.3.5. Measurements of polar anchoring energy

The Bloch wall defect (a defect caused by opposite twist of the two adjacent nematic domains, see schematic in Figure 3.3) was found in the nematic LC/polyacrylate composites with a temperature-driven anchoring transition. Such defects are formed at many places through a PDLC film if the temperature of the film is quenched through the H-to-P anchoring transition temperature, T_t, during which the anchoring changes from planar to homeotropic. The polarized microscopic observations of such walls are summarized as follows:

3.3.5.1. Optical characteristics of Bloch walls

A Bloch wall observed between cross polarizers shows symmetric color bands with respect to the center axis of the wall (Figure 3.18a). The color sequence from either edge of the wall to the center follows that of the Michel-levy birefringence chart.[90] There is a polymer filament at the right edge of the wall in Figure 3.18a, disturbing the local director structure. If the monochromatic light source is used, the wall between cross polarizers shows interference fringes parallel to the center axis (Figure 3.18b). On removal of the analyzer, the wall shows no contrast to the surrounding media that is homeotropically aligned when the wall is aligned perpendicular to the polarizer. It is due to the fact that the light with polarization perpendicular to the optical axis of the nematic molecules "sees" only the ordinary refractive index of the LC. But, the wall shows the best contrast when it aligns parallel to the polarizer, which is due to the largest refractive index variation across the width of the wall, i.e., from n_o at the edge to n_e at the center of the wall. This refractive index variation works as a focusing lens that forms a thin bright line image at several micrometers above the top of the wall.[93] All of these above

observations are consistent with the structure in Figure 3.3, suggesting us that the observed defect is a Bloch wall.

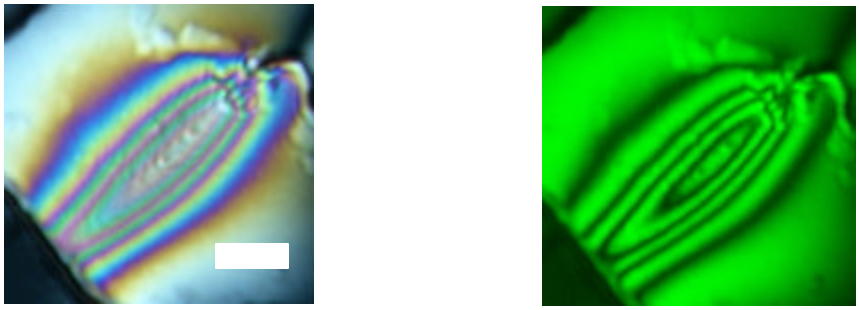

(a) **(b)**

Figure 3.18. Polarized micrographs of a Bloch wall: (a) under white light illumination; and (b) under monochromatic illumination of 532 nm. The scale bar in (a) is 10 μm.

3.3.5.2. Anchoring energy and its temperature dependence

According to Ryschenkow and Kleman,[60] polar anchoring energy strength (W_p) can be estimated from the observation of the Bloch wall. If the wall contains only pure twist deformation, equation (3.3) or (3.4) can be used for calculation. For instance, we estimated the anchoring energy of TL205 at a polyacrylate surface to be ~ 1×10^{-2} erg/cm^2 if h= 25μm, d= 9μm, and assuming twist elastic constant K_{22} = 10 pN (Appendix A), where h and d were measured by confocal microscope and polarized light microscope, respectively. The extrapolation length, $b = \frac{K_{22}}{W_p}$ = 1 μm. However, in this case, b << h, implying that the wall is a diffuse wall instead of a pure twist wall.[60] To improve the accuracy of this method based on equation 3.3, a wall structure close to that of pure twist wall is required, which was realized by reducing the sample thickness in our experiments.

It was found that the width of the wall changes as the temperature changes. The temperature variation of the Bloch wall was observed using a polarized light microscope equipped with a Linkam hotstage, which controls the temperature with accuracy up to 0.1 °C. This allows us to measure the temperature dependence of polar anchoring energy around the anchoring transition temperature, which will be helpful for understanding the mechanism of the anchoring transitions. In order to measure W_p as a function of temperature, the temperature dependence of twist elastic constant, K_{22}, has to be known. Usually, K_{22} is proportional to the order parameter of a nematic phase that drastically changes only around T_{NI}.[94] If the anchoring transition is far below T_{NI} (e.g., around room temperature), it is reasonable to assume K_{22} to be a constant within a few degree change of temperature. The absolute value of K_{22} is not important here since it doesn't affect the trend of W_p (T) calculated by using equation 3.3.

In the films with a homeotropic-to-planar anchoring transition (either a sharp one or broad one as we mentioned above), the width of the wall increases when the temperature is increased closer to T_t (Figure 3.19), consistent with the previous observation that the anchoring energy shows a minimum around T_t.[62,81] As an example, the anchoring energy versus temperature in a broad transition occurring near room temperature is plotted in Figure 3.20a.

In contrast, upon heating the film with a conical-to-homeotropic anchoring transition, the polar anchoring energy continuously increases and reaches a maximum value when this transition is over. The plot of anchoring energy versus temperature during such a broad transition is shown in Figure 3.20b. The deviation from the

monotonic trend around 20°C is likely due to that the widening of Bloch wall is limited by polymer wall boundary when the temperature decreases.

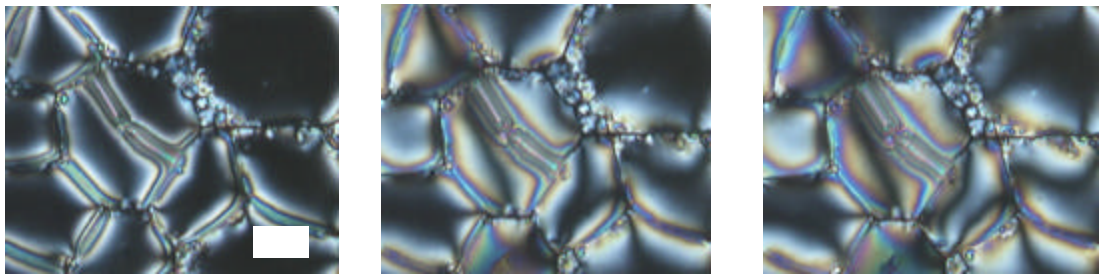

(a) 20.0 °C (b) 21.6 °C (c) 22.0 °C

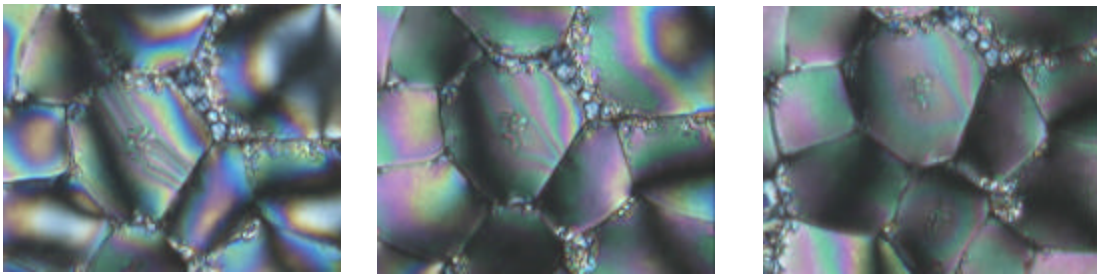

(d) 22.7 °C (e) 23.3 °C (f) 24.0 °C

Figure 3.19. Polarized light micrographs (crossed polarizers) showing the temperature dependence of the width of a Bloch wall near the H-to-P transition temperature (T_t is from 21.5 to 24.0 °C). The sample was made by the copolymerization of C10A and isobornyl acrylate (25/75, w/w). The scale bar is 10 μm.

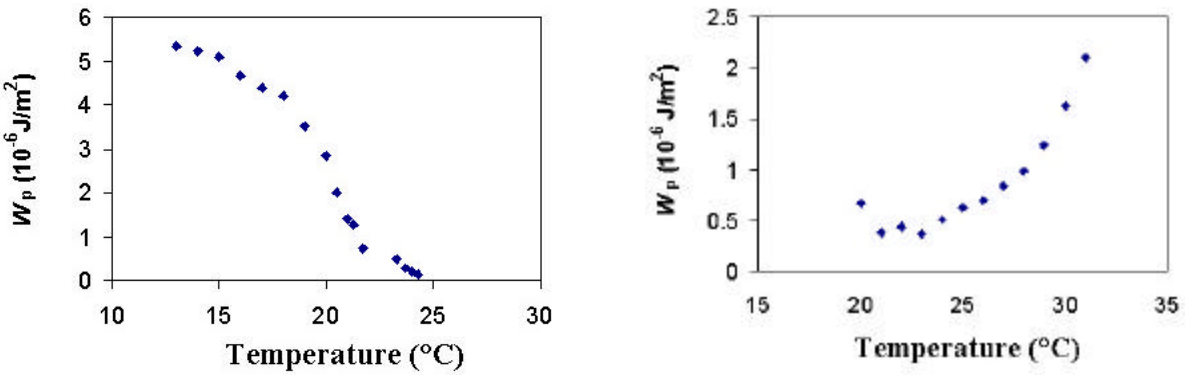

(a) **(b)**

Figure 3.20. Anchoring energy as a function of temperature in the PDLC film with a homeotropic-to-planar anchoring transition (a), and the film with a conical-to-homeotropic anchoring transition (b).

3.4. Conclusions

(1) The alignment of nematic fluids dispersed in contact with surface is found to be sensitive to the length, branching of the polymer side chains, and mixing of two different side chains (copolymers) at the interface, but insensitive to morphology of the LC-polymer composite films. Tilt angle of the alignment of the bulk nematic phase may be normal, parallel or highly tilted to the surface, depending on the side chain structure of underlying polymer substrates. This control of LC alignment is attributed to the molecular interactions between the side chain of polymers and nematic molecules.

(2) Tilted side chain conformation of poly (1-methylheptyl or 1,1-dimethylhexyl acrylate) at interface is proposed to explain the particular planar anchoring of nematic fluids in contact with these polymer surfaces.

(3) A broad homeotropic-to-planar or planar–to-homeotropic anchoring transition is found at the surfaces of the copolymer of two dissimilar acrylates (one with linear side

chain, the other with branched one), in contrast to sharp homeotropic-to-planar anchoring transition found in the case of homopolymers of linear alkyl acrylates. This is attributed to competition between two opposing anchoring forces arising from different polymer side chains at the interface. Temperature dependences of the two alignment tendencies are different, resulting in a double anchoring transition observed at some copolymer surfaces.

(4) The relationship between the anchoring transition temperature (T_t) and the composition of the monomer mixture for copolymerization of $2EH_xA$ with C7A, C8A or C10A, shows a plateau in T_t when the percentage of 2-EhxA is less than 50 mol%. Reactivity ratio difference between the two comonomers is suggested to cause such a plateau.

REFERENCES

[1] Yokoyama, H. "Interfaces and thin films," in *Handbook of Liquid Crystal Research*; Collings, P. J.; Patel, J. S., Eds.; Oxford University Press: New York, 1997, and the literatures within.

[2] Grandjean, F. *Bull. Soc. Fr. Mineral. Cristallogr.* **1916**, *39*, 164.

[3] Mauguin, C. *Bull. Soc. Fr. Mineral. Cristallogr.* **1911**, *34*, 71.

[4] Lehmann, O. in *Handbuch der Biologischen Arbeitsmeithoden,* Abderhalden, E., Ed.; Urban and Schwarzenberg: Berlin, 1922, p123.

[5] Jerome, B. "Surface effects and anchoring in liquid crystals," *Rep. Prog. Phys.* **1991**, *54*, 391-451 and the literatures within.

[6] Geary, J. M.; Goodby, J. M.; Kmetz, A.R.; Patel, J.S. "The mechanism of polymer alignment of liquid-crystal materials," *J. Apply. Phys.* **1987**, *62*, 4100-8.

[7] Ichimura, K. "Photoalignment of Liquid-Crystal Systems," *Chem. Rev.* **2000**, *100*, 1847-73 and the literatures within.

[8] Ichimura, K.; Suzuki, Y.; Seki, T.; Hosoki, A.; Aoki, K. "Reversible change in alignment mode of nematic liquid crystals regulated photochemically by command surfaces modified with an azobenzene monolayer," *Langmuir* **1988**, *4*, 1214-6.

[9] Chigrinov, V. Prudnikova, E.; Kozenkov, V.; Kwok, H.; Akiyama, H.; Kawara, T.; Takada, H.; Takatsu, H. "Synthesis and properties of azo dye aligning layers for liquid crystal cells," *Liq. Cryst.* **2002**, *29*, 1321-7.

[10] Gibbons, W. M.; Shannon, P. J.; Sun, S. T.; Swetlin, B. J. "Surface-mediated alignment of nematic liquid crystals with polarized laser light," *Nature* **1991**, *351*, 49-50.

[11] Ichimura, K. Hayashi, Y.; Kawanishi, Y.; Seki, T.; Tamaki, T.; Ishizuki, N. "P-Cyanoazobenzene as a command molecule for azimuthal anisotropy regulation of a nematic liquid crystal upon exposure to linearly polarized visible light," *Langmuir* **1993**, *9*, 857-60.

[12] Ichimura, K.; Hayashi, Y.; Goto, K.; Ishuzuki, N. *Thin Solid Films* **1993**, 235, 101-7.

[13] Thieghi, L.T.; Barberi, R.; Bonvent JJ, Oliveira, E. A.; Giacometti, J. A.; Balogh, D. T. "Manipulation of anchoring strength in an azo-dye side chain polymer by photoisomerization," *Phys. Rev. E*. **2003**, *67*, art. No. 041701.

[14] Serak, S.; Kovalev, A.; Agashkov, A.; Gleeson, H. F.; Watson, S. J.; Reshetnyak, V.; Yaroshchuk, O. "Laser-induced surface and bulk reorientation of the director in azo-dye-doped liquid crystal cells," *Opt. Commun.* **2001**, *187*, 235-47.

[15] Schadt, M.; Schmitt, K.; Kozinkov, V. "Surface-induced parallel alignment of liquid crystals by linearly polymerized photopolymers," *Jpn. J. Appl. Phys. Lett.* **1992**, *31*, 2155-64.

[16] Nishikawa, M.; Taheri, B.; West, J.L. "Mechanism of unidirectional liquid-crystal alignment on polyimides with linearly polarized ultraviolet light exposure," *Appl. Phys. Lett*. **1998**, *72*, 2403-05.

[17] Kim, J.H.; Acharya, B.R.; Kumar, S; Ha, K.R. "A method for liquid crystal alignment using in situ ultraviolet exposure during imidization of polyimide," *Appl. Phys. Lett.* **1998**, *73*, 3372-4.

[18] Skaife, J.J.; Abbott, N.L. "Quantitative Characterization of Obliquely Deposited Substrates of Gold by Atomic Force Microscopy: Influence of Substrate Topography on Anchoring of Liquid Crystals," *Chem. Mater.* **1999**, *11*, 612-23.

[19] Cognard, J. "Alignment of nematic liquid crystals and their mixtures," *Mol. Cryst. Liq. Cryst*. **1982**, Suppl, 1-77.

[20] Chaudhari, P.; Lacey, J.; Doyle, J.; Galligan, E.; Lien, S. C.; Callegari, A.; Hougham, G.; Lang, N. D.; Andry, P. S.; John, R.; Yang, K.H.; Lu, M.; Cai, C.; Speidell, J.; Purushothaman, S.; Ritsko, J.; Samant, M.; Stohr, J.; Nakagawa, Y.; Katoh, Y.; Saitoh, Y.; Sakai, K.; Satoh, H.; Odahara, S.; Nakano, H.; Nakagaki, J.; Shiota, Y. "Atomic-beam alignment of inorganic materials for liquid-crystal displays," *Nature* **2001**, *411*, 56-9.

[21] Stohr, J; Samant, M.G.; Luning, J.; Callegari, A.C.; Chaudhari, P.; Doyle, J.P.; Lacey, J.A.; Lien, S.A.; Purushothaman, S.; Speidell, J.L. "Liquid crystal alignment on carbonaceous surfaces with orientational order," *Science*, **2001**, *292*, 2299-302.

[22] Porte, G. "Tilted alignment of MBBA induced by short-chain surfactants," *J. Phys.* (France) **1976**, *37*, 1245-52.

[23] Gupta, V.K.; Abbott, N.L. "Self-Assembled Monolayers Formed from Alkanethiols on Obliquely Deposited Films of Gold as Uniform Anchors of Nematic Liquid Crystalline Phases," *Langmuir* **1996**, *12*, 2587-93.

[24] Gupta, V. K.; Abbott, N. L. "Design of surfaces for patterned alignment of liquid crystals on planar and curved substrates," *Science* **1997**, *276*, 1533-6.

[25] Miller, W.J.; Gupta, V.K.; Abbott, N.L.; Tsao, M.W.; Rabolt, J.F. "Comparison of the anchoring of nematic liquid crystals on self-assembled monolayers formed from semifluorinated thiols and alkanethiols," *Liq. Cryst.* **1997**, *23*, 175-84.

[26] Shah, R.R.; Abbott, N.L. "Principles for measurement of chemical exposure based on recognition-driven anchoring transitions in liquid crystals," *Science* **2001**, *293*, 1296-9.

[27] Folkers, J.P.; Laibinis, P.E.; Whitesides, G. M.; Deutch, J. "Phase behavior of two-component self-assembled monolayers of alkanethiolates on gold," *J. Phys. Chem.* **1994**, 98, 563-71.

[28] Kumar, A.; Abbott, N. L.; Kim, E.; Biebuyck, H.A.; Whitesides, G.M. "Patterned Self-Assembled Monolayers and Meso-Scale Phenomena," *Accounts Chem. Res.* **1995**, 28, 219-26.

[29] Abbott, N.L.; Gupta, V.K.; Miller, W.J.; Shah, R.R. "Orientations of liquid crystals on self-assembled monolayers formed from alkanethiols on gold," *ACS Sym. Ser.* **1998**, *695*, 81-102.

[30] Luk, Y.Y.; Abbott, N.L. "Surface-driven switching of liquid crystals using redox-active groups on electrodes," *Science* **2003**, *301*, 623-6.

[31] Barreman D.W. "Solid Surface Shape and the Alignment of an Adjacent Nematic Liquid Crystal," *Phys. Rev. Lett.* **1972**, *28*, 1683-6.

[32] Rastegar, A.; Skarabot, M.; Blij, B.; Rasing, T.; "Mechanism of liquid crystal alignment on submicron patterned surfaces," *J. Apply. Phys.* **2001**, *89*, 960-4.

[33] Lee, B.W.; Clark, N.A. "Alignment of liquid crystals with patterned isotropic surfaces," *Science* **2001**, *291*, 2576-80.

[34] Kim, J.H.; Yoneya, M.; Yokoyama, H. "Tristable nematic liquid-crystal device using micropatterned surface alignment," *Nature*, **2002**, 420, 159-62.

[35] Kim, J.H.; Yoneya, M.; Yamamoto, J.; Yokoyama, H. "Surface alignment bistability of nematic liquid crystals by orientationally frustrated surface patterns," *Appl. Phys. Lett.* **2001**, 78, 3055-7.

[36] Bos, P.J.; Fredley, J.; Li, J.; Rahman, J. in *Liquid Crystals In Complex Geometry*; Crawford, G. P.; Zumer S., Eds; Taylor & Francis: London, 1996.

[37] Seo, D.S. "Anchoring strength and high pretilt angle in NLC on rubbed organic solvent soluble polyimide surfaces with trifluoromethyl moieties," *J. Korean Phys. Soc.*, **2000**, *36*, 29-33.

[38] Ge J J; Li C Y; Xue G; Mann I K; Zhang D; Wang S Y; Harris F W; Cheng S Z; Hong S C; Zhuang X; Shen Y R "Rubbing-induced molecular reorientation on an alignment surface of an aromatic polyimide containing cyanobiphenyl side chains," *J. Am. Chem. Soc.* **2001**, 123, 5768-76.

[39] Lee, J.H.; Seo, D.S. "Novel alignment method for control of high pretilt angle by using a solvent dipping effect on polymer surfaces," *Liq. Cryst.* **2000**, *27*, 711-3.

[40] Filas, R. W.; Patel, J. S. "Chemically induced high-tilt surfaces for liquid crystals," *Appl. Phys. Lett.* **1987**, *50*, 1426-8.

[41] Oh, S.K.; Nakagawa, M.; Ichimura, K. "Relationship between the ability to control liquid crystal alignment and wetting properties of calix[4]resorcinarene monolayers," *J. Mater.Chem.* **2001**, *11*, 1563-9.

[42] Becker, M.E.; Kilian, R.A.; Kismoswski, B.B.; Mlynski, D.A. "Alignment properties of rubbed polymer surfaces," *Mol. Cryst. Liq. Cryst.***1986**, *132*, 167-80.

[43] Ong, H.L.; Hurd, A.J.; Meyer, R.B. "Alignment of nematic liquid crystals by inhomogeneous surfaces," *J. Appl. Phys.* **1985**, *57*, 186-92.

[44] Ramdane, O. O.; Auroy, P.; Forget, S.; Raspaud, E.; Martinot-Lagarde, P.; Dozov, I. "Memory-free conic anchoring of liquid crystals on a solid substrate," *Phys. Rev. Lett.* **2000**, *84*, 3871-4.

[45] Patel, J. S.; Yokoyama, H. "Continuous anchoring transition in liquid crystals," *Nature* **1993**, *362*, 525-7.

[46] Mauguin, C. *C. R. Acad. Sci. Paris* **1913**, *156*, 1246-7.

[47] Creagh, L.T.; Kmetz, A.R. "Mechanism of surface alignment in nematic liquid crystals," *Mol. Cryst. Liq. Crystal.* **1973**, *24*, 59-68

[48] Naemura, S. "Polar and nonpolar contributions to liquid-crystal orientations on substrates," *J. Appl. Phys.* **1980**, *51*, 6149-59.

[49] Chen, W.; Feller, M.; Shen, Y.R. "Investigation of anisotropic molecular orientational distributions of liquid-crystal monolayers by optical second-harmonic generation," *Phys. Rev. Lett.* **1989**, *63*, 2665-8.

[50] Toney, M.F.; Russell, T. P.; Logan, J. A.; Kikuchi, H.; Sands, J. M.; Kumar, S. K. "Near-surface alignment of polymers in rubbed films," *Nature* **1995**, *374*, 709-11.

[51] Ito, N.; Sakamoto, K.; Arafune, R.; Ushioda, S. "Relation between the molecular orientations of a very thin liquid crystal layer and an underlying rubbed polyimide film," *J Appl. Phys.* **2000**, *88*, 3235-41.

[52] Hiltrop, K.; Stegemeyer, H.; "On the orientation of liquid crystals by monolayers of amphiphilic molecules," *Ber. Bunsen. Phys. Chem.* **1981**, *85*, 582-8.

[53] Huang, J.Y.; Superfine, R.; Shen, Y.R. "Nonlinear spectroscopic study of coadsorbed liquid-crystal and surfactant monolayers: conformation and interaction," *Phys. Rev.* A **1990**, *42*, 3660-3.

[54] Kuhnau, U.; Petrov, A.G.; Klose, G.; Schmiedel, H. "Measurements of anchoring energy of a nematic liquid crystal, 4-cyano-4'-n-pentylbiphenyl, on Langmuir-Blodgett films of dipalmitoyl phosphatidylcholine," *Phys. Rev.* E **1999**, *59*, 578-85.

[55] Gupta, V.K.; Abbott, N.L. "Azimuthal anchoring transition of nematic liquid crystals on self-assembled monolayers formed from odd and even alkanethiols," *Phys. Rev.* E **1996**, *54*, R4540-3.

[56] Pieranski, P.; Jerome, B.; "Adsorption-induced anchoring transitions at nematic liquid crystal-crystal interfaces," *Phys. Rev.* A. **1989**, *40*, 317-22.

[57] Kitzerow, H.S.; Jerome, B.; Pieranski, P. "Strain-induced anchoring transitions," *Physica* A. **1991**, *174*, 163-94.

[58] Skaife, J.J.; Abbott, N.L. "Influence of Molecular-Level Interactions on the Orientations of Liquid Crystals Supported on Nanostructured Surfaces Presenting Specifically Bound Proteins," *Langmuir*, **2001**, *17*, 5595-5604.

[59] Zhu, Y.M.; Lu, Z.H.; Jia, X.B.; Wei, Q. H.; Xiao, D.; Wei, Y.; Wu, Z. H.; Hu, Z. L.; Xie, M. G. "Anchoring transition of liquid crystals on crown ether monolayers," *Phys. Rev. Lett*. **1994**, *72*, 2573-76.

[60] Ryschenkow, G.; Kleman, M. "Surface defects and structural transitions in very low anchoring energy nematic thin films," *J. Chem. Phys.* **1976**, *64*, 404-12.

[61] Dilisi, G.A.; Rosenblatt, C.; Griffin, A.C.; Hari, U. "Behavior of the anchoring strength coefficient near a structural transition at a nematic-substrate interface," *Liq. Cryst.* **1990**, *7*, 353-60.

[62] Amundson, K. R.; Srinivasarao, M. "Liquid-crystal-anchoring transitions at surfaces created by polymerization-induced phase separation," *Phys. Rev. E.* **1998**, *58*, R1211-4.

[63] Crossland, W.A.; Morrissy, J.H.; Needham, B. "Tilt angle measurements of nematic phases of cyano-biphenyls aligned by obliquely evaporated films," *J. Phys. D* **1976**, *9*, 2001-14.

[64] Wahlstrom, E.E. *Optical Crystallography* 4th Ed. Wiley: New York, 1969.

[65] Scheffer, T.J.; Nehring, J.; "Accurate determination of liquid-crystal tilt bias angles," *J. Appl. Phys*. **1977**, *48*, 1783-92.

[66] Lin, Q.; Zhu, H.; Tang,Y.; Yang, F. Gao, H. "Accurate optical determination of liquid crystal tilt angle by the half-leaky guided mode technique," *Displays*, **2000**, *21*, 111-9.

[67] Mattoussi, H; Srinivasarao, M.; Katz, P.; Berry, G.C. "Refractive indexes dispersion and order of lyotropic liquid crystal polymers," *Macromolecules* **1992**, 25, 2860-8.

[68] Born, M.; Wolf, E. *Principles of optics: electromagnetic theory of propagation, interference and diffraction of light*, 5th Ed., Pergamon Press: Oxford, 1975.

[69] Montarou, C.C.; Gaylord, T.K.; Villalaz. R.A.; Glytsis. E.N. "Colorimetry-based retardation measurement method with white-light interference," *Appl. Opt.* **2002**, *41*, 5290-7.

[70] Yokoyama, H. "Surface anchoring of nematic liquid crystals," *Mol. Cryst. Liq. Cryst.* **1988**, *165*, 265-316.

[71] Rapini, A.; Papoular, M. *J. Phys. (Paris) Colloq.* **1969**, *30*, C4-54.

[72] Slavinec, M.; Crawford, G. D.; Kralj, S; Zumer, S. "Determination of the nematic alignment and anchoring strength at the curved nematic-air interface," *J. Appl. Phys.* **1997**, *81*, 2153-6.

[73] Seo, D.S.; Muroi, K.; Isogami, T. "Polar anchoring strength and the temperature dependence of nematic liquid crystal (5CB) aligned on rubbed polystyrene films," *Jpn. J. Appl. Phys.*, **1992**, *31*, 2165-9.

[74] Sugimura, A.; Miyamoto, T.; Tsuji, M.; Kuze, M. "Determination of the unified surface-anchoring energy of a nematic liquid crystal on a polymer substrate," *Appl. Phys. Lett*. **1998**, *72*, 329-31.

[75] Yang, F.; Sambles, J.R.; Dong, Y.; Gao, H. "Fully leaky guided wave determination of the polar anchoring energy of a homogeneously aligned nematic liquid crystal," *J. Appl. Phys.* **2000**, *87*, 2726-35.

[76] Vilfan, M; Mertelj, A.; Copic, M. "Dynamic light scattering measurements of azimuthal and zenithal anchoring of nematic liquid crystals," *Phys. Rev. E.* **2002**, *65*, art. No. 041712.

[77] Kleman, M. *Points, Lines and Walls*; John Wiley & Sons: New York, 1983; ch.9.

[78] Guo, X.A.; Hunter, A.D.; Chen, J. "Preparation and characterization of acrylates and polyacrylates having variable fluorine contents and distributions," *J. Poly. Sci*. Part A: *Polym. Chem*. **1994**, *32*, 47-56.

[79] Mcfarland, C. A.; Koenig, J.L.; West, J.L. "Analysis of polymer-dispersed liquid crystals by infrared spectroscopy," *Applied Spectroscopy* **1993**, *47*, 321-9.

[80] Amundson, K.; van Blaaderen, A.; Wiltzius, P. "Morphology and electro-optic properties of polymer-dispersed liquid-crystal films," *Phys. Rev. E.* **1997**, *55*, 1646-54.

[81] Zhou, J.; Collard, D. M.; Park, J. O.; Srinivasarao, M. "Control of the anchoring behavior of polymer-dispersed liquid crystals: Effect of branching in the side chains of polyacrylates," *J. Am. Chem. Soc.* **2002**, *124*, 9980-1.

[82] Andrews, R.J.; Grulke, E.A. in *Polymer Handbook*; Brandrub, J., Immergut, E.H. Eds.; John Wiley and Sons: New York, 1999; VI-200.

[83] Serbutoviez, C.; Kloosterboer, J.G.; Boots, H.M.J.; Touwslager, F.J. "Polymerization-Induced Phase Separation. 2. Morphology of Polymer-Dispersed Liquid Crystal Thin Films," *Macromolecules* **1996**, *29*, 7690-8.

[84] Roussel, F.; Canlet, C.; Fung, B.M. "Morphology and orientational order of nematic liquid crystal droplets confined in a polymer matrix," *Phys. Rev. E.* **2002**, *65*, art. No. 021701.

[85] Sharlow, M.F.; Gelbart, W.M. "On the parallel perpendicular transition for a nematic phase at a wall," *Liq. Cryst.* **1992**, *11*, 25-30.

[86] Aliev, F.M.; Zgonnik, V.N. "Thermo-optics and thermal-stability of poly (alkyl methacrylates) in porous matrices," *Eur. Polym. J.* **1991**, *27*, 969-73.

[87] Walba, D. M.; Korblova, E.; Shao, R.; Maclennan, J.E.; Link, D.R.; Glaser, M.A.; Clark, N.A. "A ferroelectric liquid crystal conglomerate composed of racemic molecules," *Science* **2000**, *288*, 2181-4.

[88] Collard, D.M.; Lillya, C.P. "Structure-property relationships for the thermal phase behavior of discotic liquid crystals: the effect of branching and unsaturation in the side chains of disklike molecules," *J. Am. Chem. Soc.* **1991**, *113*, 8577-83.

[89] Greenley, R. Z. In *Polymer Handbook*, Brandrup, J.; Immergut, E. H.; Grulke E. A. Eds. John Wiley and Sons: New York, 1999; II-268.

[90] Bloss, F. D. *Optical crystallography*; Mineralogical Society of America: Washington, D. C., 1999; ch.6. and ch. 8.

[91] George, A. K. "Optical anisotropy of nematic liquid crystals,"*Phys. Chem. Liq.*; **1998**, *37*, 65-71.

[92] Dubois-Violette, E.; de Gennes, P.G. *J. Phys.* (France) **1975**, *36*, L-255.

[93] Srinivasarao, M.; Park, J. O. "Magnetic field induced instabilities in nematic solutions of polyhexylisocyanates," *Polymer* **2001**, *42*, 9187-91.

[94] Sheng, P. in *Introduction to Liquid Crystals*; Priestley, E. B.; Wojtowicz, P. J.; Sheng, P., Eds; Plenum Press: New York, 1974.

CHAPTER 4

A LC-POLYMER COMPOSITE FOR FLEXIBLE LIQUID CRYSTAL DISPLAYS BASED ON REVERSE SWITCHING OF NEMATICS

4.1. Introduction

Liquid crystal displays (LCD) are now widely used for monitors of computers, which requires high contrast, a wide viewing angle, fast response times, low switching voltages (hence low power consumption). Most of the LCDs nowadays are still based on twisted nematic devices (TN) or super-twisted nematic devices (STN).[1] However, conventional TN devices (see Figure 3.1) suffers from several disadvantages such as limited contrast, narrow viewing angles,[2] and the requirement of rubbed polymer layers as substrate.

On the other hand, a display device based on typical polymer-dispersed liquid crystal structure (PDLC) (see Figure 2.1) works by light scattering principle: scattering light in the field-off state and being transparent in the field-on state. The PDLC device has advantages of ease of manufacturing (a rub-free process), high brightness (no polarizers used), and better viewing angles compared with the TN device. The PDLC structure is also compatible with emerging applications of flexible display devices due to the mechanical flexibility afforded by polymer network.[3] The applications of light-weight and flexible displays are, for example, smart cards, personal digital assistants, electronic-books, head mounted devices, etc.[4] However, the disadvantages of a traditional PDLC display are requirement of a high driving voltage (due to smallness of LC droplets dispersed in polymer matrix), and the limited contrast (the off state is milk white instead of being completely dark).

A LCD that is able to keep most of the advantages of the PDLC device but overcomes its shortcomings would be desirable. Here we demonstrate a LC-polymer composite system potentially useful for flexible LCDs with high contrast ratio and low switching voltages, which is made similarly as traditional PDLC films but has a cellular morphology of encapsulated LC domains. Such a device works by using a homeotropic aligned nematic fluid with negative dielectric anisotropy ($-\Delta\varepsilon$), which is in contrast to a TN device or a traditional PDLC where a nematic fluid with positive dielectric anisotropy is used. The LC devices based on homeotropically aligned nematic fluids have been previously reported.[2,5,6] In these previous works, homeotropic alignment is usually obtained by deposition of surfactant molecules or special polymers to substrates and a nematic fluid is sandwiched between two pre-treated surfaces to assemble a LC cell. However, the devices based on such a structure are sensitive to external mechanical forces as there are no binders between the two substrates that can sustain mechanical forces, which are thus not good candidates for flexible displays.[7]

The structure and working principle of the LC-polymer composite we propose for the application of LCD is illustrated in Figure 4.1 It is actually a PDLC film with a cellular morphology where the top and bottom polymer substrates provide the homeotropic anchoring of a nematic fluid with $-\Delta\varepsilon$ and vertical polymer walls act as binders connecting the two substrates. The nematic fluid is aligned normal to the substrate when electric field is off and switches parallel to the substrate due to $-\Delta\varepsilon$ when electric field is on. The surface doesn't have any in-plane anisotropy so that alignment of nematic phase at the field-on state is a degenerate planar alignment and LC forms an electric field-induced Schlieren texture.

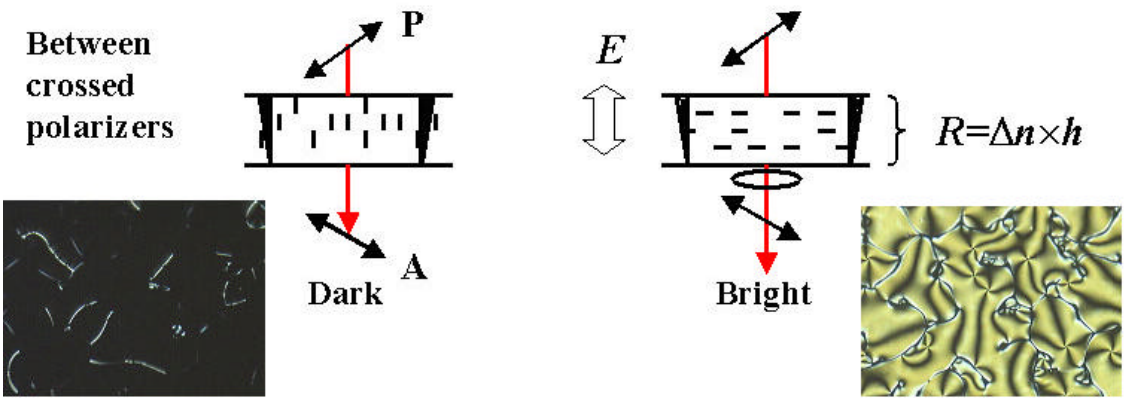

Figure 4.1. Structure and switching principle of a LC display based on the homeotropically aligned nematic LC with a negative $\Delta\varepsilon$. P: polarizer, A: analyzer, **E** is electric field and R is optical retardation given by the birefringence of LC times the sample thickness *h*. The short black bars represent the LC director and the two wedge shape lines between the top and bottom substrates represent vertical polymer walls. The microscopic pictures of both the field-on and field-off states were taken under crossed polarizers.

For the proposed LCD in Figure 4.1, the field-off state can be very dark if a perfect homeotropic alignment is obtained.[8] The brightness (i.e., the intensity of transmitted light) of the field-on state depends on optical retardation, R (i.e., effective birefringence of LC phase, (n_e-n_o), times thickness, *h*), which can be described by equation 4.1 if the light is normally incident.[9,10]

$$I = \sin^2(2\phi)\sin^2\left(\frac{\pi}{\lambda}(n_e - n_o)\cdot h\right) \tag{4.1}$$

where f is azimuthal angle of the nematic director. Although all of the f angles exist for the degenerate planar alignment in the field-on state, the total intensity still satisfies:

$$I_{total} \propto \sin^2\left(\frac{\pi}{\lambda}(n_e - n_o)\cdot h\right) \tag{4.2}$$

Based on equation 4.2, the transmittance of a monochromatic light beam versus the optical retardation, R, is plotted (Figure 4.2). As this figure suggests, both thickness

and birefringence have to be chosen appropriately to achieve the maximum output of light (corresponding to peaks of the curve), thereby the best contrast ratio.

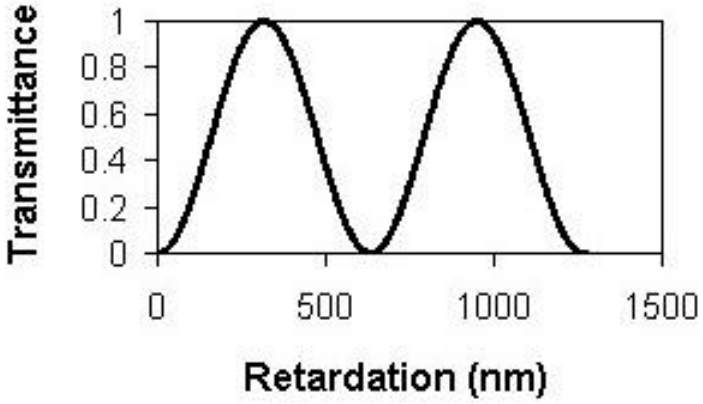

Figure 4.2. The transmitted intensity as function of the retardation (R) for a uniaxial anisotropic sample between the crossed polarizers. R varies from 0 to 1300 nm and the wavelength in equation 4.1 is chosen as 633 nm.

The switching process of the LC cell in Figure 4.1 is a Freedericksz transition. According to equations 1.12 and 1.13, i.e., $V_c = E_c \cdot h = p\sqrt{\frac{4Kp}{\Delta e}}$, the threshold electric field strength E_c is proportional to the inverse of h while the threshhold voltage V_c is independent of the thickness *h.*

The response times of a Freedericksz transition is given by: [11]

$$\tau_{rise} = \gamma_1 h^2 (\Delta e\, e_0 V^2 - K\pi^2)^{-1} \quad (4.3a)$$

$$\tau_{decay} = \gamma_1 h^2 (K\pi^2)^{-1} \quad (4.3b)$$

where γ_1 is rotational viscosity coefficient, V is the applied voltage, e_0 is the dielectric constant, K and h are the elastic constant and the sample thickness. Therefore, there is quadratic reduction of both on and off response times when decreasing the thickness, *h*.

It should be noted that the the above equations for V_c, E_c and response times are valid when the strong anchoring condition prevails, where the anchoring energy is very

large so that the alignment of LC at surface is fixed regardless of the magnitude of applied electric field.[12] This is in fact not the case of our system where a weak anchoring exists, hence equation 1.12, 1.13 and 4.3 should be modified to include the terms of anchoring energy. However, for simplicity of the discussions below and also we won't lose the generality, these equations can still be used to estimate the trend of threshold voltage/electric field and response times.

4.2. Experimental

Preparation of LC-polymer composite films and film morphology. The nematic fluid, MLC 6608 ($\Delta\varepsilon$= -4.2, Δn=0.083, T_{NI} = 90°C), is obtained from Emerck Industries. The n-alkyl acrylates and triacrylate were obtained from Scientific Polymer Products Inc. and used without further purification. The MLC 6608, monofunctional acrylate monomers and 1,1,1-trimethylol propane triacrylate were mixed in an 76:22:2 w/w ratio. The triacrylate is added to provide rigidity to the PDLC structure. The mixture was placed in a 16-μm gap of an ITO coated glass cell and illuminated with ultraviolet irradiation at 23 °C. A slow polymerization process is initiated by irradiation at 360 nm with low intensity (180-300 $\mu W/cm^2$), followed by curing at higher intensity (5 mW/cm^2).[13,14] The reactive mixture with higher LC composition (nematics, monofunctional acrylate and triacrylate ratio, 92:7:1 w/w) was also used to prepare the film that contains less amount of polymer walls in the film. The photo-polymerization was carried at 68 °C in the latter case.

Measurement of electro-optical properties. The electro-optical properties were measured using the set-up shown in Figure 4.3. Two iris apertures were used to collect

the beam only along the forward direction. The polarizer (P) and analyzer (A) are set perpendicular to each other. To measure the switching voltage (V_{90}, the voltage required for the film to reach 90% of the maximum transmittance), a 1KHz, square-wave AC voltage was applied to the film. The voltage amplitude varied from 0 to 10 Volts by step-increase. The duration between two consecutive step-increase is 1000 ms to allow the equilibrium state of LC deformation to be achieved at every step. Rise and decay times are defined as the time interval between 10% to 90%, or 90% to 10%, respectively, of the total change between the "on" and "off" transmittance.[7] Both response times are measured with application of a 0.5 HZ or 1 Hz, square-wave DC voltage (the fixed amplitude of 10 volt is used). By using the thermal chamber, the above E-O properties can also be measured as function of temperature.

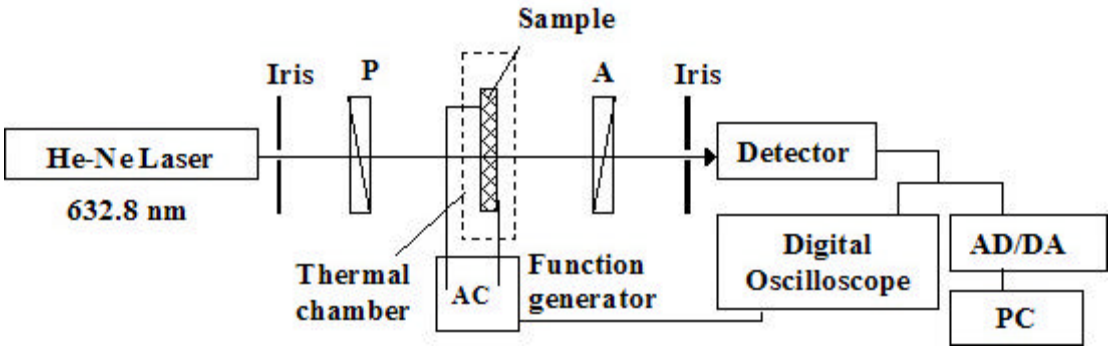

Figure 4.3. Apparatus for measurement of electro-optical properties of the LC/polymer composite film. P represents polarizer, A analyzer and AD/DA the data converter between computer (PC) and detector.

4.3. Results & Discussions

4.3.1. Anchoring behavior of MLC 6608 on different polyacrylate surfaces

For PDLC films prepared by photopolymerzation-induced phase separation of MLC 6608/acrylates system, a cellular morphology can be obtained using a slow photopolymerization process. The anchoring and anchoring transition temperature (T_t) of MLC 6608 in various polyacrylate matrices are evaluated and shown in Table 4.1 and Table 4.2. MLC 6608 at the surfaces of homopolymers of linear side chain acrylate, from *n*-hexyl through *n*-decyl acrylate, all show good homeotropic anchoring below H-to-P transition temperatures which is near $T_{NI,}$ while the branched side chain acrylates e.g., poly (2-ethylhexyl acrylate) provide only tilted or planar anchoring. If the copolymer of one linear side chain and one branched side chain acrylate is used instead of a homopolymer, the tendency of homeotropic alignment deceases as increasing the fraction of branched side chain acrylate (Table 4.2), which is similar to TL205/ poly(alkyl acrylates) system.

We study the electro-optical properties of these composite films made by using both homopolymerization or copolymerization.

Table 4.1. Effect of side chain length and branching on anchoring behavior of MLC 6608 at polyacrylate surfaces.

Acrylates	Homeotropic-to-planar transition temperature T_t /T_{NI} (°C)
n-hexyl acrylate (C6A)	80 / 89
n-heptyl acrylate (C7A)	81 / 89
n-octyl acrylate (C8A)	80 / 87
n-decyl acrylate (C10A)	83 / 89
2-ethylhexyl acrylate (2-EHA)	Tilted
Isobornyl acrylate	Planar

Table 4.2. Effect of copolymerization of *n*-decyl acrylate and isobornyl acrylate on anchoring behavior of MLC 6608.

Fraction of isobornyl acrylate (wt%)	H-to-P T_t /T_{NI} (°C)
0	80 / 87
50	53 / 87
55	41 / 88
65	18 / 88
>70	Planar

4.3.2. Plot of transmitted intensity versus applied voltage

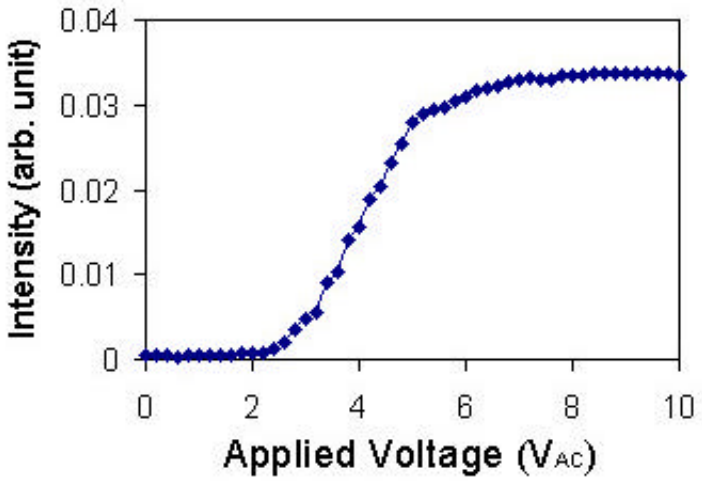

Figure 4.4. Transmitted intensity versus applied voltage for a composite film made from MLC 6608/ *n*-octyl acrylate (77/23 w/w in the prepolymerization mixture).

Figure 4.4 is a typical curve of Fredeerickz transition, from which both the switching voltage V_{90} and contrast ratio were measured to be 5.6V and 72 respectively. V_{90} is the voltage required to achieve 90% of the maximum intensity and the contrast ratio is defined as the ratio of the maximum intensity when the electric field is on and the intensity of "off " state.

To obtain a higher contrast, one can make either the "off" state darker or "on " state brighter. The major reason giving rise to high background intensity of the "off" state in the system we studied (see Figure 4.5a) is deviation from the perfect homeotropic alignment of the LC which is caused by polymer walls and polymer filaments distributed throughout the film. To improve this, a higher LC composition is used to in preparation of the LC-polymer composite film to increase the size of LC domains and reduce the amount of polymer walls and filaments.

It should be mentioned that in order to let photopolymerization of LC-monomer mixtures with a higher LC composition start from a single isotropic phase, a higher isothermal photopolymerization temperature is required. Using an empirical rule[15] (that 1% wt of acrylate results in a decrease of 3°C in T_{NI}), we found that the temperature of polymerization needs to be around 70°C for the photoreactive solution with the LC composition of 92 wt%. The polymerization was then carried out at that temperature. The resulting film in Figure 4.5b has sufficiently larger LC domains with a nice cellular morphology. The influence of polymer walls on optical texture of the film is obviously much less in (b) than in (a) of Figure 4.5. A higher contrast ratio is thus obtained, 270 for the film (b).

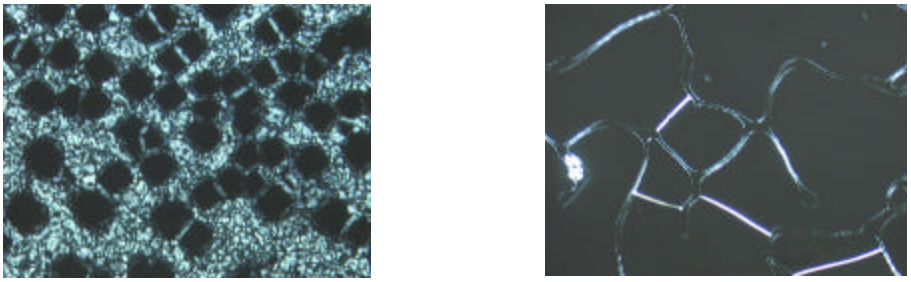

(a) LC composition = 77 wt% **(b) LC composition = 92 wt%**

Figure 4.5. Improvement of the contrast ratio using a darker off state. Both films were made from MLC6608 and *n*-octyl acrylate, but with different initial LC composition in the pre-polymerization mixture as indicated.

On the other hand, the contrast ratio can also be improved by increasing the output light intensity of "on" state. First, both the thickness and birefringence should be chosen to match one of those retardations corresponding to peaks in output intensity as shown in Figure 4.2. But it should be pointed out that the retardation in our experiments was not optimized for the wavelength of a He-Ne laser, 633nm. Second, from equation

4.1, the output intensity also depends on wavelength, which limits the optimum contrast achieved by controlling the optical retardation being valid only for a monochromatic light, not for a broad wavelength range, e.g., white light. Rosenblatt and coworkers proposed to increase the output light efficiency in "on" state by adding a small amount of chiral dopant into homeotropic aligned nematic fluids (it then becomes chiral nematic phase).[5] The principle of improved contrast is due to optical rotation of the polarization of light by the helical structure of the chiral nematic phase (i.e., similar to wave-guiding effect caused by mechanical twist in TN display devices). The optimum rotation is set to be $\pi/2$ so as to allow an incident linearly polarized light to fully pass the cross polarizers. The output intensity in such a LC cell is not sensitive to the wavelength, λ, thus having high contrast ratio for a broad range of wavelength as long as the pitch is much greater than λ (i.e., satisfying Mauguin limit for cholesteric phase[16]).

4.3.3. Response times and their composition and temperature dependences

An example of the results of the response time measurement is shown in Figure 4.6. It is interesting to note that during both "field-on" and "field-off" process, the transmittance shows a transient intensity modulation. The local magnification of the "switching-on" process is also shown. This intensity modulation is consistent with the intensity as a sine square function of the retardation (Figure 4.2). But it is noted that the transmittance doesn't reach zero during rise (switching-on) process and decay (switching-off) and also the transients in rise and decay processes are not symmetric as predicted from Figure 4.2. This may be due to either non-equilibrium process involved in fast switching process or low time-resolution of AD/DA converter that can't follow a fast variation of the intensity.

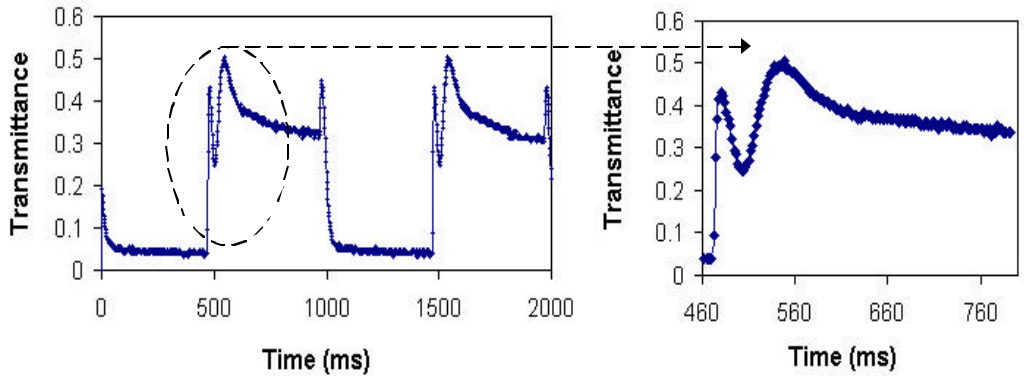

Figure 4.6. Measurement of response times of a LC-polymer composite film made from MLC6608 / C8A.

The rise time and decay time measured from Figure 4.6 are 55 ms and 40 ms respectively. It is the above transient phenomenon that causes the rise time longer than decay time. The retardation we chose permitted the two peaks showing up in a transient rise. If the sample thickness is reduced to, say 3.8 μm, which corresponds to the retardation at the first peak in Figure 4.2, the transient intensity modulation should disappear and a maximum output intensity is obtained as well. According to equation 4.3, the decease in the sample thickness will also give rise to a *quadratic* decrease of response times, but the threshold voltage can still remains intact (equation 1.13). Certainly, the thickness effects on both the output intensity and response times needs to be considered together to make a balance between them. Moreover, from choosing appropriate LC materials point of view, a nematic fluid with larger birefringence is desired since the thickness can be further lowered to match the same value of retardation, resulting in a faster response. A low rotational viscosity of the nematic fluid helps to reduce response time as well.[17]

Composition dependences of decay time and V_{90}

The decay time is useful to compare anchoring strength of different films because it is affected by surface anchoring strength but independent of applied voltage. It was found that the LC-polymer films made from long linear side chain acrylates (e.g., from C6A to C10A) show good response times (25~50ms) at room temperature. But the films made form the copolymers of a linear acrylate and a branched acrylate, e.g., *n*-decyl acrylate and isobornyl acrylate show long decay time (100~300 ms) at room temperature. This indicates weaker anchoring strength in the latter case, which has a lower T_t.

4.4. Conclusions

A LC-polymer composite system composed of a nematic fluid with negative dielectric anisotropy and a polymer network, and made by an in-situ photopolymerization, is proposed for potential application for flexible LC displays. The switching voltages, contrast ratio and response times of these composite films are measured and the approaches to improve the contrast ratio and response times are discussed. The proposed LC display based on this system has advantages such as ease of manufacturing (rub-free, one-step photopolymerization), high contrast ratio, low switching voltages, fast switching, and compatible with flexible LC displays[7].

REFERENCES

[1] West, J.L. in *Liquid Crystals In Complex Geometry*; Crawford, G. P.; Zumer S., Eds; Taylor & Francis: London, 1996.

[2] Suh, S.W.; Shin, S.T.; Lee, S. D.; "Novel electro-optic effect associated with a homeotropic to twisted-planar transition in nematic liquid crystals," *Appl. Phys. Lett.* **1996**, *68*, 2819-21.

[3] Huitema, H. E. A.; Gelinck, G.H.; van der Putten, J. B.; Kuijk, K. E.; Hart, C. M.; Cantatore, E.; Herwig, P. T.; van Breemen, A. J.; de Leeuw, D. M. "Plastic transistors in active-matrix displays. The handling of grey levels by these large displays paves the way for electronic paper," *Nature*, **2001**, *414*, 599.

[4] Acharya, B. R.; Choi, H.; Kumar, S. "Phase separated columnar structure for fabrication of flexible liquid-crystal devices, " unpublished manuscript.

[5] Crandall, K.A.; Fisch, M.R.; Petschek, R.G; Rosenblatt, C. "Homeotropic, rub-free liquid-crystal light shutter, " *Appl. Phys. Lett.* **1994**, *65*, 118-20.

[6] Seo, D.S., Lee, J.H., Kim, Y.H. "Wide viewing angle and fast response time using a novel vertical-alignment-pi cell mode on a homeotropic alignment layer," *Liquid Crystals* **2000**, *27*, 1147-50.

[7] Vorflusev, V.; Kumar, S. "Phase-separated composite films for liquid crystal displays," *Science* **1999**, *283*, 1903-5.

[8] Bloss, F. D. *Optical crystallography*; Mineralogical Society of America: Washington, D. C., 1999.

[9] Max Born and Emil Wolf, *Principles of Optics*, 5th Ed., Pergamon Press, Oxford, 1975.

[10] Mattoussi, H.; Srinivasarao, M.; Kaatz, P. G.; Berry, G. C. "Refractive indexes dispersion and order of lyotropic liquid crystal polymers," *Macromolecules* **1992**, *25*, 2860-8.

[11] Goodman, L.A. "Liquid-crystal displays - electro-optic effects and addressing techniques" in *Introduction to Liquid Crystals*; Priestley, E. B.; Wojtowicz, P. J.; Sheng, P., Eds; Plenum Press: New York, 1974, ch.14.

[12] de Gennes, P. G. *The Physics of Liquid Crystals*; Clarendon: Oxford, 1974; p.76.

[13] Amundson, K. R.; Srinivasarao, M. "Liquid-crystal-anchoring transitions at surfaces created by polymerization-induced phase separation," *Phys. Rev. E.* **1998**, *58*, R1211-4.

[14] Zhou, J.; Collard, D. M.; Park, J. O.; Srinivasarao, M. "Control of the anchoring behavior of polymer-dispersed liquid crystals: Effect of branching in the side chains of polyacrylates," *J. Am. Chem. Soc.* **2002**, *124*, 9980-1.

[15] Amundson, K.; Van Blaaderen, A.; Wiltzius, P. "Morphology and electro-optic properties of polymer-dispersed liquid-crystal films," *Phys. Rev. E.* **1997**, *55*, 1646-54.

[16] de Gennes, P. G. The Physics of Liquid Crystals; Clarendon: Oxford, 1974; p.220.

[17] Kirsch, P.; Heckmeier, M.; Tarumi, K. "Design and synthesis of nematic liquid crystals with negative dielectric anisotropy," *Liquid Crystals* **1999**, *26*, 449-52.

CHAPTER 5

ELECTRICALLY SWITCHABLE LIQUID CRYSTAL GRATINGS BASED ON PATTERNED ANCHORING

5.1. Introduction

Calamatic liquid crystals (LC) consist of molecules with highly anisotropic structures. Their use in optical or electro-optical devices relies on the bulk alignment of these elongated molecules. It is well established that external fields (electric, magnetic, and shear-flow fields) and surface anchoring forces can align bulk LC phases.[1] Control of the latter is import for making of LC-based electro-optical devices in that the equilibrium state of alignment of LC in the field-off state is determined by the anchoring. In conventional liquid crystal displays (LCD, e.g., those used for computer screens), mechanical rubbing of polymer surfaces is the dominant technique to achieve a uniform slightly tilted anchoring of LC at the surface.[2] Although this technique has reached its maturity in LCD industry, it still suffers from disadvantages such as mechanical damages to underlying layers, generation of electrostatic charges and contamination with dusts during the rubbing process. These make it inappropriate for the inexpensive production of large uniform films.[3] A variety of other techniques for treatment of surfaces to achieve a desired LC anchoring have been investigated, including oblique evaporation of inorganic materials (S_iO_x or Au),[4,5] photo-induced alignment,[3,6,7,8] use of self-assembled monolayers,[9,10,11] deposition of surfactants[12,13] and grafting of polymer brushes[14] onto the substrate.

Recently, electrically switchable LC devices with spatially periodic modulation of refractive index have attracted a lot of attentions due to their applications in optical

communications, displays, holograms and optical storage.[6,15,16,17] Such periodic structure can be obtained by either spatially modulating the concentration distribution of LC and another matrix material such as polymer,[17,18,19,20] or spatially patterning the LC alignment. As the examples of the latter, LC-based devices (e.g., diffraction gratings and Fresnel lens arrays) are fabricated by combining one of the above surface alignment techniques with various patterning methods such as microcontact printing,[9] photolithography,[16,21,] laser scanning,[22] AFM patterning,[23] and holographic recording.[24,25,26] However, with the exception of the process using both photo-induced alignment and holographic recording, these techniques to pattern the alignment of LC require multiple steps in pre-treating the substrate to align the LC phase or in the patterning process.

In this chapter, we report a simple approach to pattern the LC alignment in a periodic way using a one-step photopolymerization of a nematic LC-monomer mixture through photomask exposure, during which the closed-cell morphology is formed. There is no need to pre-teat the substrate since the LC alignment is achieved in-situ by the encapsulating polymer matrix.

As described in Chapter 3, the bulk alignment of the LC encapsulated in the closed-cell polyacrylate films is sensitive to the structure of the side chain of the polymer matrices, but generally insensitive to the morphology of the films. In particular, we have studied the effect of copolymerization of two dissimilar acrylates that favor different anchoring of LC upon the LC alignment within the polymer matrices. The anchoring behavior of nematic LC can be tuned continuously across a wide temperature window by changing the composition of the copolymer (Figure 3.10). The nonlinear relationship

between T_t and the comonomer composition is explained by the reactivity ratio difference between the two comonomers.

Based on these results, we demonstrate that the photocopolymerization of the two acrylate monomers in presence of LC through a patterning mask may lead to the definition of areas with different LC alignment. This idea is analogous to photo-induced diffusion proposed by Broer and co-workers.[27] In their case, a concentration gradient of functional photoreactive monomers was created along the thickness direction during a photopolymerization, which is due to the gradient of UV irradiation along the same direction. In our proposed method, the periodic modulation of the monomer concentrations is along a lateral direction instead, as illustrated in Figure 5.1. The process of this patterned photocopolymerization will be addressed in more detail in the following sections.

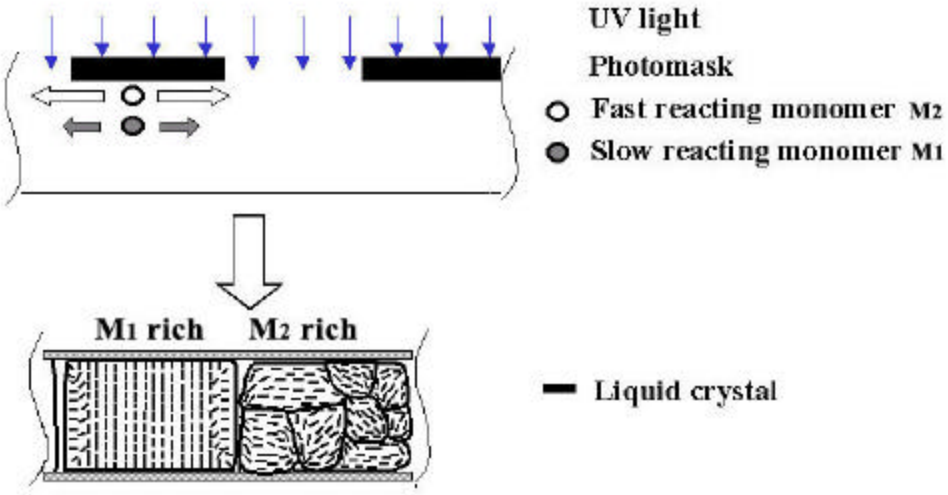

Figure 5.1. Schematics showing spatially periodic alignment of nematic LC created by a patterned photocopolymerization of the two monomers that favor different LC anchoring.

5.2. Experimental

Materials. The nematic fluid we used is TL205 (EM Industries). The birefringence of TL205 is 0.23 (at 20 °C and 589 nm). Acrylate monomers, 2-ethylhexyl acrylate (2-EH_xA), *n*-octyl acrylate (C8A) and 1,1,1-trimethylol propane triacrylate, were obtained from Scientific Polymer Products Inc. and used without further purification. The triacrylate was added as a cross-linking agent to provide rigidity to the film structure. Mixtures were prepared containing TL205, monofunctional acrylates, the triacrylate crosslinker (80:18:2, w/w) and photo-initiator (Darocur 1173, Ciba Inc, 0.5 % weight of the total acrylate monomers). The mole ratio of monofunctional acrylates, 2-EH_xA and C8A, was varied to study the effect of copolymerization. All of the mixtures of reactants are homogeneous and isotropic at room temperature.

Photopolymerization. The above photoreactive mixture was placed between two indium-tin oxide (ITO) coated glass substrates with a spacing of 15 μm (using glass microbeads of standardized size as spacer, supplied by Duke Scientific). UV exposure (360 nm) with intensity of ca. 0.5 mW/cm^2 was performed through a polymer transparency film printed with 80 μm-spaced parallel silver stripes (supplied by PageWorks Inc), placed in close proximity to the sample, until the closed-cell morphology was formed. The mask was then removed and the film was fully cured at much higher UV intensity (16 mW/cm^2), so that a constant T_{NI} was obtained.

Optical microscopy. A polarized light microscope (Leica DMRX) equipped with crossed polarziers and a digital camera is used to take microscopic images of the LC gratings made as above. A DC voltage source with adjustable output up to 50 Volts is used to apply a voltage to the sample on the microscope stage.

Measurement of electro-optical properties and diffraction patterns. A 1 kHz square wave AC voltage with the amplitude ramping from 0 to 20 Volts (HP3325A function generator) was applied across the two transparent electrodes for electro-optical measurements (Figure 5.2). The intensities of the transmitted and diffracted beams of a 1 mW He-Ne laser (633 nm) were monitored by a multifunctional powermeter (Newport model 1830-C). If not specially indicated, the polarization of the incident laser we used is parallel to the orientation of the periodic stripes in the film. The polarization dependence of diffraction intensity was also measured in a separate experiment.

A 1 Hz square wave DC voltage with amplitude from 0 to 7 V and a digital oscilloscope (Lecroy LT344) connected to a silicon photo detector (DET110, Thorlabs) were used to measure the switching times of the gratings. Diffraction patterns of the gratings at different voltages were obtained using a home-use digital camera in a dark room.

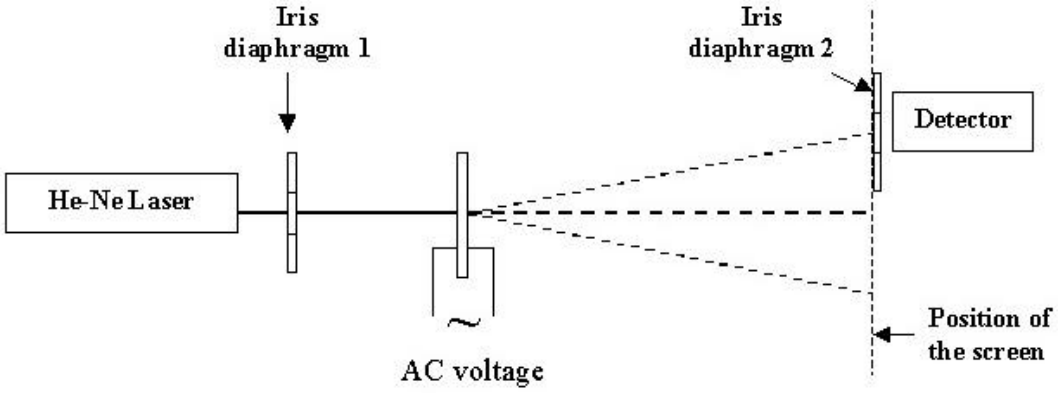

Figure 5.2. Experimental setup for measurement of diffraction efficiency of the gratings.

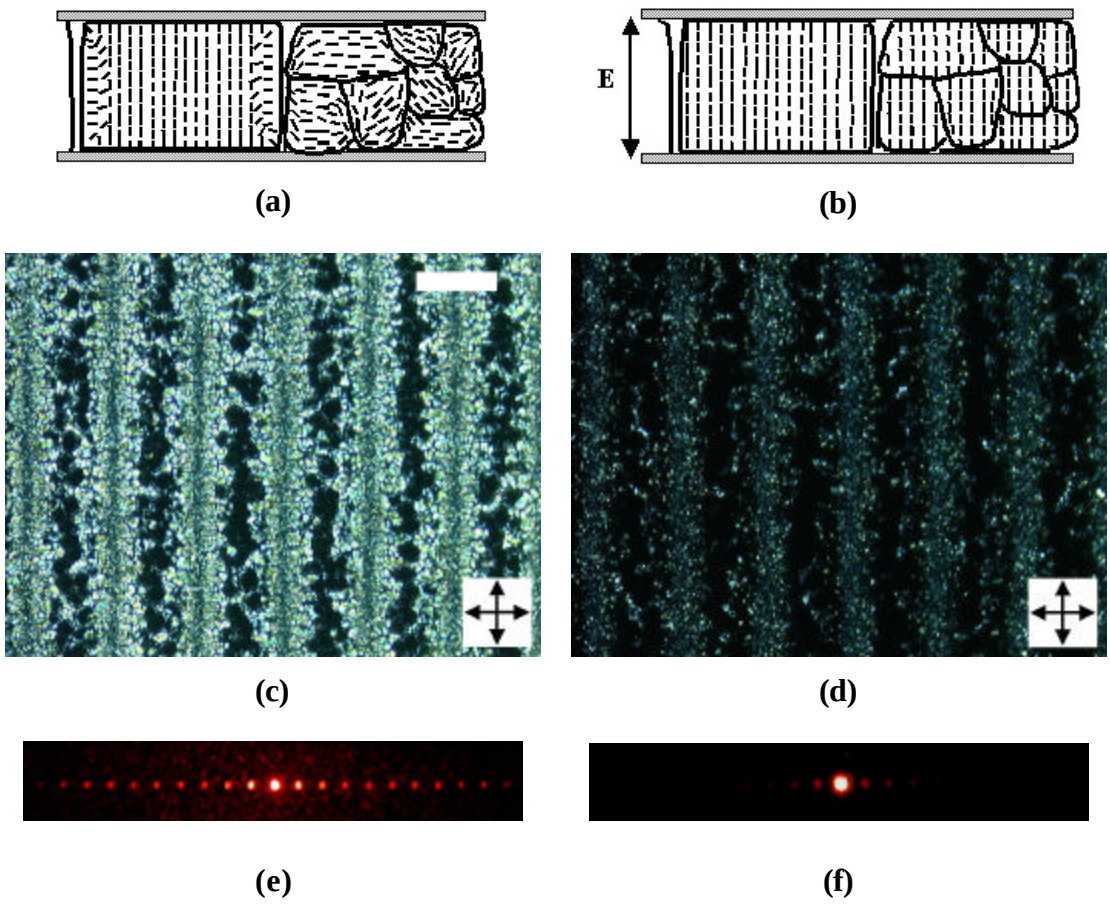

Figure 5.3. (a) and (b): schematics of the side view of two adjacent stripes with different anchoring and morphology; (c) and (d): microscopic graphs of the LC-polymer grating film under crossed polarizers; (e) and (f): diffraction patterns of the same film. (a), (c) and (e): electric field-off state; (b), (e) and (f): with an electric field **E** of 0.40 $V\mu m^{-1}$ (6V) across the thickness (square wave AC). The scale bar in (c) is 80 μm. The sample thickness is 15 μm.

5.3. Results & Discussions

5.3.1. Formation of the LC gratings with alternating anchoring, diffraction patterns and polarized microscopic observations

LC-polymer composite films made by photocopolymerization through a mask were observed by polarized optical microscopy. When the ratio of 2-EH_xA and C8A in the initial comonomer mixture is within the range from 80:20 to 90:10 (mol/mol), the photocopolymerization leads to stripes with alternating homeotropic and planar anchoring of the LC as shown in Figure 5.3c. The region with homeotropic anchoring was verified by conoscopy. There is a difference in both anchoring condition and morphology between the neighboring stripes as illustrated by schematic of Figure 5.3a.

These results can be understood in terms of the rate of photopolymerization, diffusion of monomers and the relationship between the anchoring condition and copolymerization composition (Figure 5.4, i.e., part of Figure 3.10). During a patterned photocopolymerization, the polymerization initiates in the irradiated regions. The consumption of the monomers in these regions gives rise to the diffusion of both 2-EH_xA and C8A from the unirradiated regions (Figure 5.1).[28,29] Here "unirradiated regions" are those stripes that were not directly exposed to the UV irradiation in the first stage of the photopolymerization (the film was actually fully cured after the removal of the photomask in the second stage of the photopolymerization). The fast reacting monomer (M_2), 2-EH_xA, is predicted to diffuse more than the slow reacting one (M_1), C8A during such a patterned photopolymeriztion.[27] As a result, the polymer in the irradiated region is rich in the 2-EH_xA monomer unit, which favors planar anchoring. The small LC droplets in the irradiated regions arise from fast photopolymerization that causes early phase

separation with formation of small closed-cell structure.[30] On the other hand, the polymer composition formed in the other region is richer in C8A, which favors homeotropic anchoring. The larger and polygonal LC cells in the latter regions arise due to slower photopolymerization and phase separation prior to curing across the entire film. The difference in comonomer composition between two neighboring stripes is limited by the factors such as the reactivity ratio difference between the two comonomers,[27] the balance between integral diffusion rate (the individual diffusion rates of the two monomers are assumed to be the same since they have the same molecular weight and similar structure) and polymerization rate, and the stage when solidification of the film occurs during the photopolymerization.[30]

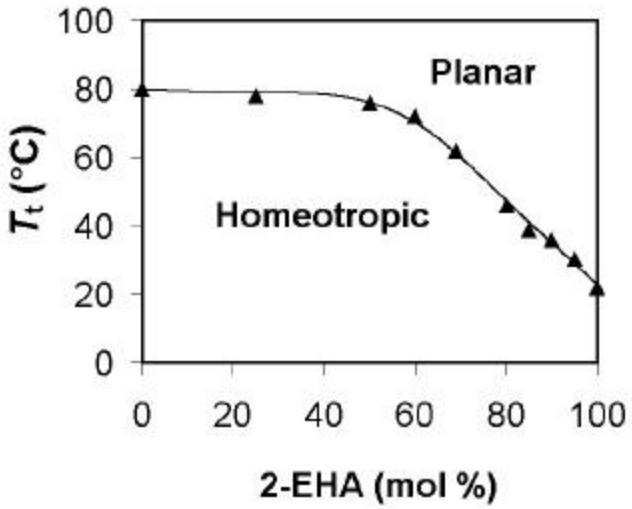

Figure 5.4. A plot of anchoring transition temperature T_t against the composition (in mole percentage) of the comonomer mixtures.

If a global comonomer composition with less than 80 mol % of 2-EH$_x$A monomer (which corresponds to an anchoring transition temperature (Figure 5.4) far above room temperature) is used, the resulting film has only homeotropic anchoring in the entire film at room temperature (i.e., stripe with alternating anchoring is not obtained). It is due to

that the concentration of 2-EH_xA in either of the two stripes is not high enough to induce planar LC anchoring at room temperature, which is generated by a limited photopolymerization-induced diffusion. Similarly, if the comonomer composition with close to 100% of 2-EH_xA monomer is used for making of the gratings, only planar anchoring can be obtained in the resulting film at room temperature or above. In the specific system we used, the appropriate ratio between the two monomers is within the range from 85/15 to 90/10 (mol/mol) in order to obtain the contrast in anchoring (i.e., homeotroic versus planar) between the adjacent stripes.

The differences in both the LC alignment and the polymer concentration give rise to a difference in the refractive index of adjacent stripes. Such a periodic structure constitutes a good diffraction grating as shown in Figure 5.3e. The periodicity of the grating, r, was calculated based on the observed diffraction pattern and Bragg's equation:

$$r = m\lambda / \sin(b_m) \qquad (5.1)$$

where m is the order of diffraction spot, λ is the wavelength and b_m is the corresponding diffraction angle. The calculated value of r is 81 μm, consistent with that measured directly by optical microscopy. When a 6 V AC voltage is applied across the sample, the contrast in the birefringence is lowered (Figure 5.3d) and the diffraction efficiency is greatly diminished (Figure 5.3f). This is due to switching of the alignment of the LC molecules from a parallel to perpendicular direction with respect to the substrates upon application of an electric field.

5.3.2. Characterizations of diffraction efficiency:

Electric field dependence of the diffraction efficiency

Diffraction efficiency (DE), defined as the percentage of the intensity of the diffraction compared to the total intensity, is an important characteristic of diffraction gratings. Depending which order of diffraction intensity is concerned, there are the zeroth order diffraction efficiency (DE_0), first order (DE_1), second order (DE_2), and so on.

The DE_1, DE_2 and DE_3 of the grating in Figure 5.3, were monitored as a function of the applied voltage. DE_1 shows a maximum value of 1.7% at approximately 2 V (i.e., the electric field E =0.13 $V\mu m^{-1}$) and a minimum at 6 V (i.e., E=0.40 $V\mu m^{-1}$). The DE_1 then slightly increases and reaches an asymptotic value of 0.3% at higher voltages. The intensity of the first order diffraction at high potential arises from the small difference between the refractive index of the polyacrylate matrix, $n_{polymer}$, and the ordinary refractive index of the LC, $n_{o,\,LC}$.

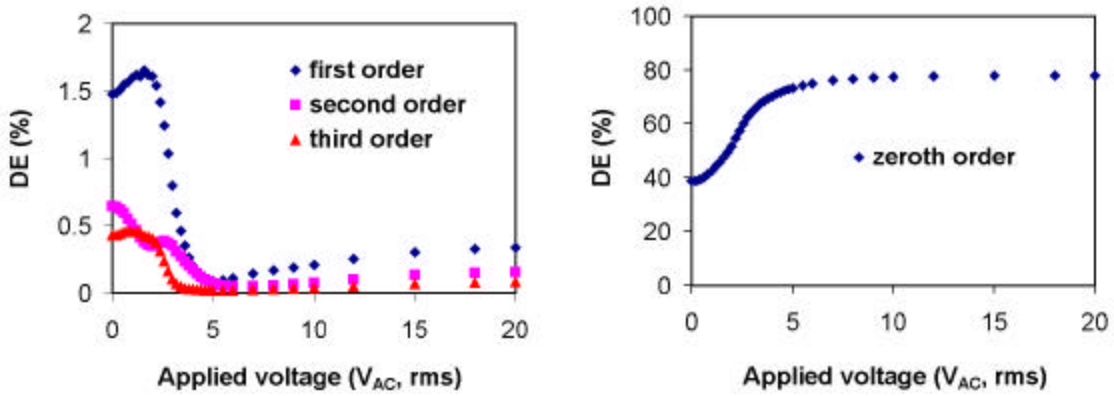

Figure 5.5. (a) Plot of first, second and third order diffraction efficiencies as a function of applied voltage. (b) The zeroth order diffraction efficiency as a function of applied voltage (1kHz, square wave AC, and rms represents the amplitude of voltage in root mean square unit).

The modulation of the DE_1 with the applied voltage can be understood in terms of a phase grating having stripes of alternating homeotropic alignment and planar alignment

of LC,[9] and a scattering effect. The effective refractive index in the stripe with homeotropic alignment of the LC (stripe 1) is approximately $n_{o,\,LC}$ (the contribution of the polymer matrix can be neglected since $n_{polymer} \approx n_{o,\,LC}$), which is independent of the applied electric field (E). The effective refractive index in the stripe with planar alignment of the LC (stripe 2) has contributions from both the polymer matrix (because $n_{polymer} < n_{eff,\,LC}$) and the LC, where the latter, $n_{eff,\,LC}$, is electric field dependent, given by equation (1.2), that is, $n_{eff,LC} = \frac{n_e n_o}{\sqrt{n_o \cos^2 \alpha + n_e \sin^2 \alpha}}$ and α is the angle between the LC director and the polarization of the light, varying with the amplitude of E. The phase difference between the rays passing through the two adjacent stripes can thus be described by:[16]

$$\Delta = \frac{2p}{l} h \quad (<n_{eff,\,LC}(E), n_{polymer}> - n_o) \tag{5.2}$$

where λ = 633nm, h the thickness of the sample (15 μm in our case), $<n_{eff,\,LC}(E), n_{polymer}>$ represents the average of $n_{eff,\,LC}(E)$ and $n_{polymer}$ in the stripe 2. A phase difference of some integral multiples of 2π corresponds to the maximum diffraction intensity, and the phase difference of some odd integral multiples of π the minimum diffraction intensity. This is consistent with the observation that the first and third order diffractions show a maximum where the second order shows a minimum (Figure 5.5a).[9,16] Based on this analysis, DE_0 is predicted to show a local minimum corresponding to the maximum of DE_1. However, this was not observed due to the following facts: (i) the rise (~0.2%) of the DE_1 before reaching the maximum is small compared with the value of DE_0 (>40%) and it induces only 0.5% of a possible drop of DE_0; (ii) the light scattering (see Figure 5.3e) arising

from the refractive index difference between $n_{polymer}$ and $n_{eff, LC}$ at the zero field state is greatly reduced (Figure 5.3f) when a low electric field is applied (since the LC molecules tilt toward parallel to the propagation of the light and $n_{eff, LC}$ gets closer to $n_{polymer}$), which contributes to the increase of DE_0.[31] Therefore, a monotonic increase of the zeroth order intensity is observed.

Based on equation 5.2, the thickness of the film can, in principle, be optimized to shift the maximum of DE_1 to zero field so that switching on and off the electric field will switch the diffraction efficiency between the maximum and the minimum.

Polarization dependence of the diffraction efficiency

For the above DE measurement, the polarization of the laser was set parallel to the stripes of the film. We also varied the polarizations of the incident laser to see the effect of polarization on the diffraction efficiency. The result is shown in Figure 5.6, in which the maximum of DE_1 is achieved with the polarization of the laser parallel to the stripes and the minimum of DE_1 with the polarization perpendicular to the stripes. It is inferred that the in-plane alignment of LC molecules in the stripe with the planar anchoring must be more or less parallel to the orientation of the stripe, instead of being degenerate (i.e., even distribution of all of the in-plane alignment directions). Thus, for the light polarized perpendicular to the stripe, the effective refractive of the LC in this stripe is $n_{o, LC}$, which is the same as that of the other stripe with homeotropic anchoring. The diffraction efficiency is hence greatly suppressed in this case. Since the diffraction efficiency is determined by the phase difference of the light passing through the two adjacent stripes, the modulation of DE_1 with rotation of the polarization of the light

should be similar to the square of a sinusoidal function, which is consistent with the observation shown in Figure 5.6. It is not yet clear to us why such an in-plane alignment was achieved within the stripe of planar anchoring. It is possibly due to a photo-aligning effect similar to that in reference 26 where the in-plane alignment of a nematic fluid encapsulated by polymer matrices was induced by the polarized UV irradiation during photopolymerization. In our case, the UV irradiation for the photopolymerization was also very likely polarized. The anisotropy of the photomask itself (a polymer transparency film with printed parallel silver stripes) was noticed by polarized light microscopy, as shown in Figure 5.7 where the optical axis of the transparency film is approximately parallel to or perpendicular to the silver stripes. Such a transparency film worked as a polarizer, giving rise to the UV irradiation polarized along the easy axis of the film (which is possibly parallel to the optical axis). Another experiment using a photomask without any optical anisotropy (e.g., a metallic mask) is desired to see whether degenerate anchoring can be obtained in the stripes of planar anchoring. If it is the case, the diffraction efficiency of the grating is expected to be polarization-independent.

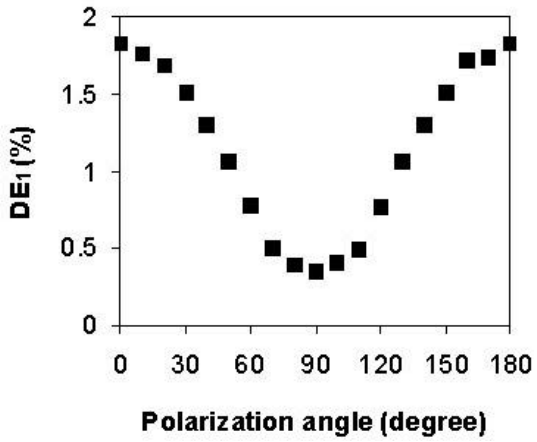

Figure 5.6. Polarization dependence of the 1st order diffraction efficiency for the LC-polymer composite grating. The polarization angle is the angle between the polarization of light and the orientation of the stripes in the film.

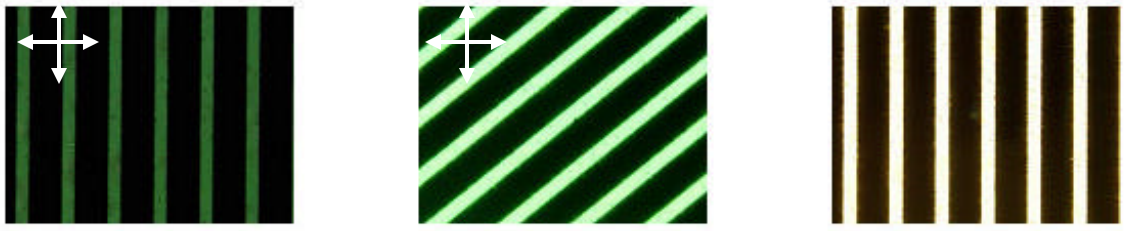

(a) **(b)** **(c)**

Figure 5.7. Anisotropy of the polyester transparency film which is used as the substrate of the photomask. Images (a) and (b) were taken under the crossed polarizers as indicated by the arrows; (c) is a bright field image. The black fringes are 80 μm-spaced.

The effect of temperature on the diffraction efficiency

Upon heating the grating film with the stripes of alternating anchoring, a homeotropic-to-planar (H-to-P) anchoring transition occurs within the stripes of *originally* homeotropically aligned, as shown in Figure 5.8 (where T_t is 35°C). There is only planar anchoring cross the entire grating film at a temperature above T_t but below T_{NI}. The DE of a film with only planar anchoring is low at the zero field due to a small difference in refractive index between the two neighboring stripes. But, as shown in Figure 5.9, with increase of the applied voltage (i.e., increase of the strength of the electric field E at the same time), the DE_1 shows a modulation with the maximum of 1.8% located at 3.8 V (E=0.25 V/μm^{-1}), which is almost the same as the maximum of DE_1 for the grating with the stripes of alternating anchoring. Here the modulation of the DE with increase of the electric field is still explained by the phase difference between the adjacent stripes. In this case, the zeroth order diffraction efficiency DE_0 (Figure 5.9b) is able to show a local maximum and minimum corresponding to the minimum and maximum of DE_1, respectively, due to a relatively larger drop and rise of DE_1 than the case shown in Figure 5.5.

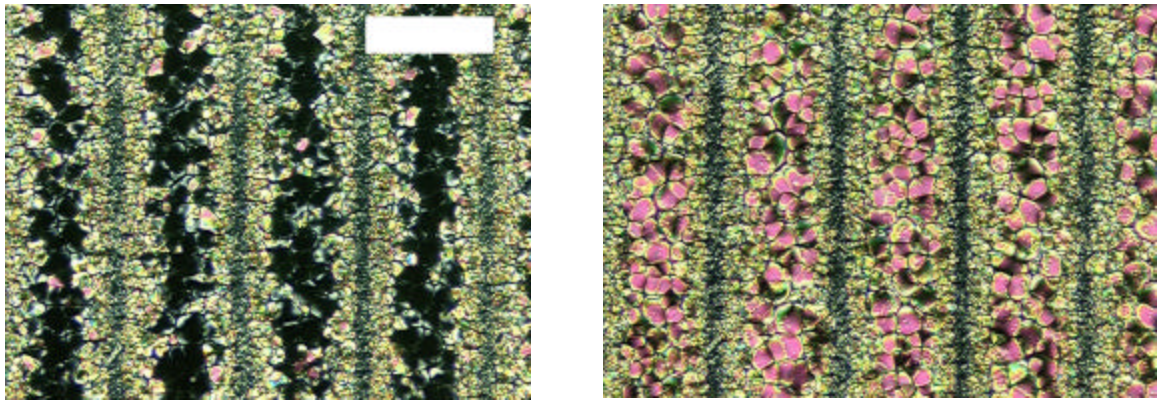

(a) **(b)**

Figure 5.8. Microscopic pictures (under crossed polarizers) showing the temperature-driven H-to-P anchoring transition of a grating film. (a) 24°C; (b) 36°C. The scale bar is 80 μm.

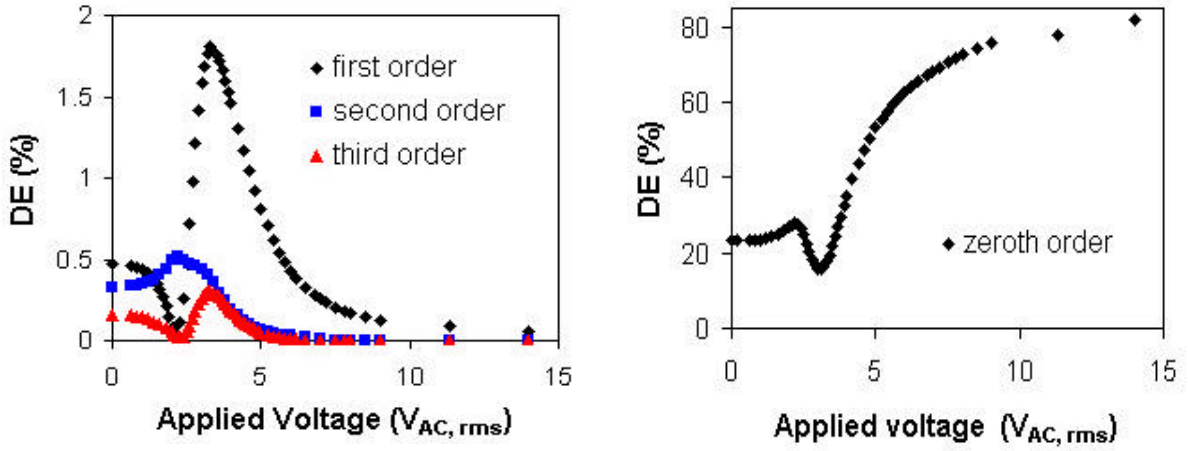

(a) **(b)**

Figure 5.9. Diffraction efficiency of the sample with only planar anchoring cross the entire film. The film thickness is 15 μm.

The similar maximum values of DE_1 in both cases can be understood by considering the size dependence of the threshold electric field, E_c, to align the encapsulated LC droplets. As we mentioned earlier, the average size of the LC droplets in one stripe is greater than that of the adjacent stripe due to the difference in dynamic of forming such a closed-cell structure. According to equation 1.12, i.e., $E_c = \frac{p}{h}\sqrt{\frac{4Kp}{\Delta e}}$, the threshold electric field of a Freedericksz transition is proportional to the inverse of the thickness. Here the size of the LC droplets should be used in place of the thickness since the bulk alignment of the LC is determined by balance of the electric field-induced aligning torque and the torque due to anchoring at the surface of polymer matrices. Thus, E_c of the larger LC droplets is lower than that of the smaller ones. This is confirmed by polarized light microscopic observation of the same film used in Figure 5.9 when it is subject to an increasing electric field. As shown in Figure 5.10a through d, the alignment of the LC phase in the stripes with larger droplets switches (hence changing the birefringence color) at a lower electric field than that in the adjacent stripes. So, the contrast in LC alignment (thereby the contrast in refractive index) between the two neighboring stripes is established by applying a low electric field (Figure 5.10b and c). Because the diffraction efficiency is mainly determined by the phase difference between the two stripes, the modulation of DE with increase of the electric field in this case should be similar to that of the case with alternating anchoring, except near zero field. The similar maximum values of diffraction efficiency in both cases are expected although they are obtained under different electric fields. But, it is noted that the grating film with the stripes of alternating anchoring has the advantage that the maximum of DE_1 can in

principle be obtained at the zero field state and therefore the grating will have low power consumption.

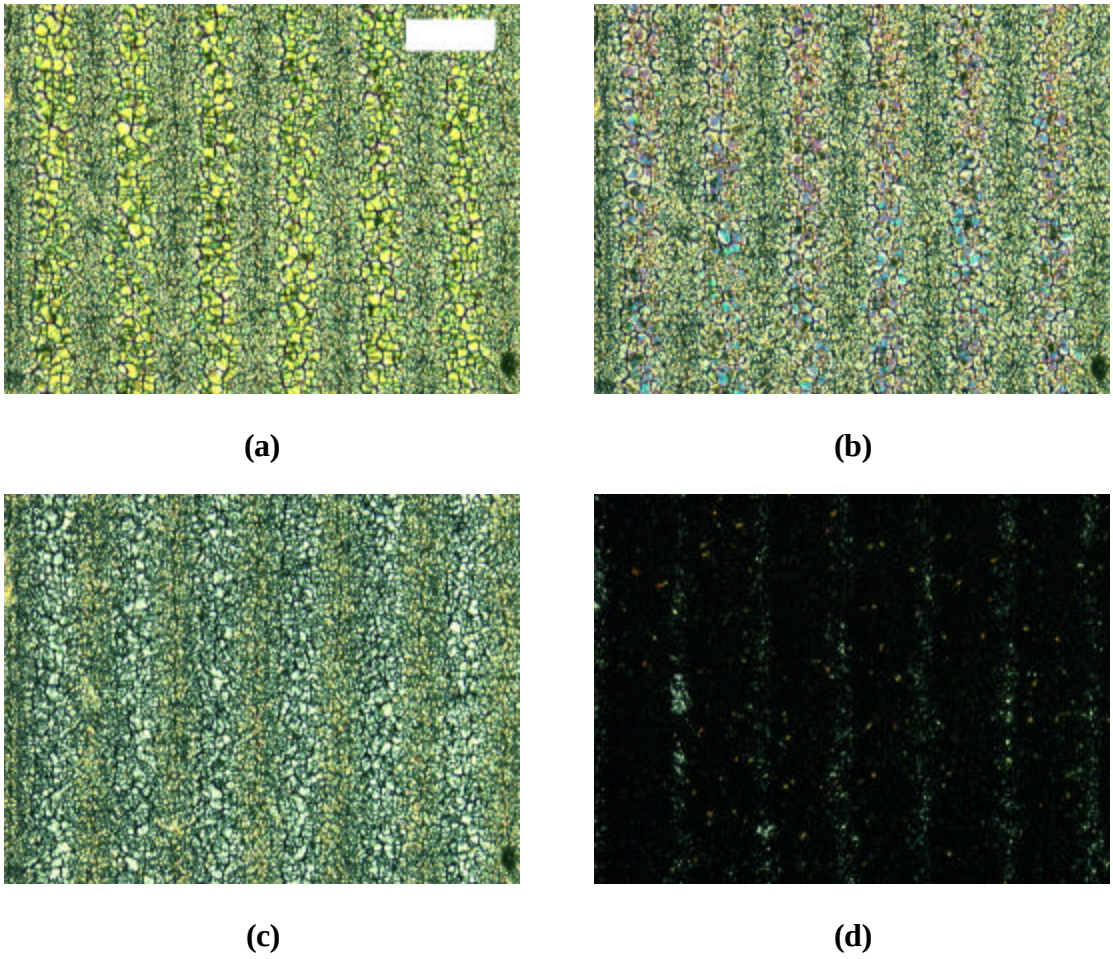

(a) **(b)**

(c) **(d)**

Figure 5.10. Microscopic pictures (under crossed polarizers) of the same grating in Figure 5.9 under an increasing electric field. (a) zero field; (b) 0.2 $V/\mu m^{-1}$; (c) 0.33 $V/\mu m^{-1}$; (d) 1 $V/\mu m^{-1}$. The film thickness is 15 μm. The scale bar in (a) is 80 μm.

5.3.3. Measurement of switching times

The switching times of the grating in Figure 5.3 were measured by monitoring the response of the zeroth order diffraction intensity under an applied DC voltage (square wave) with the amplitude varying between 0 and 7 V. This provides switching-on time of 25 ms and switching-off time of 110 ms. It should be mentioned that the fist order diffraction responds at approximately the same rate as the zeroth order one, but due to a much better signal-to-noise ratio for the detector we used, the zeroth order intensity was used to show response times here.

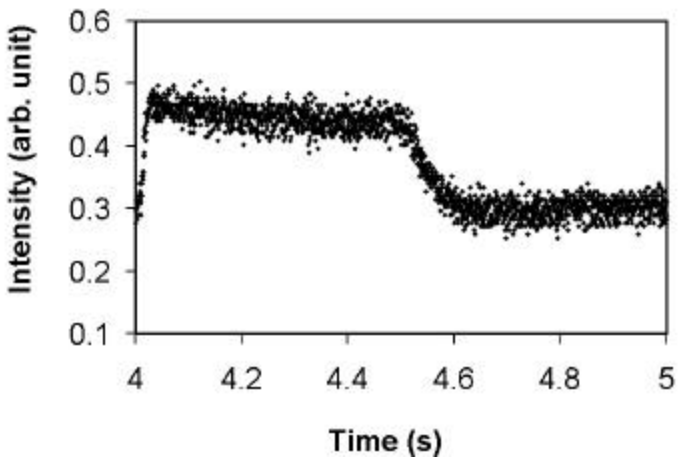

Figure 5.11. Measurement of switching times by monitoring the variation of the zeroth order diffraction intensity.

5.4. Conclusions

In summary, we have demonstrated a facile and operationally simple method to prepare electrically switchable diffraction gratings with periodic spatial alignment of LC. The method is based on polymerization-induced phase separation with the formation of a cellular structure, which affords control over the anchoring behavior of the encapsulated LC domains. The effects of electric field, polarization of the incident light, and temperature on the diffraction efficiency of the gratings are discussed. The advantages of

the LC gratings we report here are ease of manufacturing (rubbing-free, one-step photopolymerization), low switching voltages, and structure stability offered by polymer matrix. The method should also fit plastic substrates for making flexible devices.[32,33]

REFERENCES

[1]. Uchida, T.; Seki, H. In *Liquid Crystals: Applications and Uses* Vol. 3; Bahadur B. Ed.; World Scientific: Singapore, 1992; pp. 1-63.Gibbons, W. M.; Shannon, P. J.; Sun, S. T.; Swetlin, B. J. "Surface-mediated alignment of nematic liquid crystals with polarized laser light," *Nature* **1991**, *351*, 49-50.

[2]. Geary, J. M.; Goodby, J. M.; Kmetz, A.R.; Patel, J.S. "The mechanism of polymer alignment of liquid-crystal materials," *J. Apply. Phys.* **1987**, *62*, 4100-8.

[3]. Dantsker, D.; Kumar, J.; Tripathy, S. K. "Optical alignment of liquid crystals," *J. Appl. Phys.*, **2001**, *89*, 4318-25.

[4]. Armitage, D. "Alignment of liquid–crystal on obliquely evaporated silicon-oxide films," *J. Apply. Phys.* **1980**, *51*, 2552-5.

[5]. Skaife, J.J.; Abbott, N.L. "Quantitative Characterization of Obliquely Deposited Substrates of Gold by Atomic Force Microscopy: Influence of Substrate Topography on Anchoring of Liquid Crystals," *Chem. Mater*. **1999**, *11*, 612-23.

[6]. Gibbons, W. M.; Shannon, P. J.; Sun, S. T.; Swetlin, B. J. "Surface-mediated alignment of nematic liquid crystals with polarized laser light," *Nature* **1991**, *351*, 49-50.

[7]. Schadt, M.; Schmitt, K.; Kozinkov, V. "Surface-induced parallel alignment of liquid crystals by linearly polymerized photopolymers," *Jpn. J. Appl. Phys. Lett*. **1992**, *31*, 2155-64.

[8]. Ichimura, K. "Photoalignment of Liquid-Crystal Systems," *Chem. Rev.* **2000**, *100*, 1847-73 and the literatures within.

[9]. Gupta, V. K.; Abbott, N. L. "Design of surfaces for patterned alignment of liquid crystals on planar and curved substrates," *Science* **1997**, *276*, 1533-6.

[10]. Miller, W.J.; Gupta, V.K.; Abbott, N.L.; Tsao, M.W.; Rabolt, J.F. "Comparison of the anchoring of nematic liquid crystals on self-assembled monolayers formed from semifluorinated thiols and alkanethiols," *Liq. Cryst.* **1997**, *23*, 175-84.

[11]. Lee, B.W.; Clark, N.A. "Alignment of liquid crystals with patterned isotropic surfaces," *Science* **2001**, *291*, 2576-80.

[12]. Proust, J. E.; Ter-Minassian-Saraga, L.; Guyon, E. "Orientation of a nematic liquid crystal by suitable boundary surfaces," *Solid State Comm.* **1972**, *11*, 1227-&.

[13]. Porte, G. "Tilted alignment of MBBA induced by short-chain surfactants," *J. Phys.* (France) **1976**, *37*, 1245-52.

[14]. Ramdane, O. O.; Auroy, P.; Forget, S.; Raspaud, E.; Martinot-Lagarde, P.; Dozov, I. "Memory-free conic anchoring of liquid crystals on a solid substrate," *Phys. Rev. Lett.* **2000**, *84*, 3871-4.

[15] Shannon, P.J.; Gibbons, W.M.; Sun, S.T. "Patterned optical properties in photopolymerized surface-aligned liquid crystal films," *Nature*, **1994**, *368*, 532-3.

[16]. Chen, J.; Bos, P. J.; Vithana, H.; Johnson, D. L. "An electro-optically controlled liquid crystal diffraction grating," *Appl. Phys. Lett.* **1995**, *67*, 2588-90.

[17] Sutherland, R.L.; Natarajan, L.V.; Tondiglia, V.P.; Siwecki, S.A.; Chandra, S.; Bunning, T.J. "Switchable holograms for displays and telecommunications, " *Proc. SPIE* **2001**, *4463*, 1-10.

[18] Sutherland, R.L.; Tondiglia, V.P.; Natarajan, L.V.; Bunning, T.J.; Adams, W.W. "Electrically switchable volume gratings in polymer-dispersed liquid crystals, " *Appl. Phys. Lett.* **1994**, *64*, 1074-6.

[19]. Ren, H.; Wu, S.T. "Inhomogeneous nanoscale polymer-dispersed liquid crystals with gradient refractive index," *Appl. Phys. Lett.* **2002**, *81*, 3537-9.

[20]. Ren, H.; Fan, S.; Wu, S.T. "Prism grating using polymer stabilized nematic liquid crystal," *Appl. Phys. Lett.* **2003**, *82*, 3168-70.

[21]. Patel, J. S.; Rastani, K. "Electrically controlled polarization-independent liquid-crystal Fresnel lens arrays.," *Opt. Lett.*, **1991**, *16*, 532-4.

[22]. Gibbons, W. M.; Sun, S. T. "Optically generated liquid crystal gratings,"*Appl. Phys. Lett.* **1994**, *65*, 2542-4.

[23]. Wen, B.; Petschek, R. G.; Rosenblatt, C. "Nematic liquid-crystal polarization gratings by modification of surface alignment," *Appl. Opt.* **2002**, *41*, 1246-50.

[24]. Zhang, J.; Carlen, C. R.; Palmer, S.; Sponsler, M. B. "Dynamic Holographic Gratings Recorded by Photopolymerization of Liquid Crystalline Monomers," *J. Am. Chem. Soc.* **1994**, *116*, 7055-63.

[25]. Cha, S.W.; Choi, D.H.; Oh, D.K.; Han, D.Y.; Lee, C.E.; Jin, J.I. "Reversible polarization gratings on thin films of polyoxetanes bearing 4-(N,N-diphenyl)amino-4 '-nitroazobenzene chromophores," *Adv. Funct. Mat.* **2002**, *12*, 670-8.

[26]. Cipparrone, G.; Mazzulla, A.; Russo, G. "Diffraction gratings in polymer-dispersed liquid crystals recorded by means of polarization holographic technique," *Appl. Phys. Lett.* **2001**, *78*, 1186-8.

[27]. Broer, D. J.; Mol, G. N.; van Haaren, J. A. M. M.; Lub, J. "Photo-induced diffusion in polymerizing chiral-nematic media," *Adv. Mat.* **1999**, *11*, 573-8.

[28]. Fuh, A. Y. G.; Ko, T. C.; Tsai, M. S.; Huang, C. Y.; Chien, L. C "Dynamical studies of gratings formed in polymer-dispersed liquid crystal films," *J. Appl. Phys.*, **1998**, *83*, 679-83.

[29]. Bowley, C. C.; Crawford, G. P. "Diffusion kinetics of formation of holographic polymer-dispersed liquid crystal display materials," *Appl. Phys. Lett.* **2000**, *76*, 2235-7.

[30]. Drzaic, P. S. Liquid Crystal Dispersions, World Scientific: Singapore, 1995, ch.1.

[31]. Mach, P.; Wiltzius, P.; Megens, M.; Weitz, D.A.; Lin, K.H.; Lubensky, T.C.; Yodh, A. G. "Electro-optic response and switchable Bragg diffraction for liquid crystals in colloid-templated materials," *Phys. Rev. E.* **2002**, *65*, Art. No. 031720.

[32]. Vorflusev, V.; Kumar, S. "Phase-separated composite films for liquid crystal displays," *Science* **1999**, *283*, 1903-5.

[33]. Huitema, H. E. A.; Gelinck, G.H.; van der Putten, J. B.; Kuijk, K. E.; Hart, C. M.; Cantatore, E.; Herwig, P. T.; van Breemen, A. J.; de Leeuw, D. M. "Plastic transistors in active-matrix displays. The handling of grey levels by these large displays paves the way for electronic paper," *Nature*, **2001**, *414*, 599.

CHAPTER 6

MICROSCOPIC OBSERVATION OF BLOCH WALL DEFECTS

6.1. Introduction

In the previous chapters, a temperature-driven homeotropic-to-planar (H-to-P) anchoring transition was found at the interface of nematic fluids/polyacrylate system. It is found that a Bloch wall defect can be created during a quenching process through the transition temperature T_t, when the anchoring condition changes from planar to homeotropic. Since **n** is equivalent to **–n** in the nematic phase, the director have two opposite ways of rotating to align parallel to the surface normal during such a planar-to-homeotropic transition. If the transition process is fast enough, a 180° inversion wall can be trapped between the two adjacent domains with opposite rotation.[1] In Chapter 3, the Bloch wall was used to estimate the polar anchoring energy at the polymer surface. In this chapter, we explore the director-field structure of Bloch walls and related defects in three-dimensions using both polarized light microscopy and fluorescence confocal polarizing microscopy (FCPM).

6.1.1. Typical line and wall defects in nematic phase

The nematic phase has a long range orientation ordering, whose average orientation direction is referred to as the nematic director, **n**. A disclination is defined as a discontinuity in the director-field **n(r)**. The disclination in the nematic phase may be a point (zero dimensional) or a line (one dimensional). A two-dimensional disclination in nematic phase is unstable and usually smear out to disappear or become a *continuously* distorted region with finite thickness (a wall defect) if stabilized by an external field or pinned at the surfaces.[1]

The types of point disclinations have been briefly described in Chapter1. Typical line disclinations (i.e., singular lines) in nematic phase may carry the strength of +1, -1, +1/2 or –1/2. The free energy of the singular lines is much higher than that of singular points so that the system usually tends to find ways to avoid line defects. For example, the nematic phase confined in a cylindrical capillary with homeotropic surface anchoring may form "escaped" line structure at the central axis of the capillary (Figure 6.1a), which is of continuous nature, instead of a S=+1 singular line. The singular points are formed when two "escaped" line having opposite directions meet in the capillary (Figure 6.1b). The "escape" of the disclination into the third dimension was first described by Williams *et al* .[2] Meyer also gave a detailed analysis of point disclinations.[3] However, according to Cladis and Kleman,[4] a singular line in such a capillary may be metastable or stable when the diameter of the capillary R is quite small (e.g., R < 1μm).

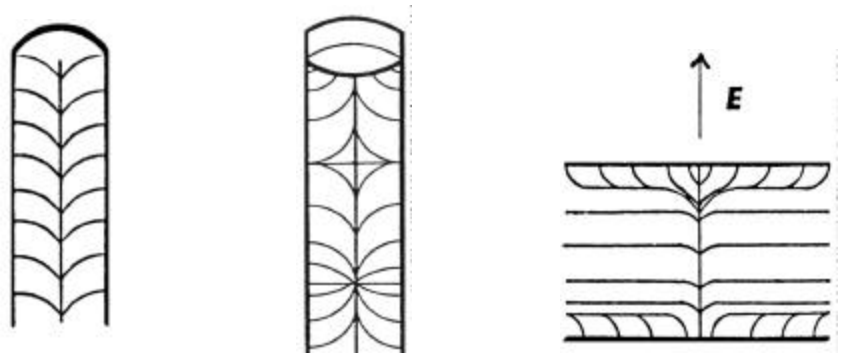

Figure 6.1. (a) Nematic director-field of "escaped line" in a capillary; (b) singular points in a capillary; and (c) bulk inversion line in a nematic domain subject to a vertical electrical field (after Saupe[5]).

Besides the disclination lines (singular ones), the line defects can have a continuous director distortion. For example, within an inversion line (or wall), the director orientations differ by an angle of 180° or less from one side of the line (or wall) to the other, but keep symmetry with respect to the line or wall direction. An inversion line can be in the bulk phase (so-called bulk inversion line[6]) as shown in the case of Figure 6.1c, or adhere to the surface. The former is indeed a one-dimensional line defect. The latter, referred to as surface inversion line here, is usually the intersection of an inversion wall with the surface. It is noted that the surface inversion line was also named as "surface disclination" by Ryschenkow and Kleman.[7,8] However, since the surface inversion line is continuous and "disclination" instead means discontinuous defect (i.e., singular) according to de Gennes,[1] we shall not use the term "surface disclination" here to avoid confusion.

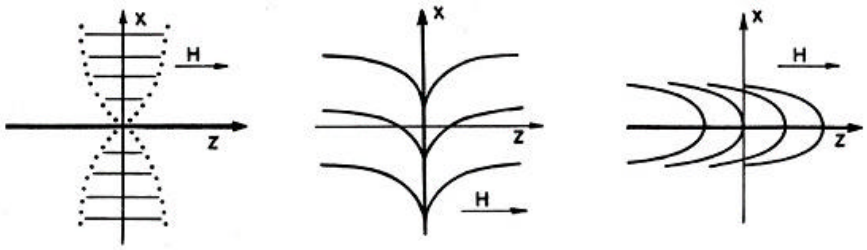

(a) **(b)** **(c)**

Figure 6.2. Schematic diagrams of alignment inversion walls in presence of a magnetic field (H): (a) Twist wall (i.e., Bloch wall); (b) Spay-bend wall perpendicular to field and (c) Spay-bend wall parallel to field (after Helfrich[9])

As mentioned above, a wall structure is a defect trapped by a fast reorientation process of nematic phase. A Freedericksz transition of nematics induced by a magnetic field or electrical field is usually used to create inversion walls. Helfrich[9] first

theoretically explored the director field of inversion walls in presence of a magnetic field. According to Helfrich's classifications, there are three different inversion walls as shown in Figure 6.2: the structure of (a) is similar to Bloch wall in ferromagnetics, therefore also referred to as Bloch walls; both (b) and (c) are splay-bend wall, whose structures are similar to Neel walls in ferromagnetics.[10] These inversion walls are of continuous nature and three-dimensional. They intersect with the surfaces to form surface inversion lines. The "line" observed under polarized light microscopes is actually the projection of the walls that is perpendicular to the substrate. Kleman predicted that either the wall or the surface inversion line can be more stable than the other depending on the sample size h compared with the extrapolation length b (defined as K/W, where K is the elastic constant of nematics and W is the anchoring strength). The wall is more stable if $b \geq h$, while the surface inversion line is more stable if $b << h$.[7] Since the apparent value of b is given by d^2/h,[7] where d is the width of the wall, the above comparison can be made between d and h instead.

The inversion walls were also observed by Nehring and Saupe:[11] "inversion walls of first kind" in their paper is the same as structure (c) of Figure 6.2; "inversion wall of second kind" is the same as structure (a) of Figure 6.2, i.e., Bloch wall.

..6.1.2. Optical characteristics of inversion walls

The alignment of the director is symmetric with respect to the center axis of the inversion wall. Therefore, the center axis of a 180° inversion wall must align at 90° to the easy axis of the surface or the field direction. The optical characteristics of inversion walls of different types are different under polarized light microscope, and hence polarized light microscopy can be used to identify them.

(i) For a Bloch wall with the twisting axis parallel to the substrates (Figure 3.3), the azimuthal angle of the director doesn't change within the wall but the tilt angle varies continuously across the wall (i.e., along a direction normal to the wall). Under crossed polarizers, if the wall axis aligns at a angle other than 0° or 90° to the polarizer, it show continuous variation of the birefringence color across the wall under while light illumination, with the highest birefringence color located at the center axis. The color bands at the two sides of the wall are symmetrical with respect to the center axis. When the analyzer is removed from the light path of the microscope, if the polarization of the incident light is normal to the wall, the wall is almost invisible because the refractive index of the nematic phase across the wall is constant and equal to the ordinary index "n_o" so that there is no refractive index contrast between the wall and the surrounding nematic domains normally aligned. However, if the polarization of the incident light is parallel to the wall, the wall shows the best contrast since there is a continuous variation of refractive index across the wall (with n_e in the center and n_o at the two edges of the wall). And a thin and bright line can also be observed in the latter case if the focus of the microscope is move up a little bit, which is due to the light focusing effect of continuously varying refractive index.[12,13]

(ii) For a splay-bend wall like Figure 6.2b that is perpendicular to the substrates and also with the easy axis parallel to the substrates, the tilt angle of the director doesn't change but the azimuthal angle varies continuously across the wall. Under the crossed polarizers, if the wall axis aligns at a angle 45° to the polarizer, two narrow dark brushes that are parallel to the wall and also located at symmetric position with respect to the center axis of the wall can be observed and the center axis of the wall is bright. If the wall

axis aligns at a angle 0° or 90° to the polarizer, the center axis of the wall is dark and the above two parallel brushes become the two bright lines. When the analyzer is removed from the light path of the microscope, the wall can always be observed regardless of the angle it aligns to the polarization of incident light. It also can focus the light to a position several micrometer above or below the sample focus plane depending on the polarization of the light.

Besides that the surface anchoring strength can be estimated from the geometry of the wall defects according to Kleman's method, Leger also indicated that microscopic observations of static or dynamic behavior of different types of inversion walls induced by a magnetic field are useful for estimating the elastic constants, twist viscosity, the critical field for Fredericks transition of nematic phases. [12]

..6.1.3. Fluorescence confocal polarizing microscopy technique (FCPM)

The estimation of anchoring strength by Kleman's method is qualitative, with the accuracy of the order of magnitude. It is partly due to the fact that the polarized light microscopy alone can neither tell the sample thickness, nor the distribution of out-of-plane alignment of the nematic director. If the three-dimensional director configuration of the Bloch wall is known, a better estimation of the polar anchoring energy can therefore be obtained. Fluorescence confocal polarizing microscopy (FCPM) has been shown to be a powerful tool to provide not only the three-dimensional morphology of the sample[14] but also the orientation information of the nematic molecules both in the plane of the substitute and out of the plane.[15,16] The typical apparatus of FCPM is illustrated by the schematic in Figure 6.3, where the two detectors, PMT1 and PMT2, collect the fluorescent light and transmitted light from the sample, respectively.

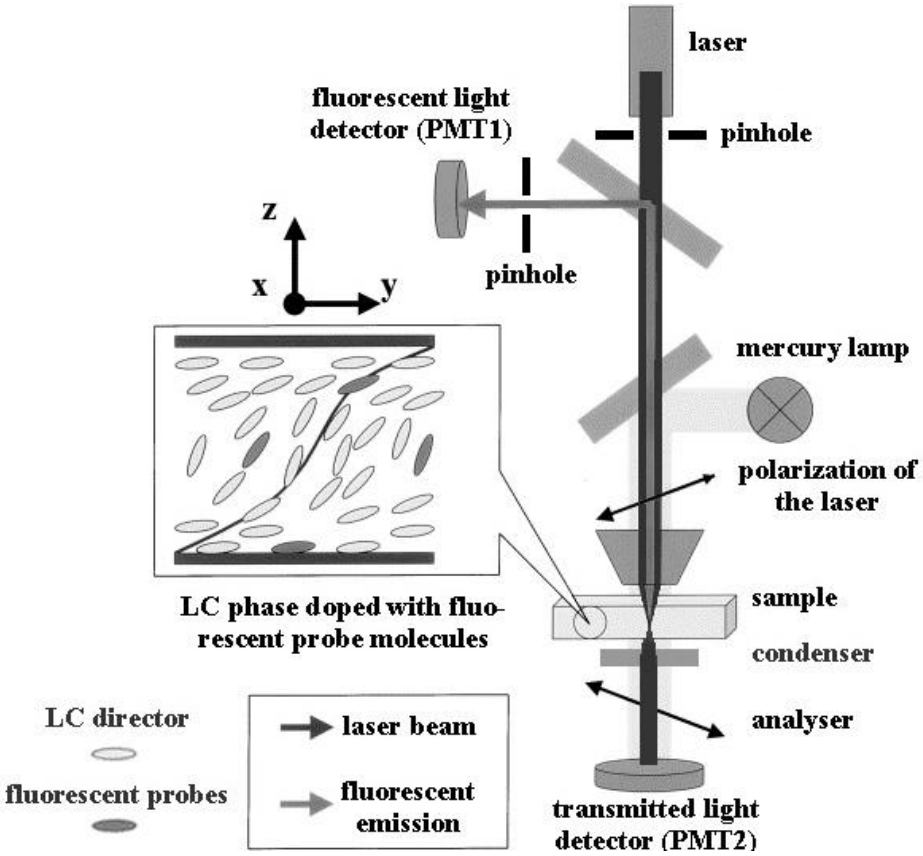

Figure 6.3. Schematics of the apparatus for fluorescence confocal polarizing microscopy (redrawn after Lavrentovich[16]).

A fluorescent probe needs to be added into the sample to image the three-dimensional director field of the nematics by FCPM. The principles of choosing appropriate fluorescent probe molecules are as follows:[16]

(i) The probe has a high quantum yield of fluorescence

(ii) The LC medium to be studied is a good solvent for the probe

(iii) The long axes of the absorption dipole and emission dipole of the probe are collinear and also parallel to the local nematic director due to the interaction between LC molecules and probe molecules.

Both (i) and (ii) make it possible that only a very small amount of probe are needed for imaging so as not to affect the original LC director field.

Since the LC phase is anisotropic and light has two propagating mode in the LC, the imaging aberration caused by a refractive index mismatch is possible.[17] To reduce the aberration in confocal imaging, a liquid crystal with a low birefringence Δn (e.g., Δn <0.1) should be used. It is also assumed that the concentration of the probe is spatially uniform through LC media to be imaged. This assumption is reasonable as long as the scale of the distortion of the director field is much greater than the molecular scale.[18]

6.2. Experimental

The nematic polymer composite films were prepared by using photopolymerization-induced phase separation method described in Chapter 3. The slow photo-polymerization is used to create the films with large polygonal LC domains of 30-50 μm wide. The Bloch walls are formed in many places through the film if the temperature of the film is quenched through the homeotropic-to-planar transition temperature. Two nematic fluids, MLC 6608 and 5CB (supplied by Emerck Industries, their physical properties are available in Appendix A), were used for making the samples. For the films made from MLC 6608, isooctyl acrylate is used as the photoreactive monomer. For the film made from 5CB, n-octyl acrylate is used. The acrylate monomers are supplied by Scientific Polymer Products Inc.. The thickness of the films is controlled by glass microbeads with a narrow diameter distribution (± 5%). Two sample thicknesses (5 and 15 μm) were used to investigate the effect of the sample thickness on the Bloch wall.

A small amount ($2\sim3\cdot10^{-5}$ weight fraction) of a fluorescent probe, pyrromethene 546 (supplied by Exciton, structure and spectra data are listed in Figure 2.5) was added to the reactive mixture before the photopolymerization to enable the director-field to be characterized by FCPM. The probe was found to align more or less parallel to the local nematic director (Chapter 3). The intensity of the fluorescence is maximum when the polarization of the excitation beam, **P**, is parallel to the director, **P** || **n,** and minimum when **P** ⊥ **n**, with the ratio of 2.0~2.2. Here we assume the collinear relation between the fluorescence transition dipole and the local nematic director. The apparatus of FCPM we used is illustrated in Figure 6.3. The dye probe is excited by an Ar^+ laser at 488 nm and

the fluorescent light is collected from 520-560 nm. The transmitted beam through the sample is collected by another detector, PMT2. The easy axis of the analyzer before the transmitted light detector is perpendicular to the polarization of the excitation beam. The microscope therefore can work simultaneously under confocal fluorescence mode and polarized transmission mode. Both 40x and 100x oil immersion objectives with numerical aperture (NA) of 1.2 and 1.4 respectively were used for imaging. Since a large NA objective is used, the beam going through the sample is highly convergent. To simplify the simulation of interference patterns obtained from the transmission, we chose to collect only the normally incident light. The iris aperture located right before the transmitted light detector is stopped down to the minimum to cut off most of the transmitted rays with high incident angles and allow only paraxial rays to pass, as illustrated in Figure 6.4. Due to the scanning of the laser beam during the imaging, some non-paraxial rays still can pass the iris, but we assume that the intensity of these rays can be neglected compared to the normally incident rays since the laser beam is a Gaussian.[17,19] with the intensity at the center of the beam much stronger than that at the edge. To test the above assumption is reasonable, interference patterns of the same sample at two different wavelengths, 458 (Ar^+ laser) and 568 nm (Kr^+ laser) are simulated based on normal incidence of the light to see if the results are consistent.

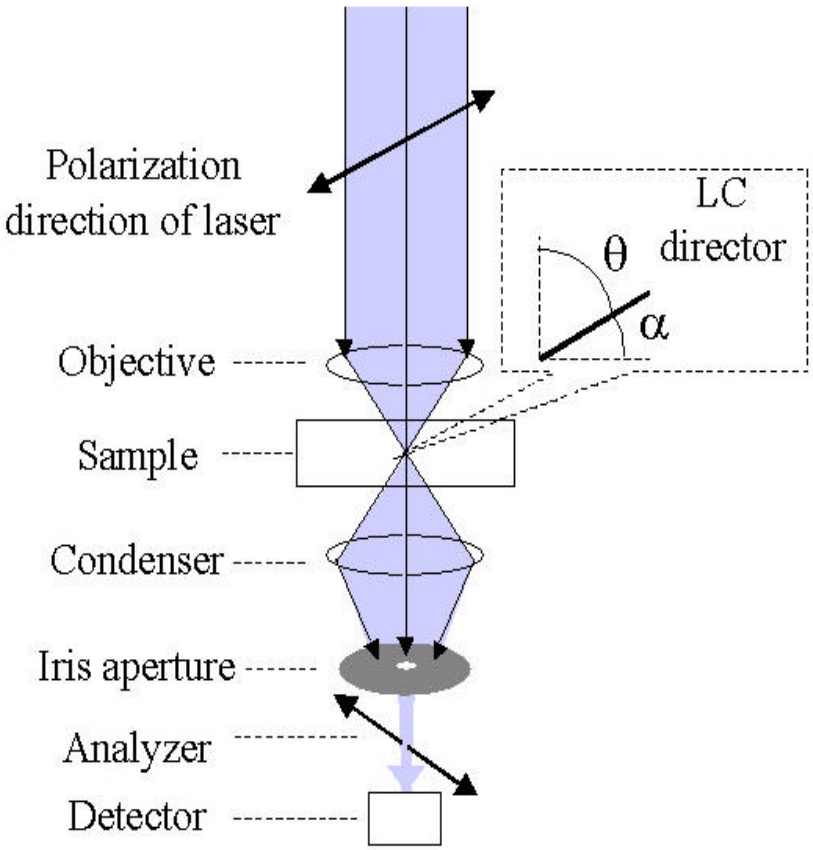

Figure 6.4. Schematic of the apparatus for collecting interference patterns of wall defects using FCPM. q is the tilt angle of local LC director. The iris aperture is stopped down to the minimum to cut off the highly convergent rays.

6.3. Results & Discussion

6.3.1. FCPM imaging of Bloch walls

The Bloch walls shown in Figure 6.5 and Figure 6.6 are the samples made from MLC6608 and isooctyl acrylate with the thickness of 15~20 μm and 5~8 μm, respectively, which are controlled by using the glass microbeads with a narrow distribution of diameter. The low birefringence of MLC6608 reduces the possibility of optical aberration due to the refractive index variation across the wall.[16] The relation between the fluorescence intensity profile and the LC director distribution can be established: the fluorescence emission of the probe molecules is proportional to the absorption of the probe to the excitation, which in turn depends on the angle between the orientation of the absorption dipole and the polarization of the incident laser, b.[19] If we assume the collinearity between the orientations of the absorption dipole of the probe molecules and the LC director, the LC director-field information can be extracted from the detected fluorescence intensity profiles. The tilt angle of the director, q, is equal to $(\pi/2-b)$ in this case. The simplified relationship between the fluorescence intensity and the orientation of the LC director is given by the equation below:

$$I_{\text{det}}(q,f=0) \propto I_{\text{em}}(q,f=0) \propto A(q,f=0) \propto \sin^2 q \qquad (6.1)$$

where q and f are the tilt and azimuthal angle of **n (r)**; I_{em} and I_{det} are the fluorescent emission intensity and the intensity collected by the detector respectively; A is the absorption; and $f=0$ is given by the direction of the projection of the wall in xy plane, which is also parallel to the polarization of the excitation.

As shown in the xz section of Figure 6.5a, the width of the Bloch wall spreads out from either the top or the bottom substrate toward to the middle plane (the half of the

thickness) of the film, with the maximum width at the middle plane. The profiles of the fluorescence intensity (I_{det}) across the wall at the different depths, i.e., close to the top and at the middle plane, are shown in Figure 6.5b.

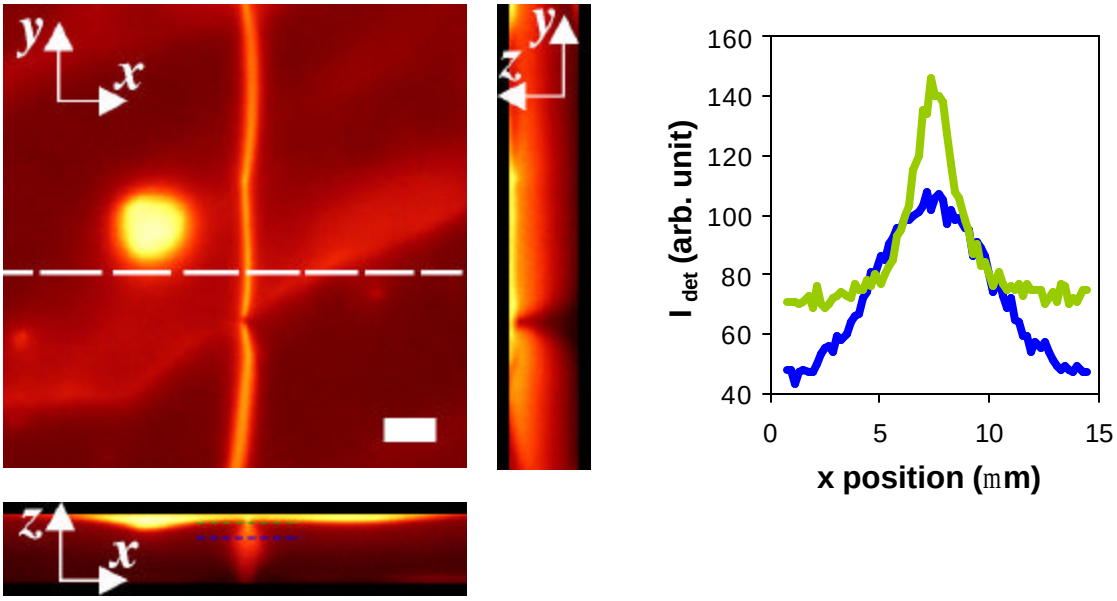

Figure 6.5. (a): the confocal fluorescence images, *xy*, *xz* and *yz* sections, of a Bloch wall where the extrapolation length is smaller than the sample thickness (~18μm); the polarization of the excitation laser is along *y* axis; (b): the fluorescence intensity profiles along the green and blue lines in the *xz* section, which are at the depth of 1 μm and 5 μm below the LC/polymer interface respectively. The scale bar is 10 μm. The system is composed of MLC 6608 and poly (isooctyl acrylate).

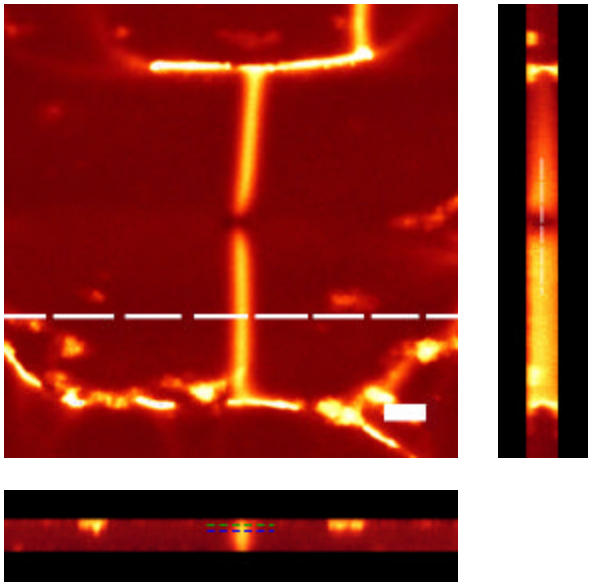

(a)

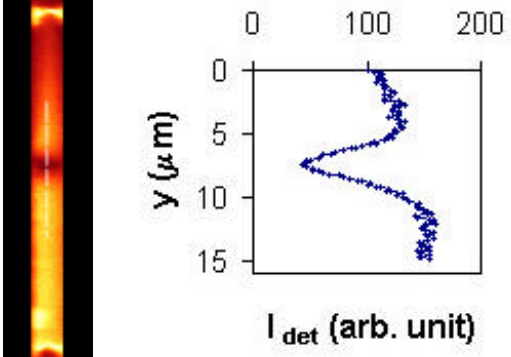

(c)

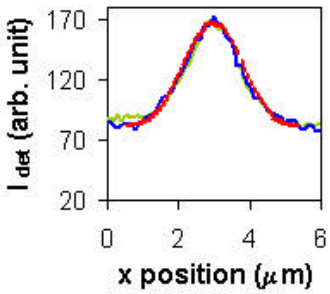

(b)

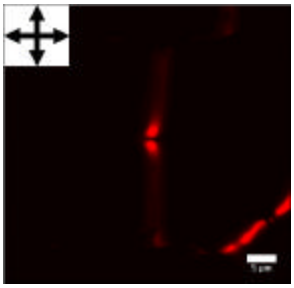

(d)

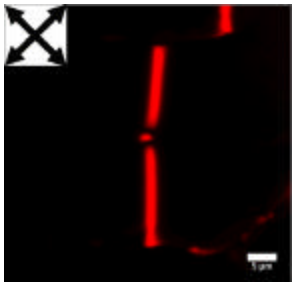

(e)

Figure 6.6. (a): the confocal fluorescence images, *xy*, *xz* and *yz* sections (the orientations of the image sections are the same as those in Figure 6.5) of a Bloch wall where the extrapolation length is comparable with the sample thickness (~5μm); the polarization of the excitation laser is along *y* axis; (b): the fluorescence intensity profiles (green and blue lines) along the two lines in the *xz* section of (a), which are at the depth of 1 μm and 2 μm respectively; (c): the fluorescence intensity profiles along the dashed line in the *yz* section of (a); (d) and (e): polarized light micrographs of the same Bloch wall under crossed polarizers. The red dotted line in (b) is the fitted curve based on the pure twist model (see section 6.3.3). The scale bar is 5 μm. The system is composed of MLC 6608 and poly (isooctyl acrylate).

Based on equation (6.1), it is clear that Figure 6.5b indicates the difference of LC director profiles at the different depth. This suggests that the director distortion along *z* axis (i.e., variation of the tilt angle *q* along z axis since *f* is a constant within the Bloch wall) has to be considered in this case, which is a splay-bend deformation. The apparent extrapolation length, *b*, estimated by the formula, $b \sim d^2/h$, is about 5 μm,[7] much smaller than the sample thickness 18 μm. It experimentally confirms Ryschenkow and Kleman's prediction: the splitting of a wall into surface lines or a diffuse wall is observed when $b << h$.[7]

In the case of Figure 6.6, the same LC-polymer system is used, but the sample thickness is smaller, ~ 5μm. The fluorescence intensity profiles across the wall at the different depth of the film almost overlap to each other (blue and green curves in Figure 6.6b), which shows that the director variation along z axis, $\partial\theta/\partial z$, is negligible. The wall therefore contains only twist deformation, i.e., it is a pure twist wall. It is noted that the apparent extrapolation length using Ryschenkow and Kleman's formula is 5~6 μm, close to the sample thickness, h. The result is again consistent with the prediction. An exact director-field model for such a pure twist wall is established in the following section, which will allow a more accurate measurement of the extrapolation length (hence anchoring strength).

6.3.2. Director-field model for a pure twist Bloch wall

The pure twist wall subject to a homeotropic anchoring of the both substrates is analogous to the inversion wall formed in presence of a magnetic field, which was considered by Helfrich[9] and also by de Gennes.[1] If we assume that the anchoring energy satisfies Rapini-Papoular equation[20] (see equation 3.2), a complete analogy between the

wall in presence of a magnetic filed and the pure twist wall in presence of a surface anchoring field can be made. The difference is that the external torque applied to nematics is from only the boundary surfaces instead of being applied throughout the whole bulk nematic phase. The director field of the Bloch wall in our case can be described by Figure 6.7.

Consider a thin slab of area, 1 (a unit length) *h in the plane parallel to y0z, extending from x to x+dx in the nematic. This slab experiences a twisting torque $-K_{22}h(d\alpha/dx)\big|_x$ at (x) and another torque $+K_{22}h(d\alpha/dx)\big|_{x+dx}$ at ($x+dx$). Moreover, it is subjected to a surface torque at both the top and bottom of this slab, $-2\frac{dW_p(\alpha)}{d\alpha}(1\cdot dx)$, where $W_p(\alpha)$ is the local polar anchoring energy at x.

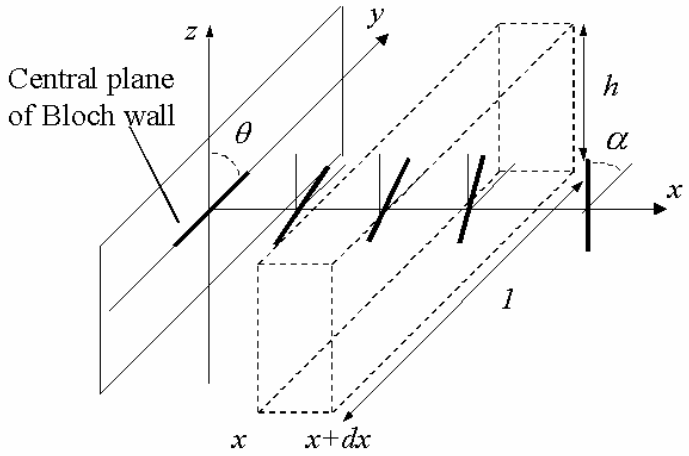

Figure 6.7. The schematic of the director-field within the half of a pure twist Bloch wall. q is the tilt angle, varying from π to 0 when x changes from $-\infty$ to $+\infty$; $a = \pi/2-q$, to satisfy the homeotropic anchoring condition.

The equilibrium equation can be written as:[1]

$$K_{22}h\frac{d^2\alpha}{dx^2}+2\frac{dW_p}{d\alpha}=0 \qquad (6.2)$$

The tilt angle dependence of W_p is given by equation 3.1:

$$W_p(\theta) = W_p \sin^2\theta = W_p \cos^2\alpha \tag{6.3a}$$

And hence:
$$-\frac{dW_p(\alpha)}{d\alpha} = 2W_p \sin\alpha\cos\alpha \tag{6.3b}$$

Then we will have

$$\left(\frac{K_{22}h}{4W_p}\right)\frac{d^2\alpha}{dx^2} + \sin\alpha\cos\alpha = 0 \tag{6.4}$$

Equation 6.4 is the same as the one analyzed by de Gennes in reference 1 except that the factor before $\frac{d^2\alpha}{dx^2}$ is different. The solution of (6.4) is:

$$\tan\left(\frac{p/2 - a}{2}\right) = \exp(-2x/(bh)^{0.5})$$
$$i.e., \quad \tan(q/2) = \exp(-2x/(bh)^{0.5}) \tag{6.5}$$

where b is the extrapolation length defined as K_{22}/W_p; h is the height of the wall, i.e., the thickness of the film. The quantity of $(bh)^{0.5}$ describes how fast the director rotates about x axis from 0 to π, which should be comparable with the wall width d. This is consistent with Ryschenkow and Kleman's result: $d^2 \sim bh$.[7]

6.3.3. Simulation of the interference and fluorescent intensity patterns of Bloch walls

Based on equation 6.5, both interference patterns and fluorescence patterns from Bloch walls can, in principle, be simulated by optical calculation.

First, the experimental fluorescence intensity profiles in Figure 6.7b are simulated using equations 6.1 ($I_{det} \propto \sin^2 q$) and 6.5. The result, i.e., the red curve of Figure 6.7b, fits the experimental data very well. The extrapolation length from the fitting is 1.4 μm, smaller than the apparent value 5 μm, calculated from $d^2 \sim bh$.

For the simulation of the interference patterns of the walls, the sample made from nematic fluid 5CB and poly (*n*-octyl acrylate) is used. The reasons are two folds: (i) 5CB

has a larger Δn (~0.2) so that more orders of interference fringes can be observed even if the sample thickness is only 5 μm (the interference fringes across the wall couldn't be observed in Figure 6.6e because of the low Δn of MLC6608, 0.083, and sample thickness being small as well; (ii) the refractive index data of 5CB under different wavelengths are available from the literature (also see Appendix A).[21]

We assume that the detected transmitted light intensity is contributed only by normally incident light as an approximation in the setup of Figure 6.4 since the iris before the transmitted light detector may cut off most of non-paraxial rays. Transmitted intensity of a normally incident polarized beam through the LC sample between crossed polarizers is given by equation 1.14, i.e., $I = \sin^2(2f)\sin^2(pR/\lambda)$, where f is the angle between the LC director and the polarizer, R the optical retardation, and λ is the wavelength. If the optical axis of the LC is at 45° to the polarizer pair, this equation can be rewritten as:

$$I \propto \sin^2\left(\frac{p}{l}(n_{eff} - n_o)\cdot h\right) \tag{6.6}$$

where n_{eff} and n_o are the effective refractive indexes for the extraordinary ray and the ordinary ray, respectively, and n_{eff} is given by equation 1.2. The angle α in equation 1.2 is defined as the angle between the polarization of the extraordinary ray and the local optical axis of the nematic phase (i.e., the direction of nematic director). α is equal to $(\pi/2-\theta)$ in this case (see Figure 6.4). Therefore, we have:

$$n_{eff} = \frac{n_e n_o}{\sqrt{n_o \sin^2\theta + n_e \cos^2\theta}} \tag{6.7}$$

Combing the equations 6.5, 6.6 and 6.7, we can calculate the transmitted light intensity profile across the wall under a monochromatic illumination, i.e., interference pattern.

As shown in Figure 6.8, the calculated interference patterns under 458nm and 568 nm match the experimental ones very well. The extrapolation length b obtained from the curve fitting is 1.5 μm (it is noted that the apparent extrapolation calculated from d^2/h, is ~ 8.4 μm) and the polar anchoring strength ($W=K_{22}/b$, K_{22} of 5CB at 24 °C is 3.9 pN) is hence 2.6×10^{-6} J/m^2.

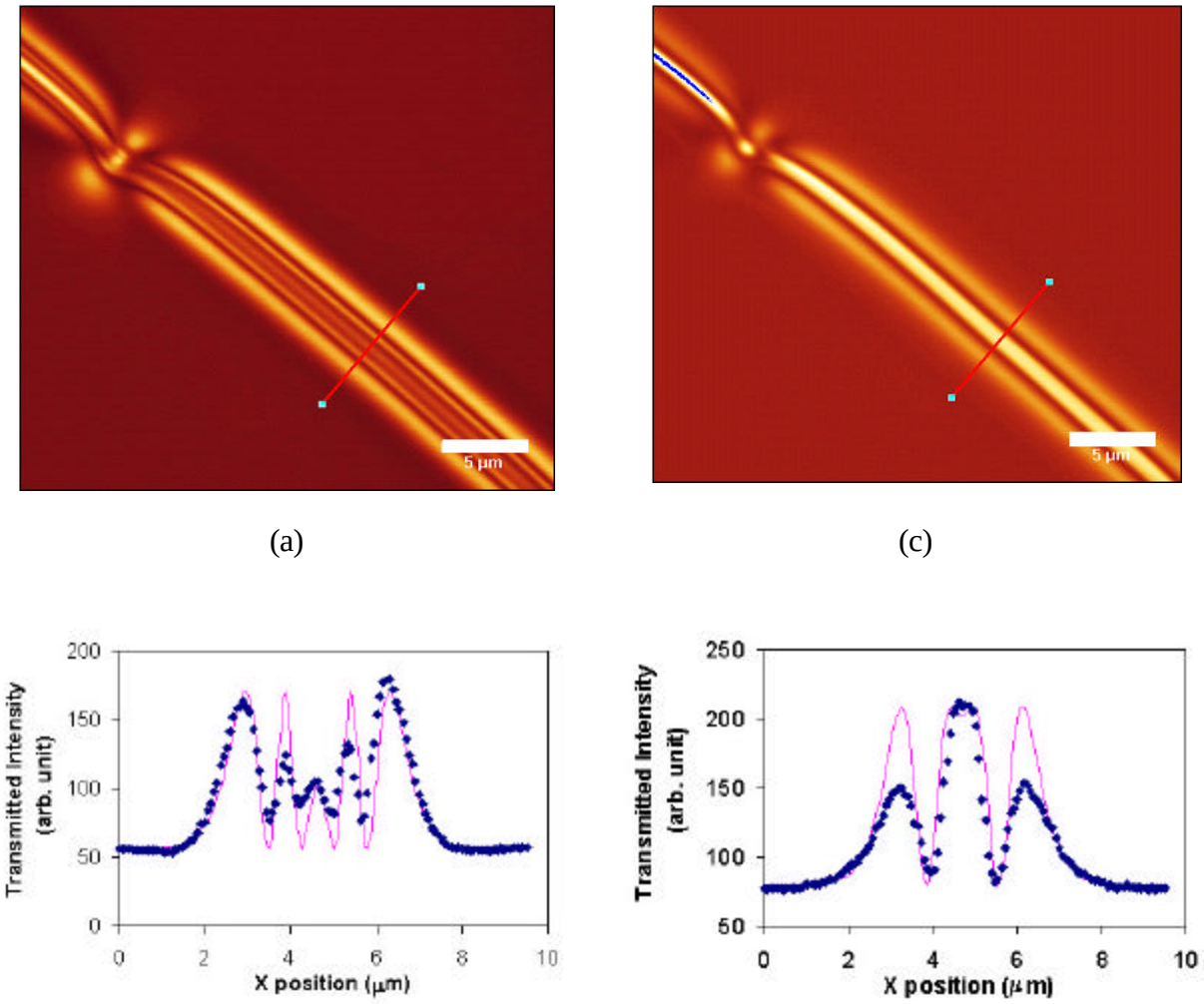

Figure 6.8. Interference patterns of a Bloch wall: experimental (blue points) and simulated ones (red curve) under the wavelength of 458 nm (a and b) and 568 nm (c and d), respectively. The film is made from 5CB and poly (*n*-octyl acrylate). The film thickness *h* is 5 μm as measured by the confocal microscopy. The scale bar is 5 μm.

6.3.4. Bloch walls and anchoring transition process

The Bloch wall formed in the system of our study is confined between the top and bottom substrates. As long as the temperature is kept far below the anchoring transition temperature (at homeotropic anchoring condition), the Bloch wall was found to be quite stable although they are the defects being trapped due to a kinetic process. They could stay intact for over a week when the environmental conditions (e.g., temperature and no external fields) are relatively fixed. The position of the Bloch wall also has some "memory" effect as long as the temperature is below the nematic-isotropic transition temperature, $T_{NI.}$ Even if the sample is repeatedly heated above T_t (but below T_{NI}) and quenched below T_t again, the walls appear at almost the same position within the encapsulated LC cells after every quench. But this memory is lost when the sample is heated above $T_{NI.}$ If the sample is quenched from above T_{NI} to below T_t, the wall newly formed may be at a different position, or if the sample is allowed to cool slowly from above T_{NI} to below T_t, the wall may disappear.

When the temperature is increased close to $T_{t,}$ the Bloch wall will become wider due to lower polar anchoring energy, at the same time, the central region of the wall also spreads out to have a finite width instead of a thin line if projected in *xy* plane (see Figure 3.19). The central region having a monostable planar anchoring was observed to act as a template to align neighboring domains parallel to itself, which is similar to epitaxial growth of a crystal. This is actually the start of homeotropic-to-planar anchoring transition. In other words, the homeotropic-to-planar anchoring transition in the LC domain containing a Bloch wall will occur first from the region of the wall and then spread out to the neighboring regions.

6.3.5. Reverse points

Another type of defect, so-called reversing point, is also often found along a Bloch wall (for example, in Figure 6.5, Figure 6.6 and Figure 6.8, the geometrical shape of these defects in *xy* plane looks like "kinked" along the *xy* projection of the wall). The reversing point defect was first reported by Ryschcenkow and Kleman.[7] As derived from both the fluorescence intensity profiles and the polarization transmission images in the above figures, the alignment of the director becomes increasingly perpendicular to the wall, but still maintains the same tilt angle within the plane parallel to the wall axis, when approaching the center of the reversing point. The director configuration of a reversing point along a pure twist wall is illustrated schematically in Figure 6.9. The characteristics of this director configuration are summarized as follows:

1) The twisting sense of the Bloch wall on the two sides of reversing point is opposite to each other, which is the origin of the name of this defect.

2) The region of reversing point is actually a blend of a Neel type wall and the Bloch wall. The Neel wall ends on two vertical wedge lines of continuous nature as shown in Figure 6.9. The wedge line at the acute side is equivalent to the *half* of a S= +1 line and the one at the obtuse side the *half* of a S= -1 line. The two wedge lines having opposite sign cannot annihilate because it is separated by the Bloch wall.

The continuous nature of the two vertical wedge lines is confirmed by polarized light microscopy. If they were singular lines or continuous lines with singular points at top or bottom end, when the analyzer is removed from a polarized light microscope, a fixed dark point should have been observed due to strong scattering of the light by the singular region.

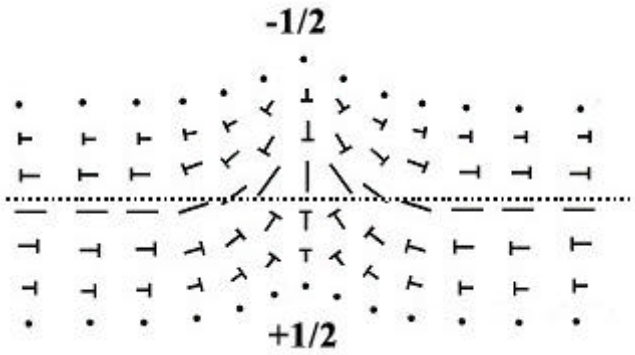

Figure 6.9. Schematics of the director field of a reversing point defect along a pure twist Bloch wall. The director variation along z is not shown since it is negligible if the apparent extrapolation length, *b*, is comparable with or greater than the sample thickness, h. The head of the nail sign, "T", representing one end of the nematic director, is behind the paper plane.

It was observed that reversing points also can stay intact for above several days if the environmental conditions were relatively fixed. They can also move along the Bloch walls from their original places to new places where another locally minimum free energy is reached. If a pair of reversing points with the opposite signs at the same side of the wall meet along a Bloch wall, they will annihilate.

6.4. Conclusions

(1) Three-dimensional director configurations of Bloch walls under the two regimes, diffuse walls and pure twist walls, were characterized by FCPM imaging. The results confirm the prediction by Ryschenkow and Kleman: pure twist wall is stable if the extrapolation length *b* is greater than or comparable to the sample thickness h; diffuse wall is stable if h is much greater than *b*.

(2) The optical simulations of a pure twist Bloch wall match very well with the experimental data i.e., the interference pattern of transmitted light and fluorescence

intensity profile across the wall. This confirms the director-field model for such a wall and also allows a more accurate measurement of polar anchoring strength.

(3) A more detailed description of “reversing point” defect along Bloch walls than those previously reported[7] is given based on the microscopic observations.

REFERENCES

[1] de Gennes, P. G. The Physics of Liquid Crystals; Clarendon: Oxford, 1974; p83.

[2] Williams, C.; Pieransk, P.; Cladis, P.E. "Nonsingular S=+1 screw disclination lines in nematics," *Phys. Rev. Lett.* **1972**, *29*, 90-2.

[3] Meyer, R.B. *Mol. Cryst. Liq. Cryst.* **1972**, *16*, 355.

[4] Cladis, P. E.; Kleman, M. "Nonsingular disclinations of strength S = + 1 in nematics," *J. de Phys.* (Paris) **1972**, *33*, 591-8.

[5] Saupe, A. "Disclinations and properties of the director field in nematic and cholesteric liquid crystals," *Mol. Cryst. Liq. Cryst.* **1973**, *21*, 211-38.

[6] Demus, D.; Richter, L. *Textures of Liquid Crystals*; Verlag Chemie: Weinheim, 1978; ch.4.

[7] Ryschenkow, G.; Kleman, M. "Surface defects and structural transitions in very low anchoring energy nematic thin films," *J. Chem. Phys.* **1976**, *64*, 404-12.

[8] Vitek, V.; Kleman, M. "Surface disclinations in nematic liquid-crystals, *"J. de Phys.* (Paris) **1975**, *36*, 59-67.

[9] Helrich, W. "Alignment-inversion walls in nematic liquid crystals in the presence of a magnetic field," *Phys. Rev. Lett.* **1968**, *21*, 1518-21.

[10] Kleman, M. *Points, Lines and Walls*; John Wiley & Sons: New York, 1983; ch.9.

[11] Nehring, J.; Saupe, A. "Schlieren texture in nematic and smectic liquid-crystals," *J. Chem. Soc. Faraday Trans. II* **1972**, *68*, 1-15.

[12] Leger, L. "Walls in nematic," *Mol. Cryst. Liq. Cryst.* **1973**, *24*, 33-44.

[13] Srinivasarao, M.; Park, J. O. "Magnetic field induced instabilities in nematic solutions of polyhexylisocyanates," *Polymer* **2001**, *42*, 9187-91.

[14] Wilson, T. in *Confocal Microscopy*; Wilson, T., Eds; Academic Press: London, 1990.

[15] Voloschenko, D.; Lavrentovich, O. D. “Optical vortices generated by dislocations in a cholesteric liquid crystal,”*Opt. Lett.* **2000**, *25*, 317-9.

[16] Smalyukh, I. I.; Shiyanovskii, S.V.; Lavrentovich, O. D. “Three-dimensional imaging of orientational order by fluorescence confocal polarizing microscopy,”*Chem. Phys. Lett.* **2001**, *336*, 88-96.

[17] Song, Y. “Study of dye diffusion in fibers by laser scanning confocal microscopy,” *Ph.D. Thesis*; North Carolina State University, 1999.

[18] Shiyanovskii, S. V.; Terentieva, Ju. G.; “Nematic-chloesteric mixture in a magnetic-field – A change in the critical behavior, ”*Phys. Rev. E.* **1994**, *49*, 916-8.

[19] Axelrod, D. In *Methods In Cell Biology*; Taylor, D. L.; Wang, Y.L., Eds; Academic Press: San Diego, 1989;Vol. 30, part B.

[20] Rapini, A.; Papoular, M. *J. Phys. (Paris) Colloq.* **1969**, *30*, C4-54.

[21] Khoo, I. C.; Wu, S. T. *Optics and Nonlinear optics of Liquid Crystals*; World Scientific: Singapore, 1993; p.81.

APPENDIX A

Table I. Typical physical properties of nematic liquid crystals (NLC) used in this thesis[a]

Physical properties of nematic fluids		TL205	TL213	5CB	MLC6608
TKN (°C)		<-20	<-20	23	—
TNI (°C)		87	88	35.5	90
Dielectric anisotropy, Δε (at 20 °C, 1 kHz)		+ 5.0	+ 5.7	+20.1	-4.2
Extraordianry refactve index, (ne) at 20 °C[b]	458 nm	—	—	1.7635	—
	568 nm	—	—	1.7212	—
	589 nm	1.7445	1.7659	1.742	1.5578
	633 nm	—	—	1.7094	—
Ordinary refractive index, (no) at 20 °C[b]	458 nm	—	—	1.5521	—
	568 nm	—	—	1.5348	—
	589 nm	1.5270	1.5271	1.530	1.4748
	633 nm	—	—	1.5300	—
Elastic constants (pN at 20 °C)[c]	K_{11}	17.3	16.8	6.6	16.7[e]
	K_{22}[d]	10.4	10.0	3.9	10.0
	K_{33}	20.4	22.0	9.3	18.0[e]

a All of the data listed here, except those specifically indicated, are provided by E-Merck Industries.

b The refractive indexes of 5CB are for 25 °C, and adopted from Khoo, I. C.; Wu, S. T. *Optics and Nonlinear optics of Liquid Crystals*; World Scientific: Singapore, 1993; p.81.

c The elastic constants of 5CB were measured at 23.5 °C: K_{11} and K_{33} are from Bogi, A.; Faetti, S. Liq. Cryst. 2000, 28, 729-739 and K_{22} is from Breddels, P.A.; Mulkens, J.C.H. *Mol. Cryst. Liq. Cryst.* 1987, 147, 107-112.

d All the K_{22} data here except that of 5CB are not measured values but assumed to be 0.6 of K11 according to Pochi, Y.; Gu, C. *Optics of Liquid Crystal Displays*; John Wiley & Sons: New York, 1999; p.12.

e The K_{11} and K_{33} data of MLC 6608 are adopted from Yang, F. Z.; Ruan, L. Z.; Sambles, J. R. *J. Applied Phys.* 2000, 88, 6175-6182.

APPENDIX B

^{1}H and ^{13}C NMR spectra of the synthesized alkyl acrylates

(±)2-Methylheptyl acrylate (2-MHA). ^{1}H NMR (300 MHz, $CDCl_3$): δ 6.35 (dd, J=17.4, 1.5 Hz, 1H), 6.10 (dd, J=17.4, 10.5 Hz, 1H), 5.75 (dd, J=10.5, 1.5 Hz, 1H), 4.00 (dd, J=10.8, 6.0 Hz, 1H), 3.89 (dd, J=10.8, 3.9 Hz, 1H), 1.75 (m, 1H), 1.06-1.40 (m, 8H), 0.88 (d, J=6.9 Hz, 3H), 0.84 (t, J=6.6 Hz, 3H). ^{13}C NMR (75 MHz, $CDCl_3$): δ166.5, 130.5, 128.8, 69.6, 33.5, 32.7, 32.2, 26.7, 22.8, 17.0, 14.2.

(±)3-Methylheptyl acrylate (3-MHA). ^{1}H NMR (300 MHz, $CDCl_3$): δ 6.38 (dd, J=17.4, 1.5 Hz, 1H), 6.10 (dd, J=17.4, 10.5 Hz, 1H), 5.80 (dd, J=10.5, 1.5 Hz, 1H), 4.19 (m, 2H), 1.69 (m, 1H), 1.52(m, 2H), 1.10-1.58 (m, 6H), 0.90 (d, J=6.9 Hz, 3H), 0.89 (t, J=6.6 Hz, 3H). ^{13}C NMR (75 MHz, $CDCl_3$): δ166.6, 130.6, 128.9, 63.4, 36.8, 35.7, 30.0, 29.3, 23.1, 19.8, 14.3.

(±)4-Methylheptyl acrylate (4-MHA). ^{1}H NMR (300 MHz, $CDCl_3$): δ 6.37 (dd, J=17.4, 1.5 Hz, 1H), 6.10 (dd, J=17.4, 10.5 Hz, 1H), 5.78 (dd, J=10.5, 1.5 Hz, 1H), 4.11 (t, J=6.6 Hz, 2H), 1.65 (m, 2H), 1.02-1.46 (m, 7H), 0.86 (t, J=6.6 Hz, 3H), 0.84(d, 6.9 Hz, 3H). ^{13}C NMR (75 MHz, $CDCl_3$): δ166.3, 130.4, 128.8, 65.1, 39.3, 33.2, 32.3, 26.3, 20.2, 19.6, 14.4.

(±)5-Methylheptyl acrylate (5-MHA). ^{1}H NMR (300 MHz, $CDCl_3$): δ 6.33 (dd, J=17.4, 1.5 Hz, 1H), 6.05 (dd, J=17.4, 10.5 Hz, 1H), 5.73 (dd, J=10.5, 1.5 Hz, 1H), 4.08 (t, J=6.6 Hz, 2H), 1.58 (m, 2H), 1.18-1.38 (m, 5H), 0.98-1.14 (m, 2H), 0.79 (t, J=6.9 Hz, 3H), 0.78 (d, J=5.1 Hz, 3H). ^{13}C NMR (75 MHz, $CDCl_3$): δ166.3, 130.4, 128.8, 64.7, 36.3, 34.4, 29.5, 29.0, 23.6, 19.2, 11.4.

1,1-Dimethylhexyl acrylate (1,1-DMHxA). ^{1}H NMR (300 MHz, $CDCl_3$): δ6.27 (dd, J=17.1, 1.5 Hz, 1H), 6.02 (dd, J=17.1, 10.2 Hz, 1H), 5.70 (dd, J=10.2, 1.5 Hz, 1H), 1.76 (m, 2H), 1.45 (s, 6H), 1.22-1.35 (m, 6H), 0.86 (t, J=6.9 Hz, 3H). ^{13}C NMR (75 MHz, $CDCl_3$): δ165.7, 130.6, 129.5, 83.1, 40.9, 32.3, 26.2, 23.7, 22.8, 14.2.

2,2-Dimethylhexyl acrylate (2,2-DMHxA). ^{1}H NMR (300 MHz, $CDCl_3$): δ6.39 (dd, J=17.1, 1.5 Hz, 1H), 6.12 (dd, J=17.1, 10.2 Hz, 1H), 5.81 (dd, J=10.2, 1.5 Hz, 1H), 3.87(s, 2H), 1.25 (m, 6H), 0.91 (s, 6H), 0.88 (t, J=7.2 Hz, 3H). ^{13}C NMR (75 MHz, $CDCl_3$): δ166.6, 130.6, 128.9, 72.7, 39.1, 34.0, 26.2, 24.5, 23.7, 14.3.

^{1}H and ^{13}C NMR spectra of poly (x-methylheptyl acrylate) prepared via solution free radical polymerization and the peak assignment*

Solutions of the polyacrylates in $CDCl_3$ were made, with concentration of approx. 3.5~ 4 wt%. NMR spectra are obtained from Mercury Vx 300 NMR instrument (300 MHz).

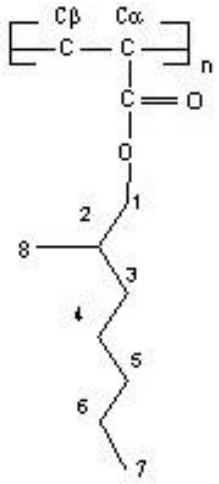

* Pham, Q.T; Petiaud, R.; Waton, H. *Proton and Carbon NMR Spectra of Polymers*, Vol. 2 and 3, John Wiley and Sons: New York, 1983.

Table II-A. ^{1}H NMR spectra data of poly(x-methylheptyl acrylates), i.e., P(x-MHA).

Polymers	Chemical shifts and assignment
Poly(n-heptyl acrylate)	3.99 (br,-O-CH_2-), 2.26 (br, -CH-C=O), 1.88,1.59, 1.28 (CH_2, 8H), 0.88(t, CH_3)
P (1-MHAC)	4.8 (br, -O-CH-), 2.24 (br, -CH-C=O), 1.85,1.56, 1.4, 0.88(CH_3)
P (2-MHAC)	3.93,3.74 (d, 54 Hz, -O-CH_2-), 2.28 (br, -CH-C=O), 1.85,1.56, 1.4, 0.88(CH_3)
P (4-MHAC)	3.98 (br, -O-CH_2-), 2.24 (br, -CH-C=O), 1.85,1.56, 1.4, 0.88(CH_3)
P (5-MHAC)	4.00 (br,-O-CH_2-), 2.3 (br, -CH-C=O), 1.85,1.56, 1.4, 0.88(CH_3)

Table II-B. ^{13}C-NMR (75MHz,CDCB) spectra data of P(x-MHA).

Polymers	Chemical shifts and assignment
Poly(n-heptyl acrylate)	174 .7(C=O), 65.0 (C1), 41.3~ 41.6(C_β), 35.5 ~36.5 (broad, C_α), 32.0 (C5), 29.2(C2), 28.8(C4), 26.0(C3), 22.8(C6), 14.3(C7)
P (1-MHAC)	174 .3(C=O), 71.4 (C1), 41.0~ 42.0 (C_β), 35 ~37 (broad, C_α), 36.0 (C2), 32.0(C5), 29.4(C4), 25.6(C3), 22.9(C6), 19.9(C8), 14.3 (C7)
P (2-MHAC)	174 .7(C=O), 69.8(C1), 41.0~ 42.0 (C_β), 35 ~37 (broad, C_α), 33.6 (C3), 32.7(C5), 32.3(C2), 26.7(C4), 22.9(C6), 17.2(C8), 14.3 (C7)
P (4-MHAC)	174 .6(C=O), 65.2(C1), 41.0~ 42.0 (C_β), 35 ~37 (C_α), 39.4 (C5), 33.1(C3), 32.5(C4), 26.4(C2), 20.3(C6), 19.7(C8), 14.6 (C7)
P (5-MHAC)	174 .6(C3), 65.0(C4), 41~ 42 (C_β), 35-37 (broad, C_α), 36.5 (C4), 34.5(C5), 29.6(C2), 29.1(C6), 23.5(C3), 19.3(C8), 11.5 (C7)

APPENDIX C

Measurement of optical anisotropy of nematic fluid TL205

Experimental:[*,†]

The nematic liquid crystal used for the study is TL205 (EMerck Industries). The refractive indices of this liquid crystal, n_o and n_e, were measured as a function of temperature using an Abbe' refractometer (Bellingham and Stanley Ltd, model 60/ED) with a large refractive index prism (prism index = 1.76142 for 589.6 nm sodium D). The value of the refractive indices measured by Abbe' refractometer were calibrated by the scale of the sodium D-line and refractive indices could be measured with an accuracy of ± 0.0001. To obtain homeotropic molecular orientation at the interface, the heated liquid crystal in the isotropic state were allowed to fall as drops on the lecithin coated surface of the fixed prism. A polarizer was attached to the eyepiece of the refractometer, the ordinary and extraordinary ray was selected by adjusting its polarization direction, and then each refractive index, n_o and n_e, was measured. The temperature of the liquid crystal was controlled by circulating water from a bath whose temperature was controlled to ± 0.1 °C.

---

* George, A. K. "Optical anisotropy of nematic liquid crystals," *Phys. Chem. Liq.*; 1998, 37, 65-71.

† de Jeu, W. H. *Physical Properties of Liquid Crystalline Materials* (Gordon and Breach, New York), 1980.

Results

Table III. Refractive indices of the nematic fluid TL205 measured as a function of temperature

Temperature (°C)	n_o	n_e	n_e-n_o
20	1.5237	1.7394	0.2157
35	1.5216	1.7286	0.207
50	1.5194	1.7126	0.1932
55	1.5191	1.7079	0.1888
60	1.5186	1.7007	0.1821
65	1.5188	1.6937	0.1749
70	1.5191	1.6854	0.1663

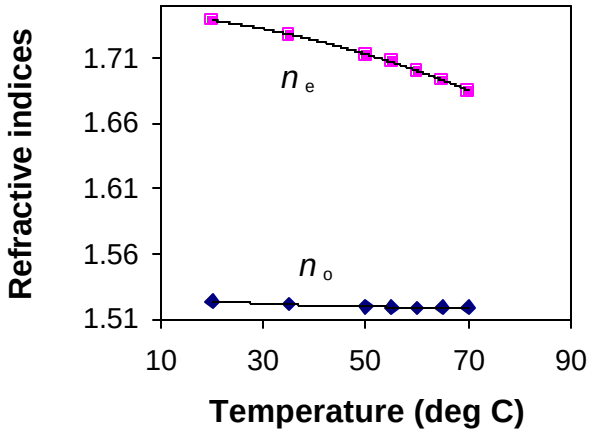

Figure I. Plot of refractive indices of the nematic fluid TL205 as a function of temperature.

BIOGRAPHY

Jian Zhou was born in Beijing, China on October 20, 1971. He received his Bachelor of Engineering (Chemical Engineering) in 1994 from Tsinghua University, and Master of Science (Polymer Chemistry and Physics) in 1997 from Institute of Chemistry, Chinese Academy of Science, Beijing, China.

From 1997 to 1999, he was employed as a chemical engineer in Beijing Research Institute of Chemical Industry. In 1999, he entered the Ph.D. program in Polymer Science at School of Polymer, Textile and Fiber Engineering, Georgia Institute of Technology. He is a student member of American Chemical Society, American Physical Society, Material Research Society.

His wife is Ms. Wei Xu.